Springer Theses
Recognizing Outstanding Ph.D. Research

Haichao Wang

The Chemistry of Nitrate Radical (NO_3) and Dinitrogen Pentoxide (N_2O_5) in Beijing

Springer

Springer Theses

Recognizing Outstanding Ph.D. Research

Aims and Scope

The series "Springer Theses" brings together a selection of the very best Ph.D. theses from around the world and across the physical sciences. Nominated and endorsed by two recognized specialists, each published volume has been selected for its scientific excellence and the high impact of its contents for the pertinent field of research. For greater accessibility to non-specialists, the published versions include an extended introduction, as well as a foreword by the student's supervisor explaining the special relevance of the work for the field. As a whole, the series will provide a valuable resource both for newcomers to the research fields described, and for other scientists seeking detailed background information on special questions. Finally, it provides an accredited documentation of the valuable contributions made by today's younger generation of scientists.

Theses are accepted into the series by invited nomination only and must fulfill all of the following criteria

- They must be written in good English.
- The topic should fall within the confines of Chemistry, Physics, Earth Sciences, Engineering and related interdisciplinary fields such as Materials, Nanoscience, Chemical Engineering, Complex Systems and Biophysics.
- The work reported in the thesis must represent a significant scientific advance.
- If the thesis includes previously published material, permission to reproduce this must be gained from the respective copyright holder.
- They must have been examined and passed during the 12 months prior to nomination.
- Each thesis should include a foreword by the supervisor outlining the significance of its content.
- The theses should have a clearly defined structure including an introduction accessible to scientists not expert in that particular field.

More information about this series at http://www.springer.com/series/8790

Haichao Wang

The Chemistry of Nitrate Radical (NO_3) and Dinitrogen Pentoxide (N_2O_5) in Beijing

Doctoral Thesis accepted by
College of Environmental Sciences and
Engineering, Peking University, Beijing, China

Springer

Author
Dr. Haichao Wang
State Key Joint Laboratory of Environmental Simulation and Pollution Control
College of Environmental Sciences and Engineering
Peking University
Beijing, China

Supervisor
Prof. Keding Lu
State Key Joint Laboratory of Environmental Simulation and Pollution Control
College of Environmental Sciences and Engineering
Peking University
Beijing, China

ISSN 2190-5053 ISSN 2190-5061 (electronic)
Springer Theses
ISBN 978-981-15-8794-8 ISBN 978-981-15-8795-5 (eBook)
https://doi.org/10.1007/978-981-15-8795-5

This Springer imprint is published by the registered company Springer Nature Singapore Pte Ltd.
The registered company address is: 152 Beach Road, #21-01/04 Gateway East, Singapore 189721, Singapore

Supervisor's Foreword

Nitrate radical (NO_3) and dinitrogen pentoxide (N_2O_5) play a pivotal role in the nocturnal atmosphere. The reaction of NO_3 with VOCs and N_2O_5 heterogeneous uptake broadly impacts the fate of NO_x and VOCs in both the regional and global scales. Over the past decades, many studies are conducted to improve our knowledge of nighttime chemistry. However, there are still many issues that remain poorly understood, especially their atmospheric processes and impacts in China. In this study, Dr. Haichao Wang sets up the first field-deployable instruments in China for the measurement of both NO_3 and N_2O_5 based on cavity-enhanced absorption spectroscopy (CEAS). The main improvements compared to the few available CEAS instruments worldwide include a mechanically aligned non-adjustable optical mounting module and a chemical titration module for determining the zero point. The new improvements also allow the new instruments to be portable, stable, and easy to operate in the field campaigns. Up to now (also after the thesis), the developed instruments have been successfully applied in about ten field campaigns, which provided key supports for the exploration of the nighttime chemistry. Besides, benefit the elucidation of the particulate nitrate formation mechanism in the major cities in China. During the thesis period, four field campaigns were conducted in Beijing with the measurement of N_2O_5 and related parameters. These data covered different seasons and a large variety of ambient conditions. Based on the obtained comprehensive dataset, the features of the ambient behaviors and the budgets of both the NO_3 and N_2O_5 in Beijing were well systematically explored and quantified. Moreover, the N_2O_5 heterogeneous uptake coefficient was determined, the relationship of N_2O_5 uptake coefficient and the particle composition and properties were elaborated, and a new parameterized equation for the N_2O_5 uptake coefficient is proposed. The impacts of NO_3–N_2O_5 chemistry on the atmospheric oxidation and the contribution to particulate nitrate formation were systematically studied and elucidated. These results significantly improved the understanding of the nighttime chemistry in the troposphere and will enlighten the thinking about the role of NO_3–N_2O_5 chemistry in other polluted regions like Beijing. The academic impact of his thesis is very good both in China and the international community. I received excellent explicit comments from Prof. Steven Brown (NOAA) and Prof. Andreas

Wahner (director of IEK-8, FZJ) to his contribution to the nighttime chemistry. The scientists from the Municipality of Milan also contacted me intensively even during the COVID-19 period to ask for help about the particulate nitrate control due to his publications, which I am the corresponding author.

Beijing, China
December 2018

Prof. Keding Lu

Abstract

Nitrate radical (NO_3) and dinitrogen pentoxide (N_2O_5) chemistry are important in the troposphere at night. The quantitative description of them is of great significance for the study of regional air quality and global climate change. This study focuses on NO_3 and N_2O_5 chemistry in Beijing, China. The NO_3 and N_2O_5 field measurement systems are developed based on the cavity-enhanced absorption spectroscopy (CEAS). The detection limits of NO_3 and N_2O_5 are 2.4 pptv and 2.7 pptv for 1 s temporal resolution. The uncertainty of NO_3 and N_2O_5 is 19% and 22–36%, respectively. Compared with other similar measuring systems in the world, there are two significant improvements. (1) The use of high-precision mechanically coupled mirror holders significantly improves the stability of the measurement system and the applicability of the field measurement. (2) The using of chemical titration modules to avoid nonlinear absorption of water vapor interference. The instrument was successfully applied in four comprehensive field campaigns in urban and suburban areas of Beijing, including the Huairou (HR) winter campaign (suburbs), Changping (CP) summer campaign (suburbs), Peking University (PKU) summer campaign (urban), and Peking University winter campaign (urban). High-quality N_2O_5 time series were acquired under four typical environmental conditions. The critical processes in NO_3 and N_2O_5 chemistry were systematically analyzed. The main findings were as follows:

1. The observation shows that the mixing ratio of N_2O_5 is significant in Beijing; the nocturnal maximum over one ppbv was observed frequently; the suburbs are significantly higher than urban areas. Based on the N_2O_5 measurements, the nighttime NO_3 concentration was derived from the thermodynamic equilibrium. The average was between 0.1 and 10 pptv, which was significantly higher in summer than in winter. The average NO_3 production rate (1–2 ppbv h^{-1}) was much higher in summer than in winter (0.1–0.2 ppbv h^{-1}). The difference between urban and suburban areas is mainly affected by the difference in NO_x concentration, and seasonal differences are mainly affected by temperature and ozone concentration.

2. The average NO_3 reactivity (k_{NO3}) for volatile organic compounds (VOCs) in PKU winter, HR winter, and CP summer is 6.6×10^{-3} s^{-1}, 3.7×10^{-3} s^{-1}, and 1.9×10^{-2} s^{-1}, respectively. Biogenic VOCs (monoterpenes) dominated k_{NO3} in CP summer, while anthropogenic VOCs dominated k_{NO3} in winter. The contribution of NO_3 to summer oxidation is significant, especially for BVOCs oxidation. NO_3 dominated more than 90% nocturnal BVOCs degradation, but the NO_3 oxidation capacity in the wintertime is weak.
3. The determined N_2O_5 uptake coefficient, $\gamma(N_2O_5)$, is generally high, ranging from 0.012 to 0.072, with an average value of 0.04 in summer in Beijing. The $\gamma(N_2O_5)$ is generally higher than those reported in Europe and the USA, which may be related to the high water content in aerosols in Beijing. $\gamma(N_2O_5)$ was ranged from 0.001 to 0.017, with an average of 0.005 in the winter suburbs of Beijing, which was much lower than that in summer. In the winter, $\gamma(N_2O_5)$ increased with the increase of relative humidity, and the aerosol liquid water content had a promoting effect on the N_2O_5 uptake, while particulate nitrate had an inhibitory effect. Both the existing organic coating model and inorganic aerosol model are difficult to accurately simulate the $\gamma(N_2O_5)$, which may be related to the underestimation of the inhibition of organic coating.
4. Both the high N_2O_5 concentration and the high aerosol surface area coexist in the $PM_{2.5}$ pollution episode in summer. The higher N_2O_5 uptake coefficient in summer resulted in a significant contribution to particulate nitrate production, with an average daily production of up to 57 μg m^{-3}, which is equivalent to the contribution of the gas-phase oxidation process (OH + NO_2) during the day. The N_2O_5 uptake coefficient was low during the winter pollution episodes, with an average daily nitrate production of 11 μg m^{-3}. The average daily amount of gas-phase oxidation contributed up to 53 μg m^{-3}, indicating that the winter nitrate production was caused by gas-phase oxidation during the daytime. In general, the heterogeneous uptake of N_2O_5 is an essential channel for nitrate production in particulate matter in urban areas. The model simulation results show that $ClNO_2$ formed by the heterogeneous reaction of N_2O_5 during the pollution process in Huairou winter has a vital role in the following daytime chemistry, which can increase the primary source of O_3 and RO_x by 21% and 13%, and become the important daytime source of O_3 and RO_x in wintertime.

Keywords Nitrate radical · Dinitrogen pentoxide · Cavity-enhanced absorption spectroscopy · Field observation · Atmospheric oxidation · Heterogeneous hydrolysis · Particulate nitrate formation

Parts of this thesis have been published in the following journal articles:

Wang, H. C., Lu, K. D*., Chen, X. R., Zhu, Q. D., Chen, Q., Guo, S., Jiang, M. Q., Li, X., Shang, D. J., Tan, Z. F., Wu, Y. S., Wu, Z. J., Zou, Q., Zheng, Y., Zeng, L. M., Zhu, T., Hu, M., and Zhang, Y. H.: High N_2O_5 Concentrations Observed in Urban Beijing: Implications of a Large Nitrate Formation Pathway, *Environ Sci Tech Let*, 4, 416–420, https://doi.org/10.1021/acs.estlett.7b00341, 2017. (Reproduced with Permission. Copyright (2017) American Chemical Society).

Wang, H. C., Chen, J., and Lu, K*. D.: Development of a portable cavity-enhanced absorption spectrometer for the measurement of ambient NO_3 and N_2O_5: experimental setup, lab characterizations, and field applications in a polluted urban environment, *Atmos Meas Tech*, 10, 1465–1479, https://doi.org/10.5194/amt-10-1465-2017, 2017. (Reproduced with Permission).

Wang, H. C., Lu, K. D. *, Guo, S., Wu, Z. J., Shang, D. J., Tan, Z. F., Wang, Y. J., Le Breton, M., Lou, S. R., Tang, M. J., Wu, Y. S., Zhu, W. F., Zheng, J., Zeng, L. M., Hallquist, M., Hu, M., and Zhang, Y. H.: Efficient N_2O_5 uptake and NO_3 oxidation in the outflow of urban Beijing, *Atmos Chem Phys*, 18, 9705–9721, https://doi.org/10.5194/acp-18-9705-2018, 2018. (Reproduced with Permission).

Wang, H. C., Chen, J., and Lu, K. D*.: Measurement of NO_3 and N_2O_5 in the Troposphere, *Prog Chem*, 27, 963–976, https://doi.org/10.7536/pc141230, 2015. (Reproduced with Permission. Copyright editorial department of Progress in Chemistry).

Acknowledgements

The five-year doctoral study at Peking University is one of the precious experiences in my life. Many people have helped me in my study. I would like to take this opportunity to express my gratitude to all of them. I would like to thank my supervisor, Prof. Keding Lu, for bringing me into the field of atmospheric chemistry. He infects and inspires me deeply by setting an good example of diligent and hard-working style. His rigorous academic style and a keen sense of scientific innovation have benefited me a lot. He gave me full freedom academically and gave me many opportunities to try various experimental designs, even if it often failed. The thesis is inseparable from his efforts. Thanks to Prof. Yuanhang Zhang for my academic guidance, his profound knowledge has always inspired me. Thanks to Prof. Min Hu for supporting me to participate in the international cooperation project "Photo-smog in China." Thanks to Prof. Limin Zeng for the help in instruments and field observation. Thanks to Prof. Xuesong Wang, Prof. Xin Li, Prof. Zhijun Wu, Prof. Song Guo, Prof. Mingjin Tang, and Dr. Shengrong Lou for the helpful discussion. Thanks to Dr. Huabin Dong and Yusheng Wu for their technical help in the experiment. Thanks to Dr. Jun Chen for his suggestions and assistance in the development of the instrument. The research group provided a friendly study atmosphere with happiness for me. Thanks to all my colleagues who helped me a lot. Thanks to my family, they will always have my back. The research carried out in the thesis was funded by the National Natural Science Foundation of China (Grant 41390240, 41390243 and 41130754).

Contents

Chapter 1
Introduction

Abstract This chapter reviews the background of the atmospheric chemistry of NO_3 and N_2O_5, the field measurement techniques of NO_3 and N_2O_5, the results from laboratory experiments, and field measurement. It summarizes the current research progress and shortcomings of NO_3 and N_2O_5 chemistry. At last, scientific problems and research targets are put forward.

1.1 Background

Since the Industrial Revolution, human activities have emitted a large number of primary pollutants into the atmosphere, such as NO_x, Volatile organic compounds (VOCs). Primary pollutants undergo a series of complex chemical and physical processes to generate secondary pollutants, such as O_3 and $PM_{2.5}$, which cause severe air pollution problems and affect human health and global climate. Nowadays, air pollution in China is severe. A better understanding of atmospheric chemical mechanisms will help clarify the nature of air pollution and provide a theoretical basis for making the control policies for the pollutant formation.

In the early 1970s, Levy firstly proposed that the tropospheric atmosphere is an oxidizing environment with the core of free radical chemistry [64]. As the most important oxidant in the atmosphere, OH radicals play a decisive role in the removal of air pollutants and determine the atmospheric lifetime of most gaseous pollutants [29, 34]. People believed that the active atmospheric self-clean process only occurred during the day, mainly because the two critical oxidants, OH radicals, and O_3, were driven by photochemistry. Since the 1990s, with the improvement of free radical measurement technology, high levels of nitrate radical (NO_3), peroxy radicals (HO_2, RO_2) and OH were observed at nighttime [19, 45, 71, 81]. It was recognized that the nighttime atmospheric environment is not inert and may also reactive. This discovery was of great significance for understanding the removal of trace gases on a global scale and the formation of free radical precursor species during the daytime, which also promoted the NO_3 chemistry attracting more and more attention at home and abroad.

H. Wang, *The Chemistry of Nitrate Radical (NO_3) and Dinitrogen Pentoxide (N_2O_5) in Beijing*, Springer Theses, https://doi.org/10.1007/978-981-15-8795-5_1

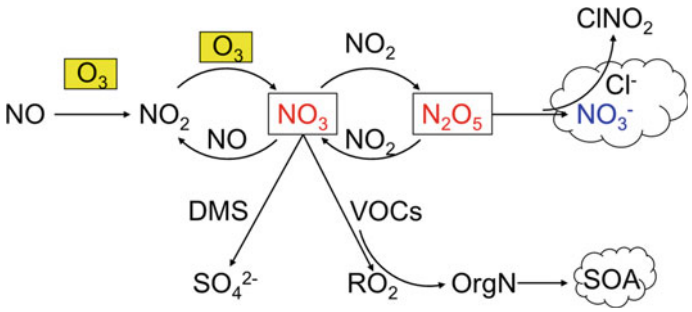

Fig. 1.1 Schematic of the NO_3 and N_2O_5 chemistry in the troposphere

Figure 1.1 shows a schematic view of the primary source and removal processes of NO_3 and N_2O_5. The reaction of NO_2 with O_3 is the main formation pathway of NO_3 (1.1), but the reaction rate constant is greatly affected by temperature. Other NO_3 formation pathways include the reaction of OH with HNO_3, photolysis of organic nitrate, etc. However, these pathways have been confirmed to contribute less to NO_3 in the troposphere. The reaction between Criegee radicals and NO_2 is considered as one of the possible sources of NO_3 [32]. However, the concentration level of Criegee radical and the quantification of the reaction rate constant are still under debate.

$$NO_2 + O_3 \rightarrow NO_3 + O_2 \tag{1.1}$$

The fast photolysis rate of NO_3 (1.2, 1.3), and NO_3 can be quickly titrated by NO (1.4), resulting in NO_3 lost fast during the daytime. The lifetime of NO_3 during the daytime is usually less than 5 s. Therefore, NO_3 chemistry is generally considered to be unimportant during the day [116]. Under the dark reaction condition, the photochemical cycle process of NO, NO_2, and O_3 stops, and NO is titrated by O_3. NO_2 reacts with O_3 to form NO_3, and NO_3 accumulates gradually, which makes the impacts of NO_3 chemical behaviors significant at night. The rapid thermodynamic equilibrium (1.5, 1.6) between NO_3 and N_2O_5 makes the relationship between NO_3 and N_2O_5 are closely connected, and the two species are usually studied together. Here K_{eq} represents the thermodynamic equilibrium constant between NO_3 and N_2O_5 (1.7).

$$NO_3 + h\nu \rightarrow O(^3P) + NO_2(\sim 90\%) \tag{1.2}$$

$$NO_3 + h\nu \rightarrow O_2 + NO(\sim 10\%) \tag{1.3}$$

$$NO_3 + NO \rightarrow 2\,NO_2 \tag{1.4}$$

$$NO_2 + NO_3 + M \rightarrow N_2O_5 + M \tag{1.5}$$

$$N_2O_5 \rightarrow NO_2 + NO_3 \tag{1.6}$$

$$K_{eq} = 5.5 \times 10^{-27} \times \exp(10,724/T) \tag{1.7}$$

The source of ambient NO_3 is relatively clear, but the research on its removal process is complicated. The direct removal pathways of NO_3 include the heterogeneous reaction of NO_3 on the particle surface and the gas-phase reaction of NO_3 and VOCs, NO, and RO_2. Although the heterogeneous reaction uptake coefficient of NO_3 on the particle surface is high, it can be ignored compared with other removal pathways. The reaction of NO_3 and VOCs is a vital reaction at night. The reaction rate of NO_3 and olefins is fast, especially biogenic VOCs (BVOCs). NO_3 oxidation is an important way to remove BVOCs and affects the atmospheric lifetime of BVOCs at night [73]. NO_3 reacts with olefins (1.8), then react with O_2 to form RO_2, and further generate organic nitrate. This reaction has a high secondary organic aerosol (SOA) mass yield. Many studies suggest the reaction of NO_3 with BVOCs is an essential source of SOA [38, 55, 61, 73, 82]. The reaction of NO_3 and BVOCs to generate SOA is a typical case of the interaction of anthropogenic emission and biological emissions. Besides, NO_3 can also react with RO_2, which has a role similar to NO during the daytime in HO_x radical regeneration [20]. In coastal areas, NO_3 dominates the oxidation reaction of dimethyl sulfide (DMS) and generates sulfates acid. The model simulation estimated that 24% of global DMS is oxidized by NO_3, which has an impact on the global sulfur cycle and cloud condensation in marine areas [3, 90, 120].

$$NO_3 + R1 - C = C - R2 \rightarrow R1 - C - C(NO_3) - R2 \tag{1.8}$$

The removal route of N_2O_5 is considered an indirect removal route of NO_3. Therefore, it is an essential loss pathway of NO_3. N_2O_5 removal includes reactions with water vapor and heterogeneous reactions on the surface of cloud droplets and particles [22]. The most important in the troposphere is the heterogeneous reaction of N_2O_5 on the particle surface (1.9). The reaction rate $k(N_2O_5)$ is calculated by the aerosol surface area (S_a), the uptake coefficient ($\gamma(N_2O_5)$), and the average molecular velocity (C) of N_2O_5 (1.10).

$$N_2O_5 + \left(H_2O \text{ or } Cl^-\right) \rightarrow (2 - f)\, NO_3^- + f\, ClNO_2 \tag{1.9}$$

$$k(N_2O_5) = 0.25 \times S_a \times \gamma(N_2O_5) \times C \tag{1.10}$$

One of the main products of the heterogeneous reaction of N_2O_5 is nitrate. Many studies have shown that the heterogeneous reaction of N_2O_5 at night in urban areas is an important NO_x removal pathway. This N_2O_5 uptake in NO_x removal is even

comparable to the reaction between NO_2 and OH during the day [42, 43, 92, 101]. Global model studies have shown that the heterogeneous N_2O_5 reaction can have an important effect on the global NO_x removal and the O_3 and OH concentration levels [2, 25]. When the value of $\gamma(N_2O_5)$ is 0.02, the heterogeneous uptake of N_2O_5 can contribute to 18% of global NO_x removal. In the quantitative N_2O_5 heterogeneous response to nitrate contribution, accurate parameterization of the uptake coefficient is the key to accurate estimation.

Laboratory studies show that N_2O_5 can generate $ClNO_2$ during the heterogeneous uptake of chlorine-containing aerosol surfaces [8, 35], where f is the $ClNO_2$ yield (1.8). Generally, high concentrations of $ClNO_2$ are prone to occur in marine areas. $ClNO_2$ in inland areas is mainly caused by human activities such as biomass and coal combustion, and salt and the melting of snow in winter [70]. A high level of $ClNO_2$ was observed in both polluted and coastal areas of the United States, respectively [75, 100]. In the early morning, the Cl radicals generated by $ClNO_2$ photolysis is significant compared with other oxidants, suggest the contribution of $ClNO_2$ to atmospheric oxidation capacity cannot be ignored [65, 75, 78, 83, 98, 112]. 25% of the alkane oxidation in the Los Angeles area is contributed by Cl radicals, and 45% of the Cl radicals are contributed by $ClNO_2$ photolysis [83]. Recent research indicates that Cl radical oxidized alkanes, alkenes, and alkynes in the London area account for 15%, 3%, and 26% of the total, respectively [7]. Besides, $ClNO_2$ photolysis enhances the photochemical reaction, and promote the increase of O_3 levels in urban areas. However, the contribution of O_3 formation to O_3 is still under debate [86].

1.2 Field Measurement Techniques of NO_3 and N_2O_5

Field observation is an essential route in promoting the understanding of the tropospheric NO_3 chemical mechanism. Many research groups try to develop NO_3 and N_2O_5 measurement techniques. NO_3 features with high reactivity, short atmospheric life, and low concentration. These characteristics require its field measurement instruments should be equipped with high time resolution, low sampling loss, and high sensitivity, which means the field measurement of NO_3 and N_2O_5 is quite tricky.

In the past 30 years, these technologies have been successfully applied to the measurement of NO_3 and N_2O_5 in the field observation: differential optical absorption spectroscopy (DOAS), cavity ring-down spectroscopy (CRDS), cavity-enhanced absorption spectroscopy (CEAS), laser-induced fluorescence (LIF), matrix isolation and electron spin resonance (MIESR), and chemical ionization mass spectrometry, CIMS). There are MIESR, DOAS, CRDS, CEAS applied to NO_3 field measurement, and CIMS, CRDS, CEAS, LIF applied to N_2O_5 measurement, among which CIMS is the only direct measurement technology of N_2O_5. The other three are based on the pyrolysis of N_2O_5 to thermal decomposed into NO_3, and then the corresponding technical method is used to measure NO_3 for quantifying N_2O_5 indirectly. In general, the measurement techniques of NO_3 and N_2O_5 can be divided into four categories:

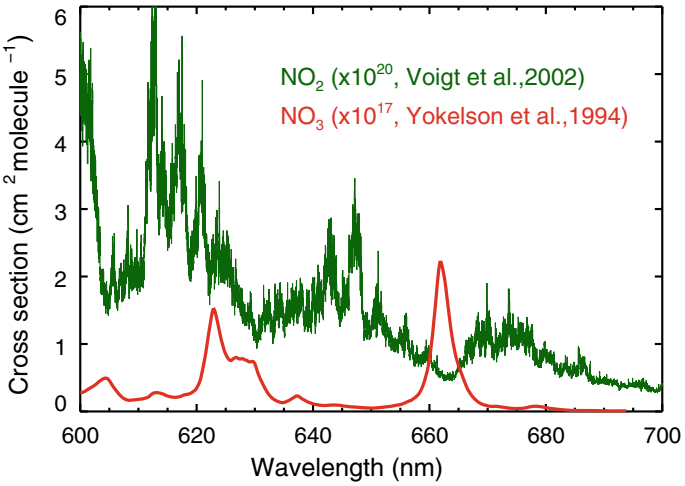

Fig. 1.2 The cross-section of NO_2 and NO_3 at 600–700 nm

absorption spectroscopy, fluorescence spectroscopy, mass spectrometry, and electron spin resonance spectroscopy.

NO_3 radicals have strong absorption at 623 and 662 nm ($B_2E' \rightarrow X_2A_2'$ electronic transition), the absorption peaks of the absorption spectrum are 1.4×10^{-17} cm^2 and 2.2×10^{-17} cm^2, respectively, which is about 10^3 times higher than that of NO_2 in the same wavelength range (Fig. 1.2). The strong absorption windows make the absorption spectroscopy ideal to measure NO_3. The absorption spectroscopy technique is based on Lambert-Beer law (1.11):

$$\log(I_0/I) = \sigma \mathrm{Ln} \tag{1.11}$$

Here I_0 is the incident light intensity, I is the transmitted light intensity, σ is the absorption cross-section of a specific gas molecule, L is the optical absorption path, and n is the atmospheric concentration of a specific gas molecule. In the atmosphere, due to the low concentration of the target species, high sensitivity can only be achieved by enlarging the optical absorption path.

The optical path of the DOAS method is usually on the order of kilometers. Differential absorption can only be used when the absorption spectrum of the species contains a marked structure within a narrow wavelength range. Based on the strong absorption feature, the differential absorption cross-section of the gas molecular absorption spectrum is used as the quantitative basis of DOAS [80]. The DOAS method is divided into passive DOAS (Max-DOAS) and active DOAS (LP-DOAS) [74]. The passive DOAS uses sunlight or moonlight as the light source. LP-DOAS usually uses a broadband light source such as a xenon lamp and uses an angled mirror to fold the optical path [52]. DOAS is one of the earliest mainstream measurement

methods applied to the observation of the troposphere NO_3. It has laid the foundation of tropospheric NO_3 chemistry. While the limitation of DOAS is the measured gas concentration represents the average value on a long-distance optical path. In addition, this method is affected by atmospheric visibility.

Optical path folding technology is another idea of absorption spectroscopy technology. The White-cell method proposed earlier, and the optical path magnification can reach more than 10^2 [53, 117]. Benefit on the development of light source (mainly LED and laser) and high-reflectivity mirrors, resonant cavity technology has become a novel and highly efficient optical path folding technology. Its optical path magnification can reach up to 10^4–10^5 levels, which significantly improves the detection capabilities of spectral technology. The application of cavity technology in NO_3 field observation includes CRDS and CEAS [18, 33, 62, 87].

The CRDS technology uses two high-reflectivity mirrors with a center wavelength of 662 nm (usually with a reflectivity >99.99%) to form a resonant cavity. The incident end of the optical cavity is a 662 nm pulsed laser light source. After the incident laser enters the resonant cavity, it forms resonance. The other end uses a high-speed response photon counter to detect the ring down time decay of the transmitted light intensity [18]. Due to the strong absorption of NO_3 in the 662 nm, the ring-down time will be reduced compared with the reference condition. The number concentration n (NO_3) of NO_3 is calculated by measuring the ring-down time with or without NO_3 gas absorption (1.12).

$$n(\mathrm{NO_3}) = \frac{R_L}{C\sigma_{NO_3}}\left(\frac{1}{\tau} - \frac{1}{\tau_0}\right) \tag{1.12}$$

Here τ_0 is the decay time of the reference spectrum, R_L represents the ratio of the distance between the high reflective lenses and the effective absorption length of the gas, and C and σ_{NO3} represent the light speed and the absorption cross-section of NO_3, respectively. The CRDS technology uses NO to dynamically titrate NO_3 to obtain the ring-down time of the reference spectrum and filtering particles with a filter to reduce the impact of aerosol extinction. Due to the high activity of NO_3, the injection, filtration, and cavity wall reaction will reduce the sampling efficiency. There is a nonlinear relationship between the use time of the membrane and the sampling efficiency. The main uncertainties of measurement include absorption cross-section, effective cavity length, membrane exchange frequency [39, 40].

CEAS is a new type of absorption spectroscopy technology [33]. Although a resonant cavity structure similar to CRDS, there are many differences between the two technologies: CEAS uses a broadband continuous light source such as an arc xenon lamp or LED; It is closer to a direct absorption spectrum measurement technology; CEAS usually uses zero air or high-purity nitrogen spectrum as the background spectrum; collects the light intensity signal of the entire band spectrum with strong NO_3 absorption (such as 640–680 nm). The concentration of each trace gas can be accurately retrieved from the absorption spectra of multiple trace gases so that multiple trace gases can be measured simultaneously (1.13):

$$n_i\sigma_i + \varepsilon_R + \varepsilon_M = \left(\frac{I_0}{I} - 1\right)\left(\frac{1-R}{d_{eff}}\right) \tag{1.13}$$

Here n_i represents the number concentration of the medium gas (such as NO_3, NO_2, H_2O), σ_i represents the gas absorption cross-section, $\varepsilon_{R,}$ and ε_M represent the absorption coefficients generated by Rayleigh scattering and Mie scattering. I_0 and I represent the reference spectral and the sampling spectral intensity. The d_{eff} represents the effective cavity length between the cavity mirrors, and R denotes the high mirror reflectivity [104]. CEAS has two types: open cavity and close cavity. Open cavity system is mainly used in smoke chamber study [103]. Close cavity CEAS is widely used in the field study. The use of a closed cavity and a sampling tube can avoid aerosol interference. However, this technology suffers from the same problem as CRDS; the uncertainty of the sampling efficiency will bring errors to the measurement. Also, the water vapor absorption at 662 nm is strong, and if it is not well subtracted in the spectral fitting, it will make errors easily. Therefore, systematic laboratory characterization and the establishment of standard systematic data analysis methods are critical for the cavity technology.

The principle of the LIF is that the trace gas to be measured by exciting it to produce a resonance transition, from the ground state electron to the excited state, the excited state gases will spontaneously emit fluorescence. The signal intensity of the fluorescence is linear dependent on the concentration of the target gas under the same experimental conditions [118]. The quantification of the signal can be quantified by the formula (1.14).

$$I_f = kqI_0Ln \tag{1.14}$$

where k is the fluorescence instrument function, q is the fluorescence quantum yield, I_0 is the excitation light signal intensity, σ is the absorption cross-section, L is the cross-intercept of the laser beam and the molecular gas beam, and n is the gas concentration to be measured. Based on the strong absorption of NO_3 in the 623 and 662 nm, the narrowband laser in one of the bands is usually used to induce the NO_3 in the sample cell, and the interference of the light source and other stray light to the measurement unit is removed by time-gating technology. In the LIF sampling process, the gas expansion sampling technology is used to make the sample enter the fluorescence detection cell at high speed to reduce the gas residence time and wall loss. LIF technology has low fluorescence background signal, high accuracy, low detection limit, and high selectivity in the measurement of free radicals. However, in terms of NO_3 radical measurement, the fluorescence quantum yield of NO_3 is low, resulting in insufficient sensitivity for measuring NO_3. Besides, the fluorescence signal of high concentration NO_2 in the ambient will cause great interference to the NO_3 signal. The measurement of NO_3 by LIF technology usually requires the use of a dual-wavelength laser method to subtract the interference of the NO_2 fluorescence signal. However, this method will reduce the detection limit of the instrument [68]. In general, LIF is not a particularly promising NO_3 and N_2O_5 measurement technology.

Chemical ionization mass spectrometry (CIMS) has fast response and high sensitivity and can realize in situ online measurement. The measurement principle of CIMS technology is that the molecular ionization reaction between the reagent ion and the sample gas ionizes the sample gas molecule, and the substance to be measured is quantified based on the measured mass spectrum. The instrument structure mainly included three parts: ion source, collision ionization chamber, and mass spectrometry detection system. For the measurement of NO_3 and N_2O_5, some research groups use 210Po as the ion source. CH_3I dissociates with the carrier gas N_2 into the ion source to generate reagent ion I^-, and the reagent ion I^- reacts with NO_3 (N_2O_5) to generate NO_3^- (R1.15, R1.16), and its concentration calculation formula is as (Eq 1.17)

$$I^- + NO_3 \rightarrow NO_3^- + I \tag{1.15}$$

$$I^- + N_2O_5 \rightarrow NO_3^- + INO_2 \tag{1.16}$$

$$n(N_2O_5) = \frac{n(NO_3^-)}{ktn(I^-)} \tag{1.17}$$

Here $n(N_2O_5)$ is the measured total concentration of NO_3 and N_2O_5, $n(NO_3^-)$ and $n(I^-)$ represent the concentration of NO_3^- and reagent ion I^-, k and t is the reaction rate and reaction time, respectively. Ionization molecular reaction region (IMR) is instead of heated inlets and flow tubes to obtain intermediate, $I(N_2O_5)^-$, by controlling the pressure of the collision ionization chamber [60]. By controlling the reaction time, $I(N_2O_5)^-$ can be achieved before dissociation, this method can effectively separate the signal of N_2O_5 and NO_3. CIMS can realize the direct measurement of N_2O_5 and $ClNO_2$ simultaneously. The disadvantage of CIMS is that it is easily interfered with by PAN, $ClONO_2$, $BrONO_2$, and other species [20]. Under high NO_2 condition, PAN can generate a large amount of 62 amu signals during the measurement and has serious interference to the measurement [114]. At present, the use of CIMS to carry out N_2O_5 field measurement is common, but the field measurement of NO_3 by CIMS has not been realized yet.

ESR measures free radicals by quantifying the unpaired electrons. In theory, all atmospheric free radicals can be measured by this method. MIESR is a combination of matrix isolation and electron spin resonance technology. The matrix isolation technology uses H_2O or D_2O as the matrix to capture and store free radicals in the gas under ultra-low temperature (77 K), and then uses ESR to quantify the signal. Electron spin resonance refers to the splitting of the Zeeman level, which is due to the interaction of the electron spin magnetic moment with the external magnetic field when the paramagnetic substance in the static magnetic field (H). The split distance is $\Delta E = g\beta H$, where g is the spectral splitting factor, and β is the Bohr magneton. An electromagnetic wave with a frequency ν is added in the vertical direction of the static magnetic field. If the electromagnetic wave energy and the Zeeman level spacing are

adapted (Eq. 1.18, where h is the Planck constant). Then the paramagnetic substance will absorb electromagnetic waves, and transition happens, resulting in absorption resonance.

$$vh = b\beta H \tag{1.18}$$

Specifically, the EPR absorption line generated by the stimulated transition of NO_3 radical is fitted to the EPR reference line of known concentration of NO_3, thereby the NO_3 concentration is determined [71]. MIESR is an offline technique with long sampling time and sample analysis time, which limited its application in field measurement.

An inter-comparison measurement by DOAS and MIESR to measure NO_3 was conducted in 1983 in Deuselbach, Germany, and in Berlin, Germany, in 1998. Although the data correlation between the two techniques is as high as 0.99, the measured value of DOAS is slightly lower than the measured value of MIESR, mainly due to the high NO_3 absorption cross-section used by DOAS. Besides, if encountered fog and haze during the measurement process, the DOAS may cause deviations [44]. In 2007, a large NO_3 measurement comparison experiment (NO_3Comp) was carried out in the SAPHIR chamber at Forschungszentrum Jülich, Germany. A total of 7 units of 3 types of measurement technology (DOAS, CEAS, CRDS) participated in the NO_3 radical measurement comparison [26]. A total of 5 units of two types of measurement technologies (CRDS, LIF) participated in the N_2O_5 measurement comparison [40]. The results show that the three NO_3 measurement techniques based on absorption spectroscopy had good consistency in NO_3 measurement ($R^2 = 0.981$). The cavity technique exhibits higher sensitivity and lower limit of detection under the same time resolution. However, under ambient atmospheric conditions, the accumulation of aerosols on the filter membrane will affect the accuracy of the cavity technology. In terms of N_2O_5 measurement, cavity technology also has excellent detection capabilities. The detection limit of LIF for measuring N_2O_5 is not so good, and only meet the measurement requirement of N_2O_5 rather than NO_3. In the RONOCO research project in 2010, the comparison experiment of CEAS and CIMS during aircraft measurement showed that the results of the two technical measurements have a good consistency ($R^2 = 0.89$) [63].

Table 1.1 summarizes the related parameters used in the field-applied instruments of NO_3 and N_2O_5. Overall, absorption spectroscopy is currently the mainstream method for measuring NO_3 and N_2O_5. As a mature measurement technology, DOAS does not need to do the calibration, but the spatial resolution is low, which is more suitable as a reference method. CRDS and CEAS have many advantages in measuring NO_3 and N_2O_5. These two technologies are simple in structure, low in cost, and have good spatial-temporal resolution and detection limits. CRDS avoids errors caused by laser energy fluctuations by measuring the decay time of light intensity, while CEAS has the advantage of measuring multiple gases at the same time, and the light source can use the cheap LEDs. The measurement sensitivity of LIF limits its ability to measure NO_3 in the field application. Since CIMS can measure N_2O_5 and $ClNO_2$

Table 1.1 Ambient measurement techniques for NO_3 and N_2O_5

Methods	Species	Principles	Resolution (s)	LOD (pptv)	Accuracy (%)	References
DOAS	NO_3	Absorption spectrum	600	3	10	[91]
MIESR	NO_3	Unpaired electrons	1800	3	5	[71]
CRDS	NO_3	Ring-down time	1	0.5	25	[27]
	N_2O_5	Ring-down time	1	1	20–40	[27]
CEAS	NO_3	Absorption spectrum	1	1.1	11	[59]
	N_2O_5	Absorption spectrum	1	2.4	14	[59]
LIF	N_2O_5	Fluorescence	600	11	8	[68]
CIMS	N_2O_5	Mass spectrum	1	11	20	[60]

Reproduced from with permission [111]. Copyright editorial department of Progress in Chemistry

simultaneously, it has its unique advantages in the study of chloride chemistry, but it is not yet possible to measure NO_3 in the field observation.

1.3 Concentration and Variation of NO_3 and N_2O_5

With the development of NO_3 and N_2O_5 measuring instruments, the field measurement of NO_3 and N_2O_5 has been gradually conducted, and it is increasingly used in large-scale observations of tropospheric chemistry research. The measurement environment includes cities, forests, polar regions, and marine regions. The measurement platform gradually evolved from simple ground observation to mobile measurement (tower base, ship base) and airborne measurement. The measurement greatly promoted the development of the chemical mechanism of free radicals at night. While the field measurement included both NO_3 and N_2O_5 is still very limited in the current stage.

Figure 1.3 summarizes the night concentration levels of NO_3 and N_2O_5 in different regions. The NO_3 and N_2O_5 concentration levels measured at high altitude (by airborne measurement, towers, etc.) are generally higher than those observed by near-ground observations. On the one hand, the vertical stratification in the boundary layer at night leads to a shallow mixing depth on the vertical scale. On the other hand, the main reason for the low concentration near-surface is the influence of NO and VOCs emitted from the near-surface [15, 109].

The formation of NO_3 and N_2O_5 is mainly affected by the NO_x concentration level of anthropogenic emissions. High NO_x occurred in the urban area and the downwind

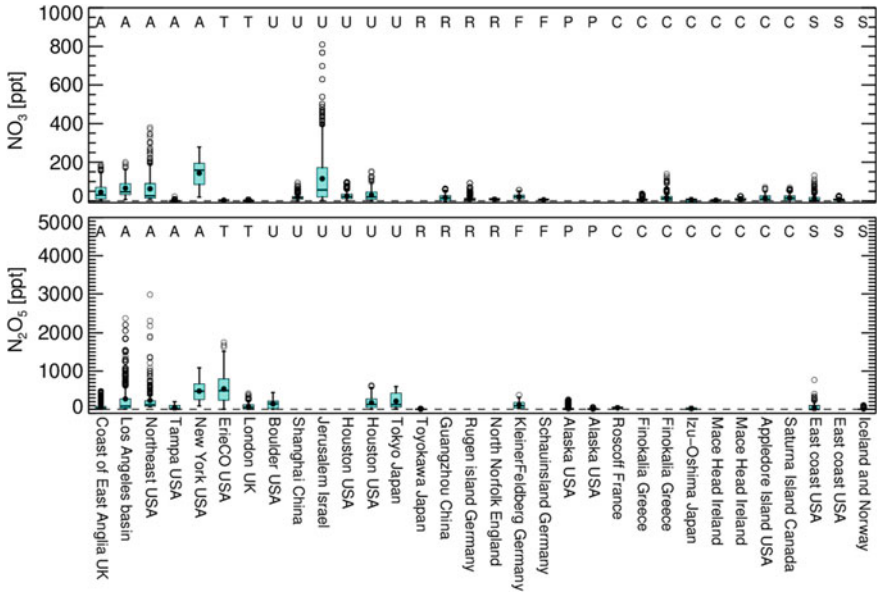

Fig. 1.3 NO_3 and N_2O_5 concentrations observed in representative geophysical regions. Type of the geophysical locations where the observation took place: A: Airborne, T: Tower, U: Urban, R: Rural, F: Forest, P: Polar, C: Coastline, S: Ship-based. Reproduced from with permission [111]. Copyright editorial department of Progress in Chemistry

direction of the urban area. In clean areas with little anthropogenic impact, such as forests, oceans, and polar regions, the concentration of NO_3 is relatively low. The average concentration of NO_3 near the ground during summer nights usually ranges from 4 to 30 pptv, and the peak during summertime in urban areas can reach 100–200 pptv [20]. The concentration of NO_3 in the Jerusalem area of Israel has been observed to be as high as 807 pptv, which is the highest value that has been observed. The high altitude of the measurement site, high concentration of precursors, and low humidity are the main reasons for the occurrence of high NO_3 values [5]. The concentration level of N_2O_5 is higher than that of NO_3 in the ambient atmosphere in general. Under the thermal equilibrium conditions, the ratio of N_2O_5 to NO_3 is related to the concentration level of NO_2 and the ambient temperature. Figure 1.4 shows that under typical urban air mass conditions, the concentration level of N_2O_5 is usually about 3–100 times that of NO_3. The average concentration of N_2O_5 at night is usually tens to hundreds of pptv. Some observations report that the nighttime peak value of N_2O_5 can reach the ppbv level. An observation reported that the N_2O_5 concentration level reached 7.7 ppbv on a mountain top site in Hong Kong (1-min time resolution). The elevated level is because the air mass came from a highly aging urban air mass with a high level of precursors, and the removal rates were relatively low [13, 112].

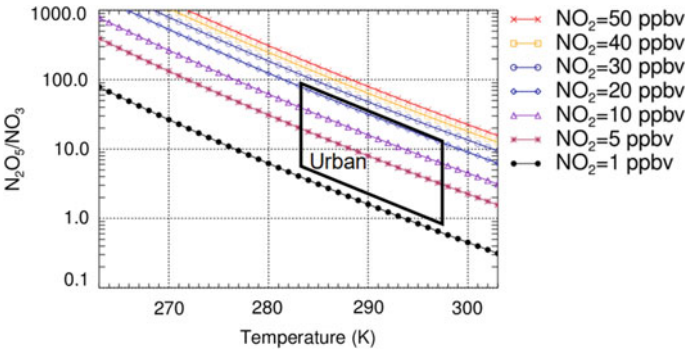

Fig. 1.4 The dependence of the ratio of N_2O_5 to NO_3 on NO_2 and temperature in the thermal equilibrium, the region in black parallelogram represents typical urban conditions

The diurnal variation of NO_3 and N_2O_5 at night is relatively clear. After sunset, NO_3 is rapidly generated and accumulated, the concentration level gradually increases, and reaches a maximum after a few hours. The NO_3 concentration gradually decreases, and after a period of consumption, the NO_3 concentration decreases to a low level or zero before sunrise. The N_2O_5 concentration usually coincides with the NO_3 trend. However, the source and removal of NO_3 and N_2O_5 are closely related to anthropogenic emissions. The atmospheric life of NO_3 and N_2O_5 is short, resulting in a very large change in the absolute concentration of NO_3 and N_2O_5 on different time scales like minute-scale, day scale [14, 23].

NO_3 concentration levels and removal pathways have an obvious seasonal difference. During the long-term observation process on the North Norfolk coast of England, it was found that the main remove pathways of NO_3 in summer are to react with DMS, during the wintertime, the thermodynamic equilibrium favors to N_2O_5 due to the low temperature. Under high aerosol loading conditions, the heterogeneous uptake of N_2O_5 becomes the main removal route [3]. Two years of long-term NO_3 observations on the Cretan islands in the Mediterranean had shown that NO_3 concentration is high in summer and low in winter [105, 106]. Long-term observations of NO_3 free radicals in the suburbs of Berlin indicated that the NO_3 removal pathway has a clear seasonal trend, with NO_3 + VOCs dominating in summer and N_2O_5 heterogeneous reaction in winter [42]. In general, NO_3 and N_2O_5 chemistry have great differences under different geophysical conditions, and more field observation data are needed to describe their atmospheric chemical behavior.

1.4 NO_3 Oxidation and N_2O_5 Uptake

The removal of trace gas at night related to NO_3 chemistry is an advanced subject worthy of attention. Kinetic experiments show that the reaction of NO_3 with olefins, especially BVOCs, has a fast reaction rate. The reaction rate of some monoterpene

species with NO_3 even exceeds its reaction rate with OH radicals. While in the current stage, there is large uncertainty about the influence of NO_3 on the atmospheric lifetime of VOCs. Besides, the reaction rates of many VOCs species with NO_3 are not quantified, which brings challenges to the subsequent analysis of NO_3 budgets.

In the US NEAQS2004 experiment, the aircraft study found that there is a clear anti-correlation between the concentration of NO_3 and isoprene at night. By measuring MVK and MACR, it was found that more than 20% of isoprene is produced by NO_3 Oxidation. The organic aerosol generated by NO_3 oxidation of isoprene accounts for 1% -17% of the total aerosol [89]. In the TexAQS2006, the petrochemical industry denominated the VOCs emission, VOCs oxidized by NO_3 is 3-5 times more than O_3 at night. The majority of VOCs emitted by industrial sources (Brown et al., [16], this conclusion is consistent with the results of the ground study during the same period [92]. As early as in 1998, it was found that the main removal of NO_3 is to react with BVOCs in the Berlioz observations in the forest area of Berlin, Germany. This pathway accounted for 30-50% of the total removal of NO_3, followed by the heterogeneous reaction of N_2O_5. Based on the simultaneous measurement of O_3, NO_3, and OH radicals, it was found that the proportion of NO_3 oxidizing VOC occupies 28%, which contributes up to 31% to the oxidation of olefinic VOCs [43]. However, there are very few comparative studies similar to this study focused on the oxidation capacity of NO_3, OH radicals, and O_3 to VOCs. The reason is that the parameters required for simultaneous measurement are relatively difficult. The oxidation of BVOCs at night will be dominated by NO_3 once the ratio of NO_x to VOCs at sunset is greater than 0.6, which further illustrated the importance of NO_3 for the removal of BVOCs [28].

Previous studies reported a large gap on the yield of SOA generated by the reaction of NO_3 and VOCs, and there are big differences in the measurement of SOA yield of certain VOCs [20]. For example, in the quantitative analysis of the yield of SOA produced by the reaction of NO_3 and β-pinene, the results obtained by the three research groups through experiments are 32–89%, 10–52%, and 46–54%, respectively [37, 46, 51]. Also, some studies have observed a certain correlation between NO_3 and RO_2 at night, and believe that the reaction of NO_3 and VOCs under low NO conditions may have a certain contribution to the recycling of HO_x free radicals at night [21, 45]. On the one hand, the reaction of NO_3 and VOCs can generate RO_2. On the other hand, NO_3 is a sink of RO_2 by acting as a role similar to NO during the daytime. In recent years, high concentrations of nighttime OH have been generally observed in forests and urban areas, suggesting that in high VOCs environments, nighttime chemistry is likely not completely dominated by NO_3 chemistry. However, the night observations for measuring both NO_3 and OH are very scarce, so there are calls for the characterization and analysis of the reaction process of free radicals throughout the night. In the observations of Pearl River Delta and Beijing, China, preliminary analysis implies that the contribution of OH to nighttime oxidation capacity will be significantly greater than that of NO_3 [67].

Until now, the research on the oxidation process of VOCs by NO_3 in the field study is still lacking. The main VOC species dominating NO_3 loss in different regions may be quite different, which leads to different products and subsequent chemical

conversion processes. In a typical high NO_x area, the oxidation capacity of NO_3 may be much higher than that of O_3 at night. However, the cycle mechanism of OH radicals at night and the role of NO_3 chemistry in the nocturnal OH cycle are still unclear. Besides, based on the simultaneous measurement of OH and NO_3, comprehensive research on the oxidation capacity at night is still lacking. The reaction mechanism of NO_3 and VOCs and the subsequent atmospheric chemical process need to be further investigated.

In order to determine the key variables affecting the uptake reactions of N_2O_5, a large number of laboratory studies conducted to investigate N_2O_5 uptake. The model aerosols included droplets, sulfate, nitrate, chloride, organic matter, black carbon, and mineral particles. $\gamma(N_2O_5)$ on the surface of pure water droplets decreases with increasing temperature. The value is 0.040 ± 0.005 at 282 K and 0.061 ± 0.004 at 271 K [102]. The heterogeneous uptake of N_2O_5 on the sulfate aerosol is greatly affected by RH. At RH < 40%, that is, before the sulfate deliquesces point, $\gamma(N_2O_5)$ increases with the increase of RH. However, at RH > 40%, with the deliquescence of sulfate, the uptake value tends to be stable, and will not change significantly with RH changes [30, 36, 47, 50]. Since different aerosols types have different deliquesce points, and the amplitude of the uptake coefficient before the deliquesce point varies with RH due to different hygroscopicity [1, 10]. For example, when the RH is less than 40%, $\gamma(N_2O_5)$ on the NH_4HSO_4 particles is less than 0.01; when RH over 40%, the value is up to 0.02 [50]. The uptake on the NaCl particles is similar to the uptake on the sulfates and is greatly affected by RH [54].

Under ambient temperature, $\gamma(N_2O_5)$ on the surface of $NaNO_3$ aerosol is 0.0018-0.0032 (RH = 50%–60%), which is an order of magnitude lower than that of sulfate at the same RH [69, 110]. Only when RH = 90%, the uptake coefficient can reach 0.02 due to the decrease of NO_3^- inhibition effect with the increase of ALWC. This mechanism was later repeatedly verified and applied to the parameterization model, called the "nitrate suppression effect" [11, 48]. Some studies have also shown that the presence of Cl^- in particulates can promote the uptake of N_2O_5 [8–10], making the $\gamma(N_2O_5)$ on the NaCl aerosol similar or slightly higher than the value on the sulfate aerosol.

The mineral dust particle is an important part of atmospheric particulate matter and a very important research matrix in the study of heterogeneous uptake. Previous studies have found that the surface area of mineral particles is the main source of uncertainty in the quantification of $\gamma(N_2O_5)$. Different surface area calculation methods can lead to the differences in the uptake coefficient up to several orders of magnitude [58, 88, 107, 108]. The $\gamma(N_2O_5)$ on the surface of Sahara dust, illite, Arizona particles, and TiO_2 particles are quite different. The $\gamma(N_2O_5)$ on illite surface is large (0.04–0.09), and on TiO_2 surface is the smallest with the value of 0.001 [93–97].

On the solid organic particles, such as malonic acid and azelaic acid, levoglucosan, abietic acid, etc., the $\gamma(N_2O_5)$ is less than 0.001 [47, 99]. In addition, $\gamma(N_2O_5)$ on the surface of methane, propane and decane carbon black is about 0.005 [57, 66]. However, $\gamma(N_2O_5)$ on the solid PAH particles is $<10^{-5}$ [49]. The presence of organic matter has an inhibitory effect on N_2O_5 uptake. However, the inhibitory effect is

largely related to the type and content of organic matter, and the mixed state of the aerosol. Specific to the influence of the reaction mechanism, on the one hand, the content of organic matter in the aerosol will affect the hygroscopicity of the particulate matter, and the heterogeneous reaction will be influenced by affecting the ALWC.

The organic substance covered by the aerosol surface may affect the mass accommodation, the liquid phase diffusion, and bulk reaction processes. Taking the externally mixed SOA formed by α-pinene ozonation as an example, it can be found that the $\gamma(N_2O_5)$ on the SOA is very low. The uptake coefficient is 3.4×10^{-3} when the volume ratio of SOA in the sulfate aerosol is 5%, with the concentration of organic matter increases, the inhibitory effect can be up to 40 times [36].

Recent studies have shown that organic matter O: C is closely related to the inhibitory effect. When O:C < 0.5, the organic matter has a significant inhibitory effect on the uptake coefficient, while when O:C > 0.8, the inhibitory effect is not significant, indicating that the oxidation state of organic matter is an important factor of N_2O_5 uptake [41]. Humic acid is similar to surfactants, which can weaken the mass accommodation of gas on the particle surface, and the higher content of humic acid in the aerosol, the lower the mass accommodation will be taking [6]. The organic matter in the well mixing SOA had no significant inhibitory effect on the $\gamma(N_2O_5)$, indicating that the mixing state of particulate matter was a key factor affecting the uptake coefficient [47, 99]. In general, the uptake mechanism of N_2O_5 affected by organic matter in aerosols is still unclear.

Based on the results of laboratory studies, many studies attempted to establish a functional relationship (parameterization) between the uptake coefficient and meteorological, aerosol composition, and mixing state. However, the mechanism of N_2O_5 uptake was poorly understood at the beginning of the study. It could only be based on the measurement results of the heterogeneous uptake coefficient of N_2O_5 on the surface of sulfate and water droplets at that time. [25, 56]. Evans et al. established a relationship with the uptake coefficient (named as EJ05) based on aerosol composition, temperature, and RH. They used an average value of 0.02 as the heterogeneous uptake coefficient for N_2O_5, making the results of the global model more in line with existing observations [31]. With the identification of the key physical and chemical parameters that affect the uptake coefficient and the deepening of the understanding of the mechanism, Riemer et al., used the weight of sulfate and nitrate in the aerosol to parameterize of the uptake coefficient (here named as R03) [85], here they limited the range of $\gamma(N_2O_5)$ (0.002–0.02). Davis et al. used seven laboratory measurement results and used statistical methods to incorporate the factors including RH, temperature, aerosol composition, and aerosol phase state into the parameterized formula (named as DV08). It is assumed that the inorganic compounds in the ambient aerosol are internal mixing, and the uptake coefficient is linearly summable [24].

Griffiths et al. parameterized the uptake coefficient based on the hydrolysis mechanism proposed by [110] and the method named as G09, by assuming that the uptake coefficient is mainly limited by the aerosol liquid phase reaction rather than surface diffusion, and based on the ion hydrolysis mechanism [47]. Based on the modified

hydrolysis mechanism [99], Bertram et al. assumed in their model that the uptake coefficient (here named as BT09) is not limited by the mass accommodation and the liquid phase reaction are not affected by the diffusion depth of N_2O_5 in the aerosol. The influence of NO_3^-, Cl^-, SO_4^{2-} and ALWC on the uptake coefficient is incorporated into the parameterization scheme [10]. Anttila et al. considered the influence of organic matter in the aerosol on the uptake coefficient in the model (here named as A06). They assumed that the organic matter was attached to the aerosol surface to form an organic thin film. The extended resistor model was used to illustrate the organic effect on N_2O_5 uptake [4]. After that, Riemer combined the early research results (R03) and A06, to obtain an expanded parameterization named as R09. R09 combines the mechanism of inorganic aerosol and organic aerosol on N_2O_5 uptake. For the uptake coefficient of the inorganic aerosol part, the formula given by R03 is used, and the uptake of the surface of the organic matter uses the formula given by A06 [84].

With the advancement of laboratory studies and parameterization of uptake coefficients, the need to verify laboratory and parameterized results through field measurements is becoming more and more urgent. Based on the field measurements of NO_3 and N_2O_5, the N_2O_5 uptake coefficient can be calculated by fitting the atmospheric lifetimes of N_2O_5 and NO_3 under pseudo-steady-state conditions [17]. Previous studies have used pseudo-steady-state methods to calculate N_2O_5 uptake coefficients in three different regions of the northeastern United States, indicating that the N_2O_5 uptake coefficient has a strong relationship with aerosol components (especially sulfate). Here organics has an inhibitory effect on the uptake coefficient. In the TexAQS2006 campaign, the field derived results are inconsistent with the results of various parameterized models, and all models have an overestimation [13]. A subsequent study in northwestern Europe has reached similar conclusions. The correlation between field derived $\gamma(N_2O_5)$, and sulfate, nitrate, and chloride are not significant. The prediction results based on the R03, EJ05, R09, and BT09 parameter methods are all overestimated, while the prediction results using the organic coating model are generally low [72]. On one hand, it may be because the parameterization method is indeed not accurate enough; on the other hand, the pseudo-steady state calculation method itself has some uncertainties.

Other methods of quantifying the N_2O_5 uptake coefficient in the field studies include the iterative box model method, the flow tube measurement method, and the product growth fitting method. The iterative box model method constrains the vertically measured N_2O_5, O_3, and NO_2, sets the initial time of the model and iterates the uptake coefficient until the predicted N_2O_5 is consistent with the measured value [109]. The flow tube method quantifies its uptake coefficient by measuring the decay of N_2O_5 by mixing the stable N_2O_5 standard and the ambient aerosol in the flow tube [12]. By simultaneously measuring N_2O_5, $ClNO_2$, and nitrate, the product growth regression method can be used to calculate the N_2O_5 uptake coefficient and $ClNO_2$ yield [79].

A large number of laboratories have shown that ambient temperature, RH, NO_3^-, Cl^-, SO_4^{2-}, water content, organic matter, and particulate matter mixed state of particulate matter are all factors that affect the N_2O_5 uptake. The inhibitory effect

of nitrate content on the uptake coefficient was gradually confirmed in field studies [109]; the inhibitory effect of high aerosol organic content on the uptake coefficient in a low humidity environment also been observed [11]. However, in the applications, most of the parameterized methods can only reflect the changing trend of the uptake coefficient. However, it is difficult to accurately predict the real values [83], indicating that in the atmosphere, these influences are complicated. The influence of organic matter on the uptake is the most important uncertainty factor in the parameterization. This discrepancy reflects the lack of understanding of the mechanism of organic matter inhibiting the N_2O_5 uptake, such as the type of organic compounds.

The uptake mechanism of N_2O_5 is mainly discovered by laboratory studies. However, the N_2O_5 uptake coefficient measured in the laboratory is quite different from the actual atmosphere, and the representativeness of the model aerosol is limited. The dataset of the N_2O_5 uptake coefficient field quantification is very limited for model study. There is a large uncertainty based on the mechanism proposed by the laboratory, and the existing parameterization schemes are difficult to accurately predict the N_2O_5 uptake coefficient, resulting in large uncertainty in the simulation of key processes in regional and global models.

In recent years, several studies are conducted in China on the discussion of NO_3 and N_2O_5 mechanism. For example, the group of Tao Wang from Hong Kong Polytechnic University used CIMS to carry out a large number of simultaneous measurements of N_2O_5 and $ClNO_2$ in the field measurement [114], including the Hong Kong, Wangdu, Jinan and Taishan in North China. The continuous observation of higher concentrations of $ClNO_2$ and lower concentrations of N_2O_5 in North China shows that there is an active N_2O_5 heterogeneous reaction process in North China, and combined with the regional model shows that this chemical process may have a certain effect on the formation of O_3 and RO_x [65, 98]; [113, 115, 119]. Based on the analysis of particulate nitrate in the Beijing area, there is a significant nitrate explosive growth process at night, and the N_2O_5 heterogeneous uptake may be the main source [76, 77]. Regional model studies indicated that the heterogeneous reaction of N_2O_5 might have a certain contribution to the nitrate formation in China [93]. Overall, there is still a gap between the research of NO_3 and N_2O_5 chemistry in China and abroad.

1.5 Main Objectives

This thesis intends to set up an instrument to measure NO_3 and N_2O_5. Based on a series of field observation experiments, the data analysis was carried. The main objectives include:

(1) Observing NO_3 and N_2O_5 concentration levels and changes.
(2) Characterizing the total reaction activity of NO_3 and revealing the key factors that are controlling N_2O_5 heterogeneous uptake.

(3) Understanding the impacts of NO_3 and N_2O_5 chemistry on atmospheric oxidation capacity and nitrate formation.

1.6 Thesis Structure

Chapter 1 Introduction. An introduction about the research background, objectives, and the thesis structure.

Chapter 2 Research method. The setup of cavity-enhanced absorption spectroscopy technology, the data quality control methods, the instrument calibration methods, and data processing methods will be introduced.

Chapter 3 Field observation. The introduction of the field campaign in Beijing, the measured NO_3 and N_2O_5 concentration level, diurnal variation, seasonal change, and spatial scale change will be described.

Chapter 4 Quantitative characterization of NO_3 reactivity and N_2O_5 heterogeneous uptake coefficient in Beijing.

Chapter 5 In this section, the environmental effects of NO_3 and N_2O_5 at night will be evaluated.

Chapter 6 Conclusions. The main conclusions of this thesis will be summarized.

References

1. Abbatt JPD, Lee AKY, Thornton JA (2012) Quantifying trace gas uptake to tropospheric aerosol: recent advances and remaining challenges. Chem Soc Rev 41(19):6555–6581
2. Alexander B, Hastings MG, Allman DJ, Dachs J, Thornton JA, Kunasek SA (2009) Quantifying atmospheric nitrate formation pathways based on a global model of the oxygen isotopic composition (delta O-17) of atmospheric nitrate. Atmos Chem Phys 9(14):5043–5056
3. Allan BJ, Carslaw N, Coe H, Burgess RA, Plane JMC (1999) Observations of the nitrate radical in the marine boundary layer. J Atmos Chem 33(2):129–154
4. Anttila T, Kiendler-Scharr A, Tillmann R, Mentel TF (2006) On the reactive uptake of gaseous compounds by organic-coated aqueous aerosols: theoretical analysis and application to the heterogeneous hydrolysis of N2O5. J Phys Chem A 110(35):10435–10443
5. Asaf D, Pedersen D, Matveev V, Peleg M, Kern C, Zingler J et al (2009) Long-Term Measurements of NO_3 Radical at a Semiarid Urban Site: 1. Extreme concentration events and their oxidation capacity. Environ Sci Technol 43(24):9117–9123
6. Badger CL, Griffiths PT, George I, Abbatt JPD, Cox RA (2006) Reactive uptake of N_2O_5 by aerosol particles containing mixtures of humic acid and ammonium sulfate. J Phys Chem A 110(21):6986–6994
7. Bannan TJ, Booth AM, Bacak A, Muller JBA, Leather KE, Le Breton M et al (2015) The first UK measurements of nitryl chloride using a chemical ionization mass spectrometer in central London in the summer of 2012, and an investigation of the role of Cl atom oxidation. J Geophys Res Atmos 120(11):5638–5657

8. Behnke W, George C, Scheer V, Zetzsch C (1997) Production and decay of ClNO2, from the reaction of gaseous N2O5 with NaCl solution: bulk and aerosol experiments. J Geophys Res Atmos 102(D3):3795–3804
9. Behnke W, Kruger HU, Scheer V, Zetzsch C (1991) Formation of atomic Cl from sea spray via photolysis of nitryl chloride—determination of the sticking coefficient of N_2O_5 on NaCl aerosol. J Aerosol Sci 22:S609–S612
10. Bertram TH, Thornton JA (2009) Toward a general parameterization of N2O5 reactivity on aqueous particles: the competing effects of particle liquid water, nitrate and chloride. Atmos Chem Phys 9(21):8351–8363
11. Bertram TH, Thornton JA, Riedel TP (2009) An experimental technique for the direct measurement of N_2O_5 reactivity on ambient particles. Atmos Measur Tech 2(1):231–242
12. Bertram TH, Thornton JA, Riedel TP, Middlebrook AM, Bahreini R, Bates TS et al (2009) Direct observations of N_2O_5 reactivity on ambient aerosol particles. Geophys Res Lett 36
13. Brown SS, Dube WP, Fuchs H, Ryerson TB, Wollny AG, Brock CA et al (2009) Reactive uptake coefficients for N_2O_5 determined from aircraft measurements during the Second Texas air quality study: comparison to current model parameterizations. J Geophys Res Atmos 114
14. Brown SS, Dube WP, Osthoff HD, Stutz J, Ryerson TB, Wollny AG et al (2007) Vertical profiles in NO_3 and N_2O_5 measured from an aircraft: Results from the NOAA P-3 and surface platforms during the New England Air Quality Study 2004. J Geophys Res Atmos 112(D22)
15. Brown SS, Dube WP, Osthoff HD, Wolfe DE, Angevine WM, Ravishankara AR (2007) High resolution vertical distributions of NO_3 and N_2O_5 through the nocturnal boundary layer. Atmos Chem Phys 7:139–149
16. Brown SS, Dube WP, Peischl J, Ryerson TB, Atlas E, Warneke C et al (2011) Budgets for nocturnal VOC oxidation by nitrate radicals aloft during the 2006 Texas air quality study. J Geophys Res Atmos 116
17. Brown SS, Ryerson TB, Wollny AG, Brock CA, Peltier R, Sullivan AP et al (2006) Variability in nocturnal nitrogen oxide processing and its role in regional air quality. Science 311(5757):67–70
18. Brown SS, Stark H, Ciciora SJ, Ravishankara AR (2001) In-situ measurement of atmospheric NO_3 and N_2O_5 via cavity ring-down spectroscopy. Geophys Res Lett 28(17):3227–3230
19. Brown SS, Stark H, Ryerson TB, Williams EJ, Nicks DK, Trainer M et al (2003) Nitrogen oxides in the nocturnal boundary layer: simultaneous in situ measurements of NO_3, N_2O_5, NO_2, NO, and O-3. J Geophys Res Atmos 108(D9):ACH18
20. Brown SS, Stutz J (2012) Nighttime radical observations and chemistry. Chem Soc Rev 41(19):6405–6447
21. Carslaw N, Carpenter LJ, Plane JMC, Allan BJ, Burgess RA, Clemitshaw KC et al (1997) Simultaneous observations of nitrate and peroxy radicals in the marine boundary layer. J Geophys Res Atmos 102(D15):18917–18933
22. Chang WL, Bhave PV, Brown SS, Riemer N, Stutz J, Dabdub D (2011) Heterogeneous atmospheric chemistry, ambient measurements, and model calculations of N_2O_5: a review. Aerosol Sci Technol 45(6):665–695
23. Crowley JN, Schuster G, Pouvesle N, Parchatka U, Fischer H, Bonn B et al (2010) Nocturnal nitrogen oxides at a rural mountain-site in south-western Germany. Atmos Chem Phys 10(6):2795–2812
24. Davis JM, Bhave PV, Foley KM (2008) Parameterization of N_2O_5 reaction probabilities on the surface of particles containing ammonium, sulfate, and nitrate. Atmos Chem Phys 8(17):5295–5311
25. Dentener FJ, Crutzen PJ (1993) Reaction of N_2O_5 on tropospheric aerosols—impact on the global distributions of NO_x, O_3, and OH. J Geophys Res Atmos 98(D4):7149–7163
26. Dorn HP, Apodaca RL, Ball SM, Brauers T, Brown SS, Crowley JN et al (2013) Intercomparison of NO_3 radical detection instruments in the atmosphere simulation chamber SAPHIR. Atmos Measur Tech 6(5):1111–1140
27. Dube WP, Brown SS, Osthoff HD, Nunley MR, Ciciora SJ, Paris MW et al (2006) Aircraft instrument for simultaneous, in situ measurement of NO_3 and N_2O_5 via pulsed cavity ring-down spectroscopy. Rev Sci Instrum 77(3)

28. Edwards PM, Aikin KC, Dube WP, Fry JL, Gilman JB, de Gouw JA et al (2017) Transition from high- to low-NOx control of night-time oxidation in the southeastern US. Nat Geosci 10(7):490+-
29. Ehhalt DH (1999) Photooxidation of trace gases in the troposphere. Phys Chem Chem Phys 1(24):5401–5408
30. Escoreia EN, Sjostedt SJ, Abbatt JPD (2010) Kinetics of N_2O_5 hydrolysis on secondary organic aerosol and mixed ammonium bisulfate-secondary organic aerosol particles. J Phys Chem A 114(50):13113–13121
31. Evans MJ, Jacob DJ (2005) Impact of new laboratory studies of N_2O_5 hydrolysis on global model budgets of tropospheric nitrogen oxides, ozone, and OH. Geophys Res Lett 32(9)
32. Fenske JD, Hasson AS, Ho AW, Paulson SE (2000) Measurement of absolute unimolecular and bimolecular rate constants for CH_3CHOO generated by the trans-2-butene reaction with ozone in the gas phase. J Phys Chem A 104(44):9921–9932
33. Fiedler SE, Hese A, Ruth AA (2003) Incoherent broad-band cavity-enhanced absorption spectroscopy. Chem Phys Lett 371(3–4):284–294
34. Finlayson-Pitts BJ, James N (2000) Chemistry of the upper and lower atmosphere: theory, experiments and applications. Academic Press, Calif
35. Finlaysonpitts BJ, Ezell MJ, Pitts JN (1989) Formation of chemically active chlorine compounds by reactions of atmospheric NaCl Particles with Gaseous N_2O_5 and $ClONO_2$. Nature 337(6204):241–244
36. Folkers M, Mentel TF, Wahner A (2003) Influence of an organic coating on the reactivity of aqueous aerosols probed by the heterogeneous hydrolysis of N_2O_5. Geophys Res Lett 30(12):1644
37. Fry JL, Kiendler-Scharr A, Rollins AW, Wooldridge PJ, Brown SS, Fuchs H et al (2009) Organic nitrate and secondary organic aerosol yield from NO_3 oxidation of beta-pinene evaluated using a gas-phase kinetics/aerosol partitioning model. Atmos Chem Phys 9(4):1431–1449
38. Fry JL, Sackinger K (2012) Model investigation of NO_3 secondary organic aerosol (SOA) source and heterogeneous organic aerosol (OA) sink in the western United States. Atmos Chem Phys 12(18):8797–8811
39. Fuchs H, Dube WP, Cicioira SJ, Brown SS (2008) Determination of inlet transmission and conversion efficiencies for in situ measurements of the nocturnal nitrogen oxides, NO_3, N_2O_5 and NO_2, via pulsed cavity ring-down spectroscopy. Anal Chem 80(15):6010–6017
40. Fuchs H, Simpson WR, Apodaca RL, Brauers T, Cohen RC, Crowley JN et al (2012) Comparison of N_2O_5 mixing ratios during NO_3Comp 2007 in SAPHIR. Atmos Measur Tech 5(11):2763–2777
41. Gaston CJ, Thornton JA, Ng NL (2014) Reactive uptake of N_2O_5 to internally mixed inorganic and organic particles: the role of organic carbon oxidation state and inferred organic phase separations. Atmos Chem Phys 14(11):5693–5707
42. Geyer A, Ackermann R, Dubois R, Lohrmann B, Muller T, Platt U (2001) Long-term observation of nitrate radicals in the continental boundary layer near Berlin. Atmos Environ 35(21):3619–3631
43. Geyer A, Alicke B, Konrad S, Schmitz T, Stutz J, Platt U (2001) Chemistry and oxidation capacity of the nitrate radical in the continental boundary layer near Berlin. J Geophys Res Atmos 106(D8):8013–8025
44. Geyer A, Alicke B, Mihelcic D, Stutz J, Platt U (1999) Comparison of tropospheric NO_3 radical measurements by differential optical absorption spectroscopy and matrix isolation electron spin resonance. J Geophys Res Atmos 104(D21):26097–26105
45. Geyer A, Bachmann K, Hofzumahaus A, Holland F, Konrad S, Klupfel T et al (2003) Nighttime formation of peroxy and hydroxyl radicals during the BERLIOZ campaign: observations and modeling studies. J Geophys Res Atmos 108(D4)
46. Griffin RJ, Cocker DR, Seinfeld JH, Dabdub D (1999) Estimate of global atmospheric organic aerosol from oxidation of biogenic hydrocarbons. Geophys Res Lett 26(17):2721–2724

47. Griffiths PT, Badger CL, Cox RA, Folkers M, Henk HH, Mentel TF (2009) Reactive uptake of N_2O_5 by aerosols containing dicarboxylic acids. effect of particle phase, composition, and nitrate content. J Phys Chem A 113(17):5082–5090
48. Griffiths PT, Cox RA (2009) Temperature dependence of heterogeneous uptake of N_2O_5 by ammonium sulfate aerosol. Atmos Sci Lett 10(3):159–163
49. Gross S, Bertram AK (2008) Reactive uptake of NO_3, N_2O_5, NO_2, HNO_3, and O-3 on three types of polycyclic aromatic hydrocarbon surfaces. J Phys Chem A 112(14):3104–3113
50. Hallquist M, Stewart DJ, Stephenson SK, Cox RA (2003) Hydrolysis of N_2O_5 on sub-micron sulfate aerosols. Phys Chem Chem Phys 5(16):3453–3463
51. Hallquist M, Wangberg I, Ljungstrom E, Barnes I, Becker KH (1999) Aerosol and product yields from NO_3 radical-initiated oxidation of selected monoterpenes. Environ Sci Technol 33(4):553–559
52. Heintz F, Platt U, Flentje H, Dubois R (1996) Long-term observation of nitrate radicals at the tor station, Kap Arkona (Rugen). J Geophys Res Atmos 101(D17):22891–22910
53. Herriott D, Harry S (1965) Folded optical delay lines. Appl Opt 4(8):883–889
54. Hoffman RC, Gebel ME, Fox BS, Finlayson-Pitts, BJ et al (2003) Knudsen cell studies of the reactions of N2O5 and ClONO2 with NaCl: development and application of a model for estimating available surface areas and corrected uptake coefficients. Phys Chem Chem Phys 5:1780–1789
55. Hoyle CR, Berntsen T, Myhre G, Isaksen ISA (2007) Secondary organic aerosol in the global aerosol—chemical transport model Oslo CTM2. Atmos Chem Phys 7(21):5675–5694
56. Jacob DJ (2000) Heterogeneous chemistry and tropospheric ozone. Atmos Environ 34(12–14):2131–2159
57. Karagulian F, Rossi MJ (2007) Heterogeneous chemistry of the NO_3 free radical and N_2O_5 on decane flame soot at ambient temperature: reaction products and kinetics. J Phys Chem A 111(10):1914–1926
58. Karagulian F, Santschi C, Rossi MJ (2006) The heterogeneous chemical kinetics of N_2O_5 on $CaCO_3$ and other atmospheric mineral dust surrogates. Atmos Chem Phys 6:1373–1388
59. Kennedy OJ, Ouyang B, Langridge JM, Daniels MJS, Bauguitte S, Freshwater R et al (2011) An aircraft based three channel broadband cavity enhanced absorption spectrometer for simultaneous measurements of NO_3, N_2O_5 and NO_2. Atmos Measur Tech 4(9):1759–1776
60. Kercher JP, Riedel TP, Thornton JA (2009) Chlorine activation by N_2O_5: simultaneous, in situ detection of $ClNO_2$ and N_2O_5 by chemical ionization mass spectrometry. Atmos Measur Tech 2(1):193–204
61. Kiendler-Scharr A, Mensah AA, Friese E, Topping D, Nemitz E, Prevot ASH et al (2016) Ubiquity of organic nitrates from nighttime chemistry in the European submicron aerosol. Geophys Res Lett 43(14):7735–7744
62. King MD, Dick EM, Simpson WR (2000) A new method for the atmospheric detection of the nitrate radical (NO_3). Atmos Environ 34(5):685–688
63. Le Breton M, Bacak A, Muller JBA, Bannan TJ, Kennedy O, Ouyang B et al (2014) The first airborne comparison of N2O5 measurements over the UK using a CIMS and BBCEAS during the RONOCO campaign. Anal Methods 6(24):9731–9743
64. Levy H (1971) Normal atmosphere—large radical and formaldehyde concentrations predicted. Science 173(3992):141–143
65. Li QY, Zhang L, Wang T, Tham YJ, Ahmadov R, Xue LK et al (2016) Impacts of heterogeneous uptake of dinitrogen pentoxide and chlorine activation on ozone and reactive nitrogen partitioning: improvement and application of the WRF-Chem model in southern China. Atmos Chem Phys 16(23):14875–14890
66. Longfellow CA, Ravishankara AR, Hanson DR (2000) Reactive and nonreactive uptake on hydrocarbon soot: HNO_3, O-3, and N_2O_5. J Geophys Res Atmos 105(D19):24345–24350
67. Lu KD, Rohrer F, Holland F, Fuchs H, Brauers T, Oebel A et al (2014) Nighttime observation and chemistry of HO_x in the Pearl River Delta and Beijing in summer 2006. Atmos Chem Phys 14(10):4979–4999

68. Matsumoto J, Kosugi N, Imai H, Kajii Y (2005) Development of a measurement system for nitrate radical and dinitrogen pentoxide using a thermal conversion/laser-induced fluorescence technique. Rev Sci Instr 76(6)
69. Mentel TF, Sohn M, Wahner A (1999) Nitrate effect in the heterogeneous hydrolysis of dinitrogen pentoxide on aqueous aerosols. Phys Chem Chem Phys 1(24):5451–5457
70. Mielke LH, Furgeson A, Osthoff HD (2011) Observation of $ClNO_2$ in a mid-continental urban environment. Environ Sci Technol 45(20):8889–8896
71. Mihelcic D, Klemp D, Musgen P, Patz HW, Volzthomas A (1993) Simultaneous measurements of peroxy and nitrate radicals at Schauinsland. J Atmos Chem 16(4):313–335
72. Morgan WT, Ouyang B, Allan JD, Aruffo E, Di Carlo P, Kennedy OJ et al (2015) Influence of aerosol chemical composition on N2O5 uptake: airborne regional measurements in northwestern Europe. Atmos Chem Phys 15(2):973–990
73. Ng NL, Brown SS, Archibald AT, Atlas E, Cohen RC, Crowley JN et al (2017) Nitrate radicals and biogenic volatile organic compounds: oxidation, mechanisms, and organic aerosol. Atmos Chem Phys 17(3):2103–2162
74. Noxon JF, Norton RB, Henderson WR (1978) Observation of Atmospheric NO_3. Geophys Res Lett 5(8):675–678
75. Osthoff HD, Roberts JM, Ravishankara AR, Williams EJ, Lerner BM, Sommariva R et al (2008) High levels of nitryl chloride in the polluted subtropical marine boundary layer. Nat Geosci 1(5):324–328
76. Pathak RK, Wang T, Wu WS (2011) Nighttime enhancement of PM2.5 nitrate in ammonia-poor atmospheric conditions in Beijing and Shanghai: plausible contributions of heterogeneous hydrolysis of N_2O_5 and HNO_3 partitioning. Atmos Environ 45(5):1183–1191
77. Pathak RK, Wu WS, Wang T (2009) Summertime PM2.5 ionic species in four major cities of China: nitrate formation in an ammonia-deficient atmosphere. Atmos Chem Phys 9(5):1711–1722
78. Phillips GJ, Tang MJ, Thieser J, Brickwedde B, Schuster G, Bohn B et al (2012) Significant concentrations of nitryl chloride observed in rural continental Europe associated with the influence of sea salt chloride and anthropogenic emissions. Geophys Res Lett 39
79. Phillips GJ, Thieser J, Tang MJ, Sobanski N, Schuster G, Fachinger J et al (2016) Estimating N_2O_5 uptake coefficients using ambient measurements of NO_3, N_2O_5, $ClNO_2$ and particle-phase nitrate. Atmos Chem Phys 16(20):13231–13249
80. Platt U, Perner D, Patz HW (1979) Simultaneous measurement of atmospheric CH_2O, O_3, and NO_2 by differential optical-absorption. J Geophys Res Atmos 84(Nc10):6329–6335
81. Platt U, Perner D, Winer AM, Harris GW, Pitts JN (1980) Detection of NO_3 in the polluted troposphere by differential optical-absorption. Geophys Res Lett 7(1):89–92
82. Pye HOT, Chan AWH, Barkley MP, Seinfeld JH (2010) Global modeling of organic aerosol: the importance of reactive nitrogen (NO_x and NO_3). Atmos Chem Phys 10(22):11261–11276
83. Riedel TP, Bertram TH, Ryder OS, Liu S, Day DA, Russell LM et al (2012) Direct N_2O_5 reactivity measurements at a polluted coastal site. Atmos Chem Phys 12(6):2959–2968
84. Riemer N, Vogel H, Vogel B, Anttila T, Kiendler-Scharr A, Mentel TF (2009) Relative importance of organic coatings for the heterogeneous hydrolysis of N_2O_5 during summer in Europe. J Geophys Res Atmos 114
85. Riemer N, Vogel H, Vogel B, Schell B, Ackermann I, Kessler C et al (2003) Impact of the heterogeneous hydrolysis of N_2O_5 on chemistry and nitrate aerosol formation in the lower troposphere under photosmog conditions. J Geophys Res Atmos 108(D4)
86. Sarwar G, Simon H, Bhave P, Yarwood G (2012) Examining the impact of heterogeneous nitryl chloride production on air quality across the United States. Atmos Chem Phys 12(14):6455–6473
87. Schulz KJ, Simpson WR (1998) Frequency-matched cavity ring-down spectroscopy. Chem Phys Lett 297(5–6):523–529
88. Seisel S, Borensen C, Vogt R, Zellner R (2005) Kinetics and mechanism of the uptake of N(2)O(5) on mineral dust at 298 K. Atmos Chem Phys 5:3423–3432

89. Sommariva R, Osthoff HD, Brown SS, Bates TS, Baynard T, Coffman D et al (2009) Radicals in the marine boundary layer during NEAQS 2004: a model study of day-time and night-time sources and sinks. Atmos Chem Phys 9(9):3075–3093
90. Stark H, Brown SS, Goldan PD, Aldener M, Kuster WC, Jakoubek R et al (2007) Influence of nitrate radical on the oxidation of dimethyl sulfide in a polluted marine environment. J Geophys Res Atmos 112(D10)
91. Stutz J, Alicke B, Ackermann R, Geyer A, White A, Williams E (2004) Vertical profiles of NO_3, N_2O_5, O-3, and NO_x in the nocturnal boundary layer: 1. Observations during the Texas air quality study 2000. J Geophys Res Atmos 109(D12)
92. Stutz J, Wong KW, Lawrence L, Ziemba L, Flynn JH, Rappengluck B et al (2010) Nocturnal NO_3 radical chemistry in Houston, TX. Atmos Environ 44(33):4099–4106
93. Su X, Tie XX, Li GH, Cao JJ, Huang RJ, Feng T et al (2017) Effect of hydrolysis of N_2O_5 on nitrate and ammonium formation in Beijing China: WRF-Chem model simulation. Sci Total Environ 579:221–229
94. Tang MJ, Camp JCJ, Rkiouak L, McGregor J, Watson IM, Cox RA et al (2014) Heterogeneous Interaction of SiO_2 with N_2O_5: aerosol flow tube and single particle optical levitation-Raman spectroscopy studies. J Phys Chem A 118(38):8817–8827
95. Tang MJ, Schuster G, Crowley JN (2014) Heterogeneous reaction of N_2O_5 with illite and Arizona test dust particles. Atmos Chem Phys 14(1):245–254
96. Tang MJ, Telford PJ, Pope FD, Rkiouak L, Abraham NL, Archibald AT et al (2014) Heterogeneous reaction of N_2O_5 with airborne TiO_2 particles and its implication for stratospheric particle injection. Atmos Chem Phys 14(12):6035–6048
97. Tang MJ, Thieser J, Schuster G, Crowley JN (2012) Kinetics and mechanism of the heterogeneous reaction of N_2O_5 with mineral dust particles. Phys Chem Chem Phys 14(24):8551–8561
98. Tham YJ, Wang Z, Li QY, Yun H, Wang WH, Wang XF et al (2016) Significant concentrations of nitryl chloride sustained in the morning: investigations of the causes and impacts on ozone production in a polluted region of northern China. Atmos Chem Phys 16(23):14959–14977
99. Thornton JA, Braban CF, Abbatt JPD (2003) N2O5 hydrolysis on sub-micron organic aerosols: the effect of relative humidity, particle phase, and particle size. Phys Chem Chem Phys 5(20):4593–4603
100. Thornton JA, Kercher JP, Riedel TP, Wagner NL, Cozic J, Holloway JS et al (2010) A large atomic chlorine source inferred from mid-continental reactive nitrogen chemistry. Nature 464(7286):271–274
101. Tsai C, Wong C, Hurlock S, Pikelnaya O, Mielke LH, Osthoff HD et al (2014) Nocturnal loss of NO_x during the 2010 CalNex-LA study in the Los Angeles Basin. J Geophys Res Atmos 119(22):13004–13025
102. Vandoren JM, Watson LR, Davidovits P, Worsnop DR, Zahniser MS, Kolb CE (1991) Uptake of N_2O_5 and HNO_3 by aqueous sulfuric-acid droplets. J Phys Chem 95(4):1684–1689
103. Varma RM, Venables DS, Ruth AA, Heitmann U, Schlosser E, Dixneuf S (2009) Long optical cavities for open-path monitoring of atmospheric trace gases and aerosol extinction. Appl Opt 48(4):B159–B171
104. Venables DS, Gherman T, Orphal J, Wenger JC, Ruth AA (2006) High sensitivity in situ monitoring of NO_3 in an atmospheric simulation chamber using incoherent broadband cavity-enhanced absorption spectroscopy. Environ Sci Technol 40(21):6758–6763
105. Vrekoussis M, Kanakidou M, Mihalopoulos N, Crutzen PJ, Lelieveld J, Perner D et al (2004) Role of the NO_3 radicals in oxidation processes in the eastern Mediterranean troposphere during the MINOS campaign. Atmos Chem Phys 4:169–182
106. Vrekoussis M, Mihalopoulos N, Gerasopoulos E, Kanakidou M, Crutzen PJ, Lelieveld J (2007) Two-years of NO_3 radical observations in the boundary layer over the Eastern Mediterranean. Atmos Chem Phys 7:315–327
107. Wagner C, Hanisch F, Holmes N, de Coninck H, Schuster G, Crowley JN (2008) The interaction of N_2O_5 with mineral dust: aerosol flow tube and Knudsen reactor studies. Atmos Chem Phys 8(1):91–109

108. Wagner C, Schuster G, Crowley JN (2009) An aerosol flow tube study of the interaction of N_2O_5 with calcite, Arizona dust and quartz. Atmos Environ 43(32):5001–5008
109. Wagner NL, Riedel TP, Young CJ, Bahreini R, Brock CA, Dube WP et al (2013) N_2O_5 uptake coefficients and nocturnal NO_2 removal rates determined from ambient wintertime measurements. J Geophys Res Atmos 118(16):9331–9350
110. Wahner A, Mentel TF, Sohn M, Stier J (1998) Heterogeneous reaction of N_2O_5 on sodium nitrate aerosol. J Geophys Res Atmos 103(D23):31103–31112
111. Wang HC, Chen T, Lu KD (2015) Measurement of NO_3 and N_2O_5 in the troposphere. Prog Chem 27(7):963–976
112. Wang T, Tham YJ, Xue LK, Li QY, Zha QZ, Wang Z et al (2016) Observations of nitryl chloride and modeling its source and effect on ozone in the planetary boundary layer of southern China. J Geophys Res Atmos 121(5):2476–2489
113. Wang T, Xue LK, Brimblecombe P, Lam YF, Li L, Zhang L (2017) Ozone pollution in China: a review of concentrations, meteorological influences, chemical precursors, and effects. Sci Total Environ 575:1582–1596
114. Wang X, Wang T, Yan C, Tham YJ, Xue L, Xu Z et al (2014) Large daytime signals of N_2O_5 and NO_3 inferred at 62 amu in a TD-CIMS: chemical interference or a real atmospheric phenomenon? Atmos Measur Tech 7(1):1–12
115. Wang Z, Wang WH, Tham YJ, Li QY, Wang H, Wen L et al (2017) Fast heterogeneous N_2O_5 uptake and $ClNO_2$ production in power plant and industrial plumes observed in the nocturnal residual layer over the North China Plain. Atmos Chem Phys 17(20):12361–12378
116. Wayne RP, Barnes I, Biggs P, Burrows JP, Canosamas CE, Hjorth J et al (1991) The nitrate radical—physics, chemistry, and the atmosphere. Atmos Environ Part A-General Topics 25(1):1–203
117. White JU (1942) Long optical paths of large aperture. J Opt Soc America 32(5):285–288
118. Wood EC, Wooldridge PJ, Freese JH, Albrecht T, Cohen RC (2003) Prototype for in situ detection of atmospheric NO_3 and N_2O_5 via laser-induced fluorescence. Environ Sci Technol 37(24):5732–5738
119. Yun H, Wang T, Wang WH, Tham YJ, Li QY, Wang Z et al (2018) Nighttime NO_x loss and $ClNO_2$ formation in the residual layer of a polluted region: Insights from field measurements and an iterative box model. Sci Total Environ 622:727–734
120. Yvon SA, Plane JMC, Nien CF, Cooper DJ, Saltzman ES (1996) Interaction between nitrogen and sulfur cycles in the polluted marine boundary layer. J Geophys Res Atmos 101(D1):1379–1386

Chapter 2
Instrumentation

Abstract This chapter introduces the homemade instrument of cavity enhanced absorption spectroscopy for measuring NO_3 and N_2O_5 in field studies. The layout of the optical layout and flow system, as well as the sampling loss and sampling efficiency of NO_3 and N_2O_5 in sampling line are characterized by lab experiments. The accuracy and uncertainties of the instrument are analyzed. In the end, the field performance is presented.

2.1 Instrument Layout

The CEAS instrument is designed to measure the ambient NO_3 and N_2O_5 and features a small size, easy portability, and low power consumption. The total weight is less than 25 kg, approximate dimensions are 95 × 40 × 25 cm, and the power consumption is less than 300 W, which potentially meets the requirements for future applications on mobile platforms. The system is distinct from previous CEAS systems [12, 14] because of its rigid cavity design, fast setup, and stable operation (e.g. the thermal alignment drift is minimized) in field campaigns. A dynamic NO titration setup was used to obtain the reference spectrum, which removed the influence of ambient water vapor so that the fitting precision was significantly enhanced.

2.1.1 Optical Layout

The schematic layout of the instrument is shown in Fig. 2.1a. The optical layout consists of a temperature stabilized light source, collimating optics, and a commercial spectrograph with CCD detector. The light source and collimating optics were concentrically integrated on an aluminium profile (75 × 8 × 5 cm).

A single-color LED (LZ1-10R200, LedEngin, Marblehead, MA, USA) is used as the light source and is mounted on a three dimensional (3D) adjustable bracket. The manufacturer-specified full luminosity output is about 800 mW, centred at the deep red light region (660 nm); and the full width at half maximum (FWHM) is 25 nm.

H. Wang, *The Chemistry of Nitrate Radical (NO_3) and Dinitrogen Pentoxide (N_2O_5) in Beijing*, Springer Theses, https://doi.org/10.1007/978-981-15-8795-5_2

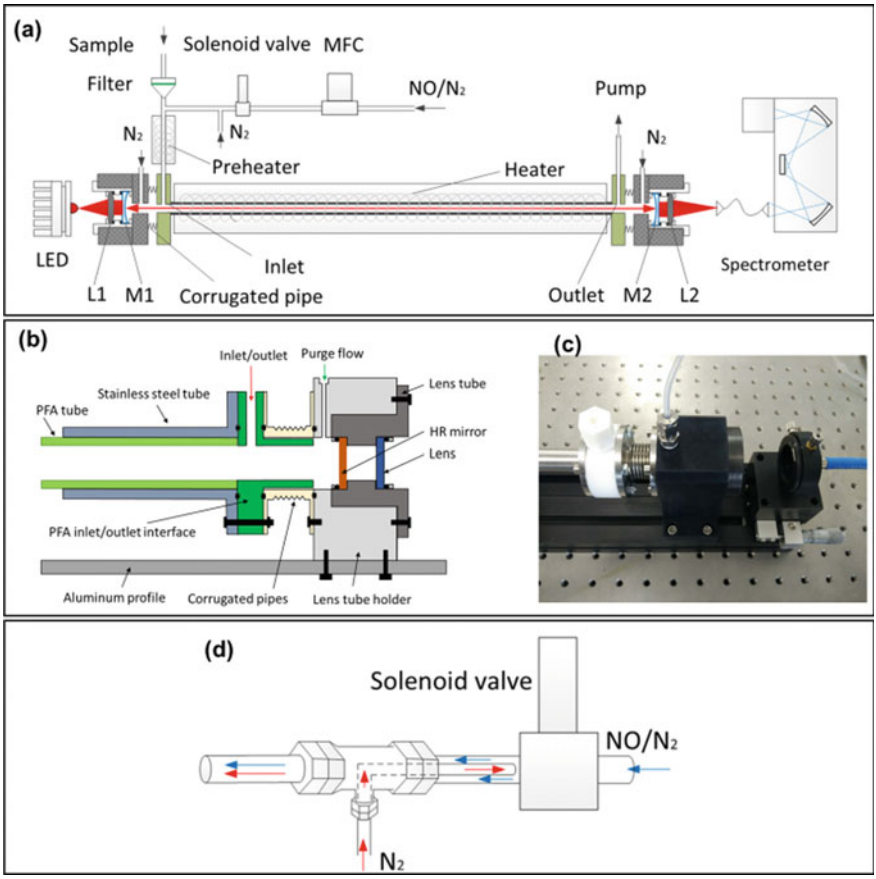

Fig. 2.1 A schematic of the newly developed IBBCEAS instrument for the detection of NO_3 and N_2O_5. **a** Overview of the optical layout (LEDs, collimating optics, high-finesse cavity, and spectrometer) and the flow system (aerosol filter, inlet, NO titration module, preheating tube, and detection cell). **b** The schematic layout of the mirror mounts, which enables a mechanical alignment of the high reflectivity (HR) mirrors. **c** A photograph of the mirror mounts. **d** The schematic layout of the NO titration module; the red arrow denotes the N_2 gas flow, and the blue arrow denotes the NO gas flow. Reproduced from with permission [28]

To minimize the wavelength shift and intensity drift caused by the LED temperature drift, the LED plate is mounted on an aluminium block and uses a thermo-electric cooler (TEC) control module to stabilize the temperature of the aluminium block at 17.5 ± 0.1 °C. The aluminium block is thermally insulated to reduce heat exchange with the ambient surroundings.

Before light is emitted into the high-finesse cavity, a Plano-Convex lens ($f = 30$ mm) is concentrically installed into the lens tube (shown in Fig. 2.1a as L1) to collimate the red light into the high-finesse cavity. The high-finesse cavity is formed by a pair of high reflectivity (HR) mirrors (102116, Layertec GmbH, Mellingen,

Germany) with a diameter of 25.0 mm (+0.00/−0.10 mm). The peak reflectivity of the HR mirrors at 660 nm is reported to be larger than 99.99% with a radii of curvature of 100 ± 5 cm. The two HR mirrors are mounted on two customized lens tubes, and the lens tubes are mechanically mounted on two matching lens tube holders, which are installed on an aluminium profile to maintain the distance between the two mirrors at 50.0 cm. Due to the high precision machining and assembly, the two lens tubes (shown as the scheme in Fig. 2.1b and the corresponding photograph in Fig. 2.1c) and the HR mirrors are mechanically aligned to have concentricity (<0.01°). Each HR mirror is continuously purged by 100 ml/min high purity nitrogen flow to prevent particle contamination by the sample gas flow.

The optical cavity is enclosed by a sample gas detection cell with a sample inlet, outlet, and two welded corrugated pipes connected at two ends. The light exiting the cavity is further imaged by a Plano-Convex lens (f = 50 mm) installed on the lens tube (shown in Fig. 2.1a as L2) that couples the output light onto the lead of a 100 μm diameter, 0.22 numerical aperture optical fibre (QP100-2-UV-VIS, Ocean Optics, Dunedin, FL, USA). The lead of the fibre is mounted on a 3D adjustable bracket and integrated on the aluminium profile. The other lead of the fibre directs the cavity output light into the spectrometer (QE65PRO, Ocean Optics, Dunedin, FL, USA). The charged couple device (CCD) in the QE65000 spectrograph is thermally regulated at −20.0 °C to minimize the dark current. The line density of the diffraction grating of the spectrometer is 1200 mm^{-1}, the entrance slit width is 100 μm, and the spectral resolution FWHM is 0.85 nm with the wavelength coverage of 580–710 nm. The instrument works under a signal to noise ratio (SNR) estimated to be larger than 500:1.

2.1.2 Flow System

The instrument sample flow system includes the aerosol filter, the inlet tube, the preheating tube and heated detection cell, and sensors for temperature, pressure, and relative humidity. During the field measurements, we operate with a sample flow rate of 2.0 L min^{-1}. A Teflon polytetrafluoroethylene (PTFE) filter (25 μm thickness, 4.6 cm diameter, 2.5 μm pore size, Typris, China) is used in the front of the sample module to remove ambient aerosols. After the filtration of the aerosols, the sample gas flow is delivered into the preheating tube through a 1.5 m PFA inlet tube (Entegris, I.D. = 4.35 mm). A 35 cm long PFA tube (Entegris, I.D. = 4.35 mm) is installed in the front of the inlet interface as a preheating tube to dissociate N_2O_5 to NO_3. This preheating tube is heated and stabilized at 120 °C. With this setup of temperature and residence time, N_2O_5 is completely decomposed to NO_3 in the preheating tube.

In Fig. 2.1b, the central part of the detection cell is constructed using a 35.6 cm long PFA tube (marked in light green) (Entegris, I.D. = 10.0 mm), enclosed by a stainless tube (marked in grey). Each end of the stainless tube is connected with a PFA interface (marked in green) which set up the inlet and outlet and further connected with the corrugated pipes. With this combination, the loss of NO_3 during detection

is minimized. The total PFA cell length is 44.0 cm, but the length from the inlet to the outlet is only 39.2 cm. The sample gas flow cell is heated and stabilized at 80 °C to prohibit the reverse reaction of NO_3 and NO_2 producing N_2O_5.

2.1.3 Dynamic Reference Spectrum

The effect of non-Lambert-Beer behaviour of water vapour absorption lines near 660 nm has to be well accounted for to achieve accurate and precise NO_3 detection [8, 14]. A few groups reported that the water vapour absorption can be determined with an "effective" water vapour absorption cross section from a look up table approach or a real-time iterative calculation approach under atmospheric conditions [12, 14]. In this work, we solve this problem by using a dynamic reference spectrum through frequent addition of NO into the inlet. This method has previously been used to acquire the chemical zero in the CRDS method [4, 7]. Through the frequent addition of NO, the reference spectrum contain optical extinction from other absorbers in this spectral region, for example water vapour, NO_2, O_3, and any aerosols not removed by the filter. For the CRDS method, the NO addition is carefully designed so that the resulting extinction of increased NO_2 in the reference measurement compared to that of NO_3 is negligible. For the CEAS method, the NO addition is a little less precise since this method allows for observation of NO_3 separately from NO_2 due to their different spectral shapes. In both cases, the effect of water vapour is removed, and the fitting precision increases significantly in our applications.

The NO titration module is connected to the inlet tube by a PFA tee-piece. Using a computer controlled solenoid valve, the instrument measures reference and sample spectrum sequentially by switching the NO injection on and off (NO = 98.0 ppmv, flow rate = 10.0 ml min^{-1}). A high purity N_2 line (I.D. = 1.50 mm) is added at the exit of the solenoid valve by a PFA tee-piece to flush the residual NO after the NO injection is switched off (Fig. 2.1d). The resulting NO mixing ratio is about 480 ppbv in the sample flow when NO injection is performed. Since 7.7 ppbv N_2O_5 was once observed and reported in Hong Kong [29] as an extreme case, the ambient NO_3, N_2O_5, and O_3 were set at about 1 ppbv, 10 ppbv, and 100 ppbv, respectively, for the simulation, proving that the ambient NO_3 and N_2O_5 can be removed within a time scale of 0.05 s when NO is injected (Fig. 2.2).

The NO_2 impurity in the used NO standard is analysed by a commercial NO_x instrument (TE-42i). The NO_2 impurity is found to be around 0.8%, which means 4 ppbv of NO_2 is present in the reference spectrum measurement with the presence of 480 ppbv NO. The NO_3 and O_3 in the preheating tube and detection cell react with the high concentration of NO and generate NO_2. In the case shown as Fig. 2.2, the additional NO_2 produced during the measurement of the reference spectrum can reach up to 55 ppbv (with the initial additional NO_2 set at 4 ppbv). Therefore, to use this dynamic reference spectrum, we normally fit both NO_3 and NO_2 to cover the limiting cases when the generated NO_2 is high. Nevertheless, the fitted NO_2 concentration will be negative since the NO_2 concentrations are higher in the reference spectrum.

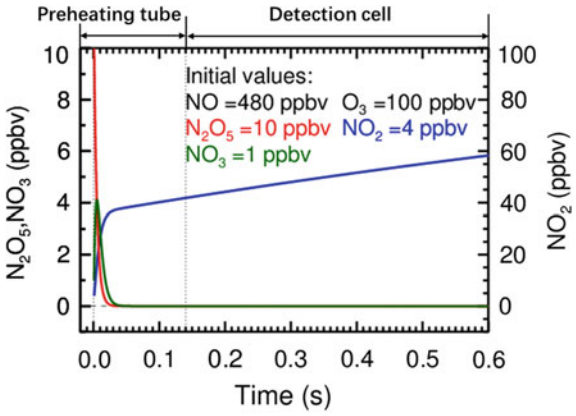

Fig. 2.2 Simulation of the change of the mixing ratios of NO_3, N_2O_5 and NO_2 during the NO titration mode in the preheating tube and detection cell for an extremely high NO_3 and N_2O_5 case. The initial ambient NO_3, N_2O_5 and O_3 were set at 1 ppbv, 10 ppbv and 100 ppbv, respectively. The initial NO_2 was set at 4 ppbv from the impurity of the used NO standard. Reproduced from with permission [28]

2.2 Characterizations

The principle of the IBBCEAS system was systematically introduced by [10] and will only be introduced briefly here. The extinction coefficient ($\alpha(\lambda)$) in the cavity intrinsically consists of the absorption, the Rayleigh and the Mie scattering, caused by the gas samples (2.1). The $\alpha(\lambda)$ can be determined through measurements of the intensity of the sample spectrum, reference spectrum, the mirror reflectivity, and the effective cavity length

$$\alpha(\lambda) = \left(\frac{I_0(\lambda)}{I(\lambda)} - 1\right)\left(\frac{1 - R(\lambda)}{d_{eff}}\right) = \sum_i n_i \cdot \sigma_i(\lambda) + \alpha_{Mie}(\lambda) + \alpha_{Rayl}(\lambda) \quad (2.1)$$

Here λ is the wavelength of light; n_i and $\sigma_i(\lambda)$ are the number density and absorption cross section of the i_{th} gas compound, respectively, which causes absorption of the incident light; d_{eff} is the effective cavity length; $R(\lambda)$ is the mirror reflectivity; $\alpha_{Rayl}(\lambda)$ is the extinction due to Rayleigh scattering; $\alpha_{Mie}(\lambda)$ is the extinction due to Mie scattering; $I_0(\lambda)$ is the reference spectrum; and $I(\lambda)$ is the sample spectrum. The parameters include the cross section of the strongly light absorbing gases in the target wavelength range, the effective cavity length, and mirror reflectivity that have to be quantified before deriving the mixing ratio of target gas species.

2.2.1 The Absorption Cross Section ($\sigma_i(\lambda)$)

The effective absorption cross section of the abundant ambient absorbers, NO_3 and NO_2, in the wavelength window of 640–680 nm needs to be determined to retrieve the molecule number density of NO_3. Since we used a dynamic reference spectrum, which contains the same amount of water vapour as that of the measured sample spectrum (Sect. 2.3), the calculation of the strong nonlinear absorption lines of H_2O in this wavelength window is avoided. The NO_3 absorption cross section is known to be temperature dependent [18, 32]. Under the heated cavity conditions (353 K), the effective absorption cross section of NO_3 is calculated by two steps: (1) the reported cross section of NO_3 [32] is scaled to the ratio of the band's peak intensity at 662 nm between 298 K and 353 K according to [18] and (2) the scaled absorption cross section is further convoluted with an instrument function determined with the neon emission line at 659.48 nm. Consequently, the calculated effective cross section at 353 K is about 1.77×10^{-17} cm^2 molecule^{-1} at 662 nm, the uncertainty of the temperature correction and convolution is estimated to be 13%. Under cold cavity conditions (298 K), the NO_3 cross section is convoluted directly to our spectral resolution with a peak value of 2.02×10^{-17} cm^2 molecule^{-1} at 662 nm, the uncertainty of the convolution is estimated to be 10% [12]. The NO_2 cross section is reported to be not sensitive to the temperature change [26], so that only convolution is performed to derive its effective absorption cross section for our instrument setup. Figure 2.3 shows the temperature scaled and instrumental resolution convolved NO_3 absorption cross section at 353 K and the convolved NO_2 absorption cross section, respectively. The cross section of NO_3 near 662 nm is three orders of magnitude larger than that of NO_2.

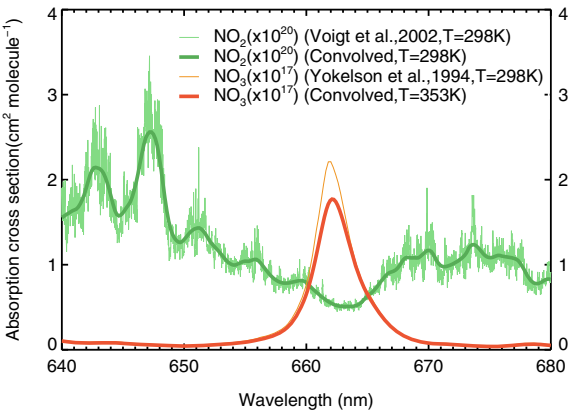

Fig. 2.3 Absorption cross section of NO_3 and NO_2 from 640 to 680 nm. The green thin line is the original cross section of NO_2 at 298 K determined by [26], the green thick line is the convolved result, the orange thin line is the original cross section of NO_3 at 298 K determined by [32], and the red thick line is the temperature scaled and convolved cross section at 353 K. Reproduced from with permission [28]

2.2.2 The Mirror Reflectivity ($R(\lambda)$)

The mirror reflectivity ($R(\lambda)$) is an important parameter to be determined for the CEAS type of instrument. In previous work, $R(\lambda)$ had been determined through four different methods, including the detection of a stable trace gas compound with known concentrations [25], the differentiation of pure gases with distinct Rayleigh scattering cross section [6, 16, 30], the using of low loss optics [24], and the determination of the phase shift or ring down time [14]. In this study, $R(\lambda)$ is determined through the differentiation of pure gases (N_2 and He) in the cavity (Eq. 2.2) during the field campaigns. The Rayleigh scattering cross sections for N_2 ($\sigma_{Rayl,\,N2}(\lambda)$) and He ($\sigma_{Rayl,\,He}(\lambda)$) are found in [21], respectively.

$$R(\lambda) = 1 - d\left(\frac{I_{N2}(\lambda)\cdot n_{N2}\cdot\sigma_{Rayl,N2}(\lambda) - I_{He}(\lambda)\cdot n_{He}\cdot\sigma_{Rayl,He}(\lambda)}{I_{He}(\lambda) - I_{N2}(\lambda)}\right) \quad (2.2)$$

In Eq. (2.2), d is the distance between the two high reflective mirrors (50.0 cm); $I_{N2}(\lambda)$ and $I_{He}(\lambda)$ represent the light out spectrum determined when the cavity is filled by N_2 or He through the purge flow injection lines, respectively; and n_{N2} and n_{He} are the calculated number density of N_2 and He, respectively, at the measured temperature and pressure in the cavity. Figure 2.4 shows the mirror reflectivity calibration results during the field measurements performed at the campus of the University of Chinese Academy of Science (UCAS) in Beijing during winter 2016. The bold black line is the average reflectivity of the five measurements of $R(\lambda)$. It is noted that the peak of the $R(\lambda)$ is 0.999936 ± 0.000002 at 662 nm. Under the protection of the purge flow and due to the mechanically aligned setup of the cavity system, the determined $R(\lambda)$ is remarkably stable during this field campaign. The bold red line is the average

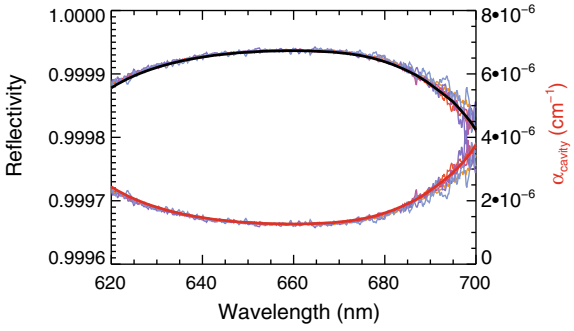

Fig. 2.4 Mirror reflectivity and cavity losses calibrated with high purity He and N_2 in the current experimental setup during the field measurements. The original calibration results were depicted by varying coloured lines: the smoothed black bold line is the average R(λ) and the smoothed bold red line is the average cavity loss (1 − R(λ))/d) from five measurements. The mean (±1σ) value at 662 nm of reflectivity and the cavity loss are 0.999936 ± 0.000002 and $(1.28 \pm 0.01) \times 10^{-6}$, respectively. The effective path length at 662 nm reached 6.13 km. Reproduced from with permission [28]

cavity loss, which is equal to $(1 - R(\lambda))/d$, with the maximized point near 662 nm of $(1.28 \pm 0.01) \times 10^{-6}$ (1σ). The total uncertainty of the reflectivity is about 5%, which is dominated by the scattering cross sections of N_2, according to [23]. The uncertainty for He makes a negligible contribution [31].

2.2.3 The Effective Cavity Length (d_{eff})

The effective cavity length (d_{eff}) represents the cavity length occupied by the absorbing gas when the sample flow is stable. Since the continuous purge flow occupies the two ends of the cavity to protect the mirrors, the d_{eff} is usually shorter than the distance between the two high reflective mirrors (defined as d, which is 50.0 cm in our setup) and longer than the distance between the sample inlet and outlet (defined as d_{sample}, which is 39.2 cm in our setup). We determine the d_{eff} by supplying a NO_2 gas standard (200 ppbv) with a constant flow into the cavity with purge flow and retrieving the d_{eff}. The 200 ppbv NO_2 sample is prepared by a bottle standard of NO_2 (80.8 ppm) diluted with high purity synthetic air (O_2: 20.5%, N_2: bal) through a gas mixer (TE-146i). The uncertainty of the prepared NO_2 standard is estimated to be 2%, while the uncertainty of the NO_2 absorption cross section is estimated to be 4.7% according to [26]. In our measurement, the d_{eff} is determined to be 45.0 cm, which occupies 90.0% of the total length of the optical cavity. Moreover, d_{sample} is 78.4% of the length of the total optical cavity. The difference between the d_{eff} and d_{sample} shows that there is the gas sample flows turbulent mixed into the purge volumes. Since the possibility of this turbulent mixing is slow relative to the rate of the NO_3 wall losses, the determination of the d_{eff} for NO_3 is associated with an additional uncertainty of 12%, and the total uncertainty of the determined d_{eff} with this approach is about 13%.

2.3 Spectral Fitting

A least square spectral fitting software package was developed for retrieving the molecule number densities of NO_3 and NO_2. The optimized spectral fitting window was found to be from 640 to 680 nm, and a third-order polynomial was applied to fit the background drift and unaccounted scattering effect. Figure 2.5 shows an example of the spectral fitting of a measurement spectrum of NO_3 at 5 s integration time with ambient measurement. By using the dynamic reference spectrum, the spectral fitting is targeted at NO_3 and NO_2 as explained above. The retrieved mixing ratio of NO_3 (that actually represents the $NO_3 + N_2O_5$ concentration in the gas samples) is 64 pptv and that of NO_2 is -33 ppbv, which was mainly caused by the conversion of ambient O_3 (80 ppbv) with the added NO in the measurement of the reference spectrum. The corresponding fitting residual is in the range of $\pm$ 4.0 $\times 10^{-9}$ cm^{-1}, and the H_2O absorption is found to be cancelled out in the residual

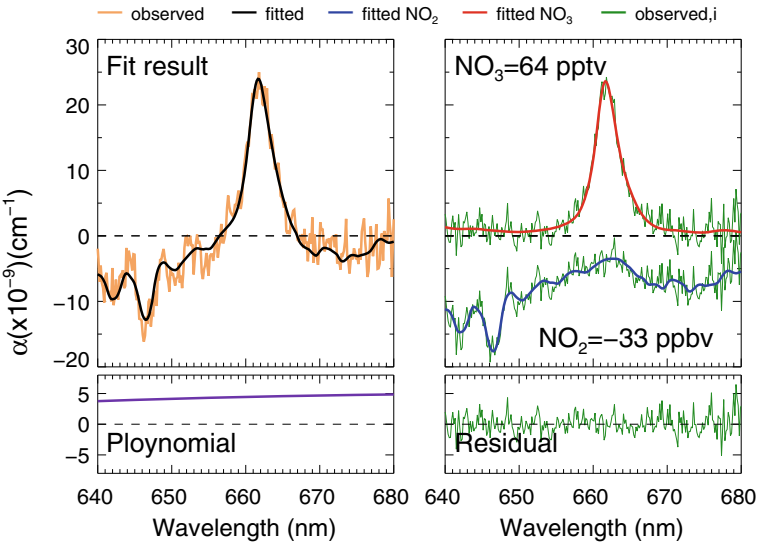

Fig. 2.5 An example of the spectral fit for an extinction spectrum measured (5 s average) during field measurements. The fitted results of NO_3 and NO_2 are shown as well as the third-order polynomial, the total fit result, and the residual. Reproduced from with permission [28]

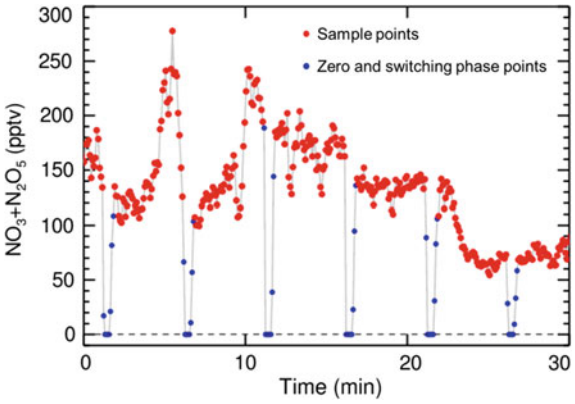

Fig. 2.6 An example time series of $NO_3 + N_2O_5$ detection performed at a rural site in Beijing with 5 s spectrum integral time. The red points denote the ambient measurement mode without NO addition, and the blue points denote the 20 s zero points (determination of the dynamic reference spectrum) with NO addition and 20 s switching time between the titration mode and the sample mode. Reproduced from with permission [28]

spectrum. Moreover, an example time series of $NO_3 + N_2O_5$ measurement results during ambient measurements is shown in Fig. 2.6. During ambient measurement, the NO titration is performed periodically to acquire the dynamic reference spectrum.

In Fig. 2.6, the red points mark the effective ambient measurement result, which covered 4 min 20 s of every 5 min, and the blue points include 20 s for the zero points and a 20 s switching phase between the two modes, which is discarded from the data analysis.

2.4 Sampling Transmission Efficiency

For the accurate measurement of NO_3 and N_2O_5, the wall loss reactivity of the sample manifold and the detection cell need to be determined. This includes: (1) the wall loss on the filter, (2) the wall loss on the inner surface of the inlet tube, and (3) the wall loss in the preheating tube and the detection cell. To determine the wall loss reactivity, a NO_3/N_2O_5 source module with stable mixing ratio ($\pm 2\%$) is set up in the lab. In this module, high purity synthetic air and NO_2 is supplied to a gas mixer (TE-146i), and O_3 is generated in this gas mixer through the irradiation of a mercury lamp. The supplied NO_2 and the produced O_3 is further delivered into a 160 L smog chamber to generate stable concentrations of NO_3 and N_2O_5. Commercial NO_x (TE-42i) and O_3 monitors (TE-49i) are operated to quantify the mixing ratio of NO_2 and O_3 in the chamber. According to the detected concentration of NO_2 and O_3, we can modulate the delivered concentration levels of the NO_3 and N_2O_5 with the help of a box model.

2.4.1 Filter Loss

The filter transmission efficiency of NO_3 and N_2O_5 is determined through the differentiation of an inlet without a filter, with a clean filter (25 μm thickness, 4.6 cm diameter, 2.5 μm pore size, Typris, China), and with used filters saved during typical pollution episodes during field measurements. According to previous field measurements of NO_3 and N_2O_5 (e.g. [4, 20]), frequent filter change is suggested, and the frequency is proposed to be 0.5–3 h depending on the aerosol loadings to reduce the impact of the filter aging caused by aerosol accumulation. For this reason, we changed the filter with a regular time interval (once every hour) during pollution episodes. For clean conditions, the filter exchange frequency was reduced to be once every two hours.

For the determination of the NO_3 filter transmission efficiency, an additional preheating tube is inserted in front of the detection system to convert all the generated N_2O_5 delivered by the calibration source to NO_3. The determined clean filter transmission efficiency is 75% for NO_3 and is slightly lower than the previous results of NO_3 transmission efficiency on Teflon filters [1, 20]. The filter transmission efficiency of NO_3 on used filters is determined to be 5% less than that on the clean filter. For the field calculation of the NO_3 concentrations, the filter transmission efficiency

is then estimated to be 72 ± 3%. For the determination of the N_2O_5 filter transmission efficiency, the mixing ratio of NO_2 and O_3 is modulated to achieve a high ratio of N_2O_5/NO_3 (>100) before being fed into the instrument. The transmission efficiency of the N_2O_5 on the clean filter is determined to be 96%, which is consistent with the previous studies on the filter loss of N_2O_5 [1, 11, 20]. The filter transmission efficiency of N_2O_5 on a used filter is determined to be 6% smaller than that on the clean filter. Therefore, the filter transmission factor for N_2O_5 is estimated to be 93 ± 3%.

2.4.2 Wall Loss in the Sampling Line

To determine the wall loss reactivity of NO_3, the heated detection cell is used as a flow tube. Gas samples with a stable amount of N_2O_5 are delivered by the NO_3/N_2O_5 source described above. By stopping the sample gas flow, the observed NO_3 versus the elapsed time determines the first order loss rate of NO_3 in the heated detection cell. In this experiment, the fitted first order uptake coefficient of NO_3 reflects the contribution from three processes: (1) the wall loss of the NO_3 in the detection cell; (2) the change of the effective cavity length due to the adding of the purge flows; and (3) the production of NO_3 from the reaction of NO_2 and O_3. The NO_2 concentration determined in the running sample gas flow is used to determine the change of d_{eff} corresponding to the elapsed time after stopping the sample flow (in the way it is used to quantify the d_{eff} in Sect. 3.3). A time series of d_{eff} is determined with high time resolution data acquisition (0.5 s) that is then used to quantify the mixing ratio of NO_3 in the corresponding time intervals. Figure 2.7 shows the decay of the observed NO_3 concentrations on a logarithmic scale versus the elapsed time. The fitted first order decay rate is 0.13 ± 0.02 s^{-1} with a good correlation coefficient ($R^2 = 0.991$). Finally, the fitted first order decay rate is corrected by the chemistry of R1 and R4 with a box model constrained to observed NO_2 and O_3. The NO_3 wall reactivity of the heated detection cell surface is determined to 0.16 ± 0.02 s^{-1}, which is similar to previous results of 0.1–0.3 s^{-1} [3, 7, 12, 27].

The surface materials are the same as that of the inlet tube, the preheating tube, and the detection cell. Therefore, the wall loss reactivity of NO_3 in the detection cell will be applicable for the inlet and the preheating tubes. As shown in Fig. 2.1a, the instrument has only one mixing point at the setup of the NO titration module. In addition, there is no blockage of the main sample gas flow of the PFA tee-piece. Therefore, we think the influence of the mixing point can be neglected. As reported by [12], the NO_3 wall loss reactivity in the cold PFA piping (inlet) is the same as in the heated ones with a value of 0.27 s^{-1}. Nevertheless, we noticed that [7] reported that the NO_3 wall loss reactivity of the cold PFA tube could be a factor of two larger than that of the heated tube. We assume our NO_3 wall loss reactivity for the cold PFA tube to be between 0.16 and 0.32 s^{-1}, and the average NO_3 wall loss reactivity for the cold PFA tube is estimated to be 0.24 s^{-1} with an uncertainty of 0.08 s^{-1}.

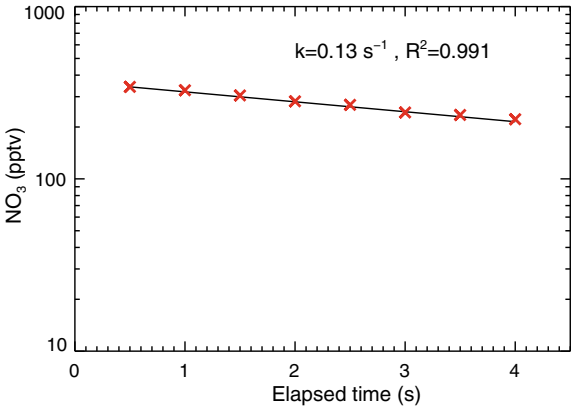

Fig. 2.7 The determined concentration decay of the NO_3 radical in the heated detection cell caused by the wall loss. Red cross denote the observation results, and the black line depicts the corresponding exponential fit. The net wall loss reactivity of NO_3 is corrected to be 0.16 ± 0.02 s^{-1} with a box model simulation of the chemical reactions occurring in the detection cell. Reproduced from with permission [28]

To determine the wall loss reactivity of the N_2O_5 in the PFA inlet tube, PFA tubes (Entegris, I.D. = 4.35 mm) with different lengths (0.5, 3.5, 5.5, 7.5, and 10.5 m) are inserted between the outlet of the NO_3/N_2O_5 source and the inlet of the preheating tube. The apparent first order loss rate of N_2O_5 (0.015 s^{-1}) is deduced by an exponential fit of the observed N_2O_5 concentrations to the varied residence times with different tube lengths (Fig. 2.8). The actual situation is more complicated in these

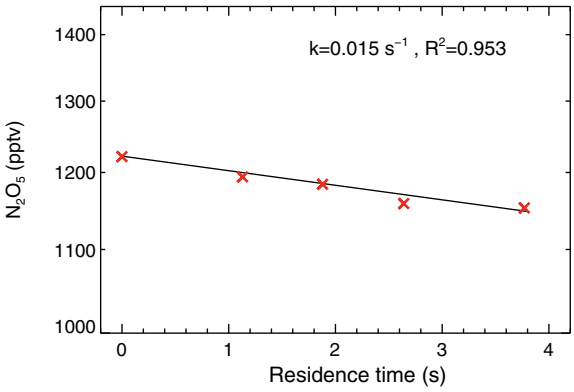

Fig. 2.8 The determined concentrations of N_2O_5 versus the residence time of the sample gas flows in the inlet tube. The change of the residence time is achieved by changing the inlet tubes having different lengths. Red cross denote the observation results, and the black line depicts the corresponding exponential fit. The net wall loss reactivity of N_2O_5 is corrected to be 0.019 ± 0.002 s^{-1} with a box model simulation of the chemical reactions occurring in the inlet tubes. Reproduced from with permission [28]

Table 2.1 The transmission efficiency of NO_3 and N_2O_5 for the sample module setup for the developed instrument

Gases	Filter (%)	Inlet tube (0.7 s) (%)	Preheating tube (0.14 s) (%)	Cavity (0.46 s) (%)	Total (%)
NO_3	72 ± 3[a]	84 ± 4 ($k = 0.24\ s^{-1}$)[b]	98 ($k = 0.16\ s^{-1}$)	93 ($k = 0.16\ s^{-1}$)	55 ± 6
N_2O_5	93 ± 3[a]	99 ($k = 0.019\ s^{-1}$)	99 ± 1[c]	93 ($k = 0.16\ s^{-1}$)	85 ± 3

Reproduced from with permission [28]
[a]Filter aging contributed an uncertainty of 3%
[b]The uncertainty of the NO_3 wall loss reactivity in the cold inlet tube caused an uncertainty of 4%
[c]The location of the N_2O_5 dissociation in the preheating tube had an uncertainty of 1%

PFA tubes due to the formation reaction of NO_3 and N_2O_5, the shift of thermal equilibrium, and the wall losses of both NO_3 and N_2O_5. The wall loss reactivity of N_2O_5 is retrieved from the observed apparent decay rate with a box model. In this model, initial NO_2 and O_3 are the observed values of the NO_3/N_2O_5 source. The retrieved N_2O_5 wall loss reactivity is $0.019\ s^{-1} \pm 0.002\ s^{-1}$. Moreover, the variation of ambient mixing ratio of NO_2 will change the N_2O_5 dissociated location in the preheating tube which would also influence the transmission efficiency of N_2O_5. By assuming the N_2O_5 is totally dissociated in the middle of the preheating tube, we determine the transmission efficiency of N_2O_5 in the preheating tube to be $99 \pm 1\%$.

The total transmission efficiencies as well as the detailed contributions due to the corresponding filter/wall loss and residence time for NO_3 and N_2O_5 are summarized in Table 2.1 for the experimental setup during field applications. The total estimated transmission efficiency of NO_3 (T_{NO3}) and N_2O_5 (T_{N2O5}) is determined to be $55 \pm 6\%$ and $85 \pm 3\%$, respectively. T_{NO3} is dominated by the loss on the filter and the inlet tube, the difference of T_{NO3} between cold cavity and heated cavity is negligible, while the T_{N2O5} is dominated by the loss on the filter and the detection cell.

2.5 Uncertainty and the Limit of Detection

As outlined above, the uncertainty of the NO_3 absorption is estimated to be 10% (298 K) and 13% (353 K), respectively; the uncertainty of the effective cavity length calculation is about 13% mainly due to the fast NO_3 wall loss; the uncertainty of the mirror reflectivity determination is about 5% controlled by the error of the scattering cross section of N_2; and the uncertainty of the T_{NO3} is about 6%, according to the Gaussian error propagation, the associated uncertainty is estimated to be 19% for the ambient NO_3 measurement. The uncertainty of the transmission efficiency in the heated cavity is estimated about 4 and 11% when N_2O_5 or NO_3 dominate the concentrations of $NO_3 + N_2O_5$, respectively, according to the Gaussian error propagation, the associated uncertainty for the ambient $NO_3 + N_2O_5$ measurement

Table 2.2 Details of the uncertainties of the measurement of ambient NO_3 and $NO_3 + N_2O_5$

Parameters	Uncertainty (NO_3) (%)	Uncertainty ($NO_3 + N_2O_5$) (%)
Cross section of NO_3	13	10
Mirror reflectivity	5	5
Transmission efficiency	6	4–11
Effective cavity length	13	13
Associated above	19	19–22

Reproduced from with permission [28]

is estimated to be 19–22%. The uncertainties of the observed mixing ratio of NO_3 and $NO_3 + N_2O_5$ are summarized in Table 2.2.

For the ambient N_2O_5 measurement, two parallel cavity are required with one cold cavity measure NO_3 and another heated cavity measured $NO_3 + N_2O_5$ like previous studies [5, 7, 14], here we estimated the uncertainty of N_2O_5 by following the expression proposed by [9].

$$\delta(N_2O_5) = \sqrt{\frac{[\delta(SUM)SUM]^2 + [\delta(T_{NO3})T_{NO3}NO_3]^2}{[SUM - T_{NO3}NO_3]^2} + \delta(T_{N2O5})^2} \tag{2.3}$$

In Eq. (2.3), the $\delta(N_2O_5)$ represents the uncertainty of N_2O_5 measurement, *SUM* is the measured $NO_3 + N_2O_5$ in the heated cavity and NO_3 is the ambient mixing ratio of NO_3 derived by the cold cavity, $\delta(T_{NO3})$ and $\delta(T_{N2O5})$ denotes the uncertainty of T_{NO3} and T_{N2O5}, $\delta(SUM)$ denotes the uncertainty of $NO_3 + N_2O_5$ measurement in the heated cavity. As reported by [12, 19], the uncertainty of N_2O_5 is increased with the decreasing of the ratio of N_2O_5/NO_3, when the N_2O_5/NO_3 is larger than 1 in the field measurement, the uncertainty of N_2O_5 is in the range of 22–36%.

The best integration time is determined through an Allan Variance method. Figure 2.9a depicts the Allan Variance analysis of the 12 000 zero measurement spectrums in the laboratory with 1 s integration time. According to the Allan deviation plot, increasing the integration time could improve the sensitivity of our instrument when the averaging time was smaller than 30 s. When the average time interval ranges from 30 to 100 s, the best detection capability is achieved; and when the average time interval is larger than 100 s, increasing the average time does not improve the sensitivity further and actually decreases it, which is most likely due to the drift of the light source. The limit of detection can be estimated by the standard deviation calculation from zero air measurement with the best integration time estimated above. Figure 2.9b, c show the histogram analysis of 12 000 zero measurement results for a 1 s and 30 s average, respectively. The limit of detection (LOD) is 2.4 pptv (1σ) for

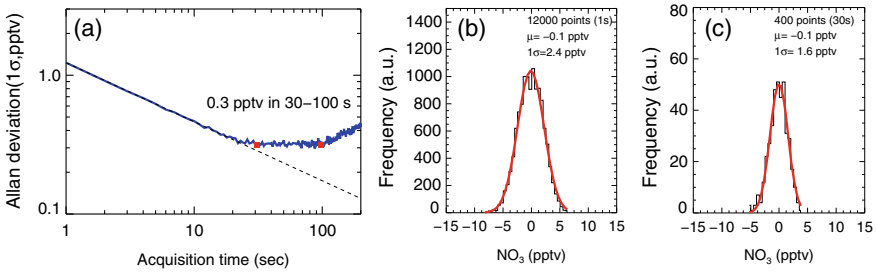

Fig. 2.9 The instrument performance with different integration times. **a** Allan deviation plots for measurements of NO_3 with 1 s integration time. **b** and **c** Show the histogram analyses of the measurements of NO_3 with 1 s and 30 s integration time, respectively. Reproduced from with permission [28]

the 1 s data and improved to be 1.6 pptv (1σ) for the 30 s data. Due to the smaller cross section of NO_3 was applied in the measurement of N_2O_5 at 353 K, the LOD is estimated 2.7pptv (1σ) with 1 s integral time. Referring to the observed mixing ratios of NO_3 and N_2O_5 in the typical regions [27], the developed instrument has the ability to measure NO_3 and N_2O_5 in the field. The LOD and uncertainty of our instrument is further compared with the existing field measurement techniques for NO_3 and N_2O_5 (Table 2.3). For the NO_3 measurement, CRDS, CEAS and LIF are available with LOD values of 0.2–10 pptv and uncertainties lower than 25%. For the N_2O_5 measurement, the three methods mentioned above and CIMS are available with LOD values of 0.5–12 pptv and uncertainties lower than 40%. Our instrument compares well with the available field instruments for the detection of NO_3 and N_2O_5. Nevertheless, we have so far only probed the field sites with the presence of high concentrations of $NO_3 + N_2O_5$, and, therefore, the NO_3 measurement mode is not used in the field studies.

2.6 Performance in Field Campaigns

The instrument has been deployed in two comprehensive field campaigns in Beijing in 2016. The first campaign took place at the campus of the University of Chinese Academy of Sciences (UCAS), and the data shown in Fig. 2.10b is from 27 February to 4 March, while the second campaign took place at Peking University Changping (PKU(CP)) campus and the data shown in Fig. 2.10c is from 23 May to 29 May. As shown in Fig. 2.10a, both sites are located in the northern rural areas in Beijing, about 60 and 40 km from the centre of Beijing, respectively. According to our current understanding of the NO_3–N_2O_5 chemistry, rural areas are lack of fresh NO emissions, and the air masses transported from urban is well aged and featured with high NO_2, O_3 and low NO, so that the influence of the NO_3–N_2O_5 chemistry can be

Table 2.3 Limits of Detection (LOD) and uncertainty of the existing field deployable instruments of NO_3 and N_2O_5

Reference	Method	NO_3		N_2O_5	
		LOD	Uncertainty (%)	LOD	Uncertainty (%)
This work	CEAS	2.4 pptv (1 s)	19–22	2.7 pptv (1 s)	22–36
Kennedy et al. [12]	CEAS	1.1 pptv (1 s)	11	2.4 pptv (1 s)	14
Bitter et al. [2]	CEAS	1 pptv (100 s)			
Schuster et al. [20]	CRDS/CEAS	2 pptv (5 s)	14	2 pptv (5 s)	13
Nakayama et al. [17]	CRDS	1.5 pptv (100 s)			
Dube et al. [9]	CRDS	0.2 pptv (1 s)	25	0.5pptv (1 s)	20–40
Ayers et al. (2005)	CRDS	2 pptv (25 s)			
Wang et al. [27]	CRDS	3.2 pptv (10 s)	8		
Matsumoto et al. [15]	LIF	10 pptv (600 s)	17	12 pptv (600 s)	17
Slusher et al. [22]	CIMS			12 pptv (1 s)	
Kercher et al. [13]	CIMS			2.7 pptv (60 s)	20
Wang et al. [29]	CIMS			4 pptv (60 s)	20

Reproduced from with permission [28]

maximized. We therefore expected these two sites to be ideal locations to probe the NO_3–N_2O_5 chemistry in Beijing.

During the UCAS campaign, our instrument was deployed at a roof lab, and the sample inlet was about 15 m above the ground. The measurement site was close to the mountainous area in Beijing and also was influenced by nearby traffic emissions. When the northerly wind appeared, we sampled clean air masses entrained with local traffic and residential emissions; when the southerly wind appeared, we could then capture the outflow from Beijing. In this campaign, the average night-time temperature and NO_2 mixing ratio is -4.3 °C and 15.5 ppbv, respectively. The calculated ratio of N_2O_5/NO_3 based on the thermodynamic equilibrium was found to be larger than 300; therefore the mixing ratio of NO_3 was ignorable compared with N_2O_5. Therefore, the amount of the detected $NO_3 + N_2O_5$ represented that of N_2O_5 for this campaign. Figure 2.10b shows the mixing ratio of $NO_3 + N_2O_5$ during

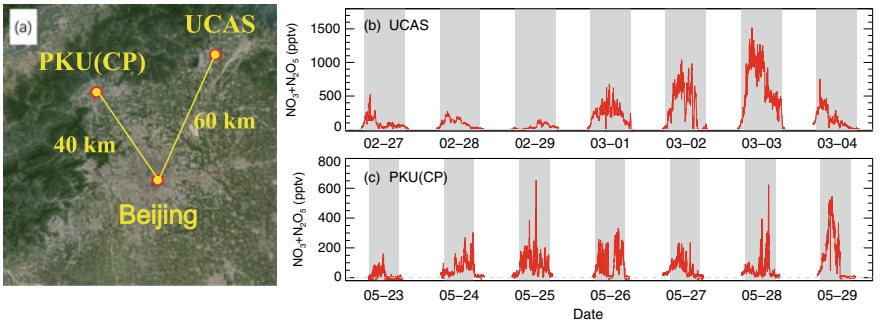

Fig. 2.10 Two example time series of the observed mixing ratios of $NO_3 + N_2O_5$ measured during the UCAS winter campaign 2016 and the PKU(CP) summer campaign. The grey box indicates the time span for night-time. **a** Depicts the map of the two sites indicating the UCAS site and PKU(CP) site that are about 60 km and 40 km away from the centre of Beijing, respectively. **b** Shows a typical development of the observed mixing ratio of $NO_3 + N_2O_5$ from clean to polluted air masses at UCAS. **c** Shows the observed mixing ratio of $NO_3 + N_2O_5$ during a typical pollution episode at PKU(CP). Reproduced from with permission [28]

a typical time when such air mass change from clean to polluted conditions. High mixing ratios of $NO_3 + N_2O_5$ were observed near the ground surface at the UCAS site. During the pollution episodes, the maximum $NO_3 + N_2O_5$ reached more than 1 ppbv on the night of 02–03 Mar 2016. A rapid variation of $NO_3 + N_2O_5$ was also observed, which may have been due to local traffic emissions during stagnant conditions. In all these days, the observed $NO_3 + N_2O_5$ continuously accumulated during a few hours after sunset, reached its maximum before midnight, and then gradually decreased to zero before sunrise. The decrease of the $NO_3 + N_2O_5$ at night in this location may be related to the typical running style of the heavy-duty vehicles (HDV). It is known that HDV would emit large amounts of fresh NO. The emitted NO is titrated with the O_3 and NO_3 and then reduces the accumulation of N_2O_5 or enhances the loss of N_2O_5 during the time scale of thermal dissociation (0.1–20 min from summer to winter time). Typically, more heavy-duty cars appear on the nearby street after 22:00 since the ban of HDV entering downtown Beijing is lifted after 22:00. The $NO_3 + N_2O_5$ measurement results of the PKU(CP) summer campaign are presented in Fig. 2.10c. During the summer campaign, the instrument was set up on the fifth floor of the main building at the PKU(CP) campus. The inlet was also about 15 m above ground. The average night-time temperature and NO_2 mixing ratio were 10.0 °C and 17.5 ppbv, respectively. High O_3 events frequently occurred in this season compared to that of winter. Together with the atmospheric processes with high NO_2 conditions, the calculated ratio of N_2O_5/NO_3 based on the thermodynamic equilibrium was estimated to be larger than 20, and the amount of $NO_3 + N_2O_5$ also represented that of N_2O_5 mostly at the PKU(CP) site.

2.7 Summary

A new portable CEAS instrument was developed for the ambient measurement of NO_3 and N_2O_5 incorporating two unique features:

(1) Novel non-adjustable mechanically aligned mirror mounts were designed and tested successfully. The new design offered a fast setup of the instrument in the field and proved to be stably operable by checking the mirror reflectivity.
(2) An addition chemical titration module was tested by adding NO into the sample flow and proved to be very helpful for the ambient spectral analysis, which enhanced the fitting precision by avoiding the complicated fitting of the water vapour absorption.

The total transmission efficiencies of NO_3 and N_2O_5 were determined to be 55 $\pm$ 6% and 85 $\pm$ 3%, respectively. The total uncertainty of the measurement of NO_3 and N_2O_5 was determined to be 19% and 22%–36%, respectively. The best limit of detection was quantified to be 2.4 pptv (1σ) and 2.7 pptv (1σ) with a 1 s integration time for NO_3 and N_2O_5, respectively. Compared to the other field instruments used worldwide, the new instrument was capable of measuring both NO_3 and N_2O_5, since only one channel was established at the moment. The instrument was deployed successfully in the $NO_3 + N_2O_5$ measurement in two comprehensive field campaigns conducted in the northern rural areas of Beijing in 2016, where high ratios of N_2O_5/NO_3 were present due to the presence of high NO_2. In these two campaigns, high mixing ratios of near surface $NO_3 + N_2O_5$ (mostly N_2O_5) up to 1 ppbv were detected. The observed high $NO_3 + N_2O_5$ concentrations in the summer campaign indicated that high concentrations of NO_3, up to 50 pptv, could be present at night. Since significant night-time OH concentrations (up to 1×10^6 cm^{-3}) were also found for these environments (e.g. Lu et al. 2014; Tan et al. 2017), the contribution of NO_3–N_2O_5 and HO_X chemistry toward the night-time oxidation capacity in Beijing is worthy of future exploration.

References

1. Aldener M, Brown SS, Stark H, Williams EJ, Lerner BM, Kuster WC et al (2006) Reactivity and loss mechanisms of NO_3 and N_2O_5 in a polluted marine environment: results from in situ measurements during New England air quality study 2002. J Geophys Res Atmos 111(D23)
2. Bitter M, Ball SM, Povey IM, Jones RL (2005) A broadband cavity ringdown spectrometer for in-situ measurements of atmospheric trace gases. Atmos Chem Phys 5:2547–2560
3. Brown SS, Stark H, Ciciora SJ, McLaughlin RJ, Ravishankara AR (2002) Simultaneous in situ detection of atmospheric NO_3 and N_2O_5 via cavity ring-down spectroscopy. Rev Sci Instrum 73(9):3291–3301
4. Brown SS, Stark H, Ciciora SJ, Ravishankara AR (2001) In-situ measurement of atmospheric NO_3 and N_2O_5 via cavity ring-down spectroscopy. Geophys Res Lett 28(17):3227–3230
5. Brown SS, Stark H, Ryerson TB, Williams EJ, Nicks DK, Trainer M et al (2003) Nitrogen oxides in the nocturnal boundary layer: simultaneous in situ measurements of NO_3, N_2O_5, NO_2, NO, and O-3. J Geophys Res Atmos 108(D9): ACH18

6. Chen J, Venables DS (2011) A broadband optical cavity spectrometer for measuring weak near-ultraviolet absorption spectra of gases. Atmos Measur Tech 4(3):425–436
7. Crowley JN, Schuster G, Pouvesle N, Parchatka U, Fischer H, Bonn B et al (2010) Nocturnal nitrogen oxides at a rural mountain-site in south-western Germany. Atmos Chem Phys 10(6):2795–2812
8. Dorn HP, Apodaca RL, Ball SM, Brauers T, Brown SS, Crowley JN et al (2013) Intercomparison of NO_3 radical detection instruments in the atmosphere simulation chamber SAPHIR. Atmos Measur Tech 6(5):1111–1140
9. Dube WP, Brown SS, Osthoff HD, Nunley MR, Ciciora SJ, Paris MW et al (2006) Aircraft instrument for simultaneous, in situ measurement of NO_3 and N_2O_5 via pulsed cavity ring-down spectroscopy. Rev Sci Instr 77(3)
10. Fiedler SE, Hese A, Ruth AA (2003) Incoherent broad-band cavity-enhanced absorption spectroscopy. Chem Phys Lett 371(3–4):284–294
11. Fuchs H, Dube WP, Cicioira SJ, Brown SS (2008) Determination of inlet transmission and conversion efficiencies for in situ measurements of the nocturnal nitrogen oxides, NO_3, N_2O_5 and NO_2, via pulsed cavity ring-down spectroscopy. Anal Chem 80(15):6010–6017
12. Kennedy OJ, Ouyang B, Langridge JM, Daniels MJS, Bauguitte S, Freshwater R et al (2011) An aircraft based three channel broadband cavity enhanced absorption spectrometer for simultaneous measurements of NO_3, N_2O_5 and NO_2. Atmos Measur Tech 4(9):1759–1776
13. Kercher JP, Riedel TP, Thornton JA (2009) Chlorine activation by N_2O_5: simultaneous, in situ detection of $ClNO_2$ and N_2O_5 by chemical ionization mass spectrometry. Atmos Meas Tech 2:193–204
14. Langridge JM, Ball SM, Shillings AJL, Jones RL (2008) A broadband absorption spectrometer using light emitting diodes for ultrasensitive, in situ trace gas detection. Rev Sci Instr 79(12)
15. Matsumoto J, Imagawa K, Imai H, Kosugi N, Ideguchi M, Kato S et al (2006) Nocturnal sink of NO_x via NO_3 and N_2O_5 in the outflow from a source area in Japan. Atmos Environ 40:6294–6302
16. Min KE, Washenfelder RA, Dube WP, Langford AO, Edwards PM, Zarzana KJ et al (2016) A broadband cavity enhanced absorption spectrometer for aircraft measurements of glyoxal, methylglyoxal, nitrous acid, nitrogen dioxide, and water vapor. Atmos Measur Tech 9(2):423–440
17. Nakayama T, Ide T, Taketani F, Kawai M, Takahashi K, Matsumi Y (2008) Nighttime measurements of ambient N_2O_5, NO_2, NO and O-3 in a sub-urban area, Toyokawa, Japan. Atmos Environ 42:1995–2006
18. Osthoff HD, Pilling MJ, Ravishankara AR, Brown SS (2007) Temperature dependence of the NO(3) absorption cross-section above 298 K and determination of the equilibrium constant for NO(3) + NO(2) < - > N(2)O(5) at atmospherically relevant conditions. Phys Chem Chem Phys 9(43):5785–5793
19. Osthoff HD, Sommariva R, Baynard T, Pettersson A, Williams EJ, Lerner BM et al (2006) Observation of daytime N_2O_5 in the marine boundary layer during New England air quality study—intercontinental transport and chemical transformation 2004. J Geophys Res Atmos 111(D23)
20. Schuster G, Labazan I, Crowley JN (2009) A cavity ring down/cavity enhanced absorption device for measurement of ambient NO_3 and N_2O_5. Atmos Measur Tech 2(1):1–13
21. Shardanand S, Rao ADP (1977) Absolute Rayleigh scattering cross sections of gases and freons of stratospheric interest in the visible and ultraviolet regions. NASA Technical Note
22. Slusher DL, Huey LG, Tanner DJ, Flocke FM, Roberts JM (2004) A thermal dissociation-chemical ionization mass spectrometry (TD-CIMS) technique for the simultaneous measurement of peroxyacyl nitrates and dinitrogen pentoxide. J Geophys Res-Atmos 109:Artn D19315
23. Sneep M, Ubachs W (2005) Direct measurement of the Rayleigh scattering cross section in various gases. J Quant Spectrosc Radiat Transfer 92(3):293–310
24. Varma RM, Venables DS, Ruth AA, Heitmann U, Schlosser E, Dixneuf S (2009) Long optical cavities for open-path monitoring of atmospheric trace gases and aerosol extinction. Appl Opt 48(4):B159–B171

25. Venables DS, Gherman T, Orphal J, Wenger JC, Ruth AA (2006) High sensitivity in situ monitoring of NO_3 in an atmospheric simulation chamber using incoherent broadband cavity-enhanced absorption spectroscopy. Environ Sci Technol 40(21):6758–6763
26. Voigt S, Orphal J, Burrows JP (2002) The temperature and pressure dependence of the absorption cross-sections of NO_2 in the 250-800 nm region measured by Fourier-transform spectroscopy. J Photochem Photobiol a-Chem 149(1–3):1–7
27. Wang D, Hu RZ, Xie PH, Liu JG, Liu WQ, Qin M et al (2015) Diode laser cavity ring-down spectroscopy for in situ measurement of NO_3 radical in ambient air. J Quant Spectrosc Radiat Transfer 166(23–29)
28. Wang HC, Chen J, Lu KD (2017) Development of a portable cavity-enhanced absorption spectrometer for the measurement of ambient NO_3 and N_2O_5: experimental setup, lab characterizations, and field applications in a polluted urban environment. Atmos Measur Tech 10(4):1465–1479
29. Wang T, Tham YJ, Xue LK, Li QY, Zha QZ, Wang Z et al (2016) Observations of nitryl chloride and modeling its source and effect on ozone in the planetary boundary layer of southern China. J Geophys Res-Atmos 121:2476–2489
30. Washenfelder RA, Attwood AR, Flores JM, Zarzana KJ, Rudich Y, Brown SS (2016) Broadband cavity-enhanced absorption spectroscopy in the ultraviolet spectral region for measurements of nitrogen dioxide and formaldehyde. Atmos Measur Tech 9(1):41–52
31. Washenfelder RA, Langford AO, Fuchs H, Brown SS (2008) Measurement of glyoxal using an incoherent broadband cavity enhanced absorption spectrometer. Atmos Chem Phys 8(24):7779–7793
32. Yokelson RJ, Burkholder JB, Fox RW, Talukdar RK, Ravishankara AR (1994) Temperature-dependence of the NO_3 absorption-spectrum. J Phys Chem 98(50):13144–13150

Chapter 3
Field Measurements

Abstract This chapter introduces the basic information of the comprehensive field experiment that participated by PKU-CEAS. Four comprehensive field campaigns were conducted in Beijing, which is the Huairou Winter campaign (Huairou, HR), Changping Summer campaign (Changping, CP), Peking University Summer campaign (Peking University, PKUS), and Peking University Winter campaign (PKUW). The four campaigns are ground-based measurements. This chapter systematically summarizes the meteorological conditions, chemical conditions, NO_3 and N_2O_5 concentration levels, and variations in the above four field studies.

3.1 Introduction of Field Measurements

Table 3.1 summarizes the basic situation of all field observation experiments. The period of the Huairou campaign is from January to March 2016. The site is on the top of the first teaching building of Yanqi Lake Campus, University of Chinese Academy of Sciences, Huairou District, Beijing. It is about 60 km away from the urban area of Beijing. It is a typical suburban site. The site is located in the northeast of Beijing. The site is shown in Fig. 3.1. There is no large industrial zone around the Huairou site. The Yanqi Lake is to the southwest of the site. The west and north of the campus are mountains, National Highway G111 at 120 m in the east, and Huaibei Village in the northeast. When the wind direction is west or north, the air mass mainly comes from Siberia, which is a typical background situation. When the wind direction is south or southwest, the air mass mainly comes from the air masses in the North China Plain or Beijing City. This site is an ideal site to study the regional air pollution. When the wind direction is east or northeast, it is occasionally affected by local scattered coal, biomass combustion emissions, and traffic source emissions. The main experimental instruments of this site are installed in two laboratories on the fourth floor and the top of the experimental building. The sampling height of the experimental instruments is about 20 m from the ground. In terms of NO_3 and N_2O_5 chemistry, the measured parameters are comprehensive. N_2O_5 is directly measured, and NO_3 is calculated by thermodynamic equilibrium using N_2O_5 and NO_2. Besides, it also includes the key precursors of NO_3 and N_2O_5, NO_2 and O_3, the parameters

H. Wang, *The Chemistry of Nitrate Radical (NO_3) and Dinitrogen Pentoxide (N_2O_5) in Beijing*, Springer Theses, https://doi.org/10.1007/978-981-15-8795-5_3

Table 3.1 Summary of the field campaigns in Beijing

Time	Sites	Region	Season	Longitude, latitude	
2016/01-03	Huairou (HR)	Suburban	Winter	40.41 °N, 116.68 °E	
2016/05-06	Changping (CP)	Suburban	Summer	40.22 °N, 116.23 °E	
2016/09-10	Peking University (PKUS)	Urban	Summer	39.99 °N, 116.30 °E	
2017/11-12	Peking University (PKUW)	Urban	Winter	39.99 °N, 116.30 °E	

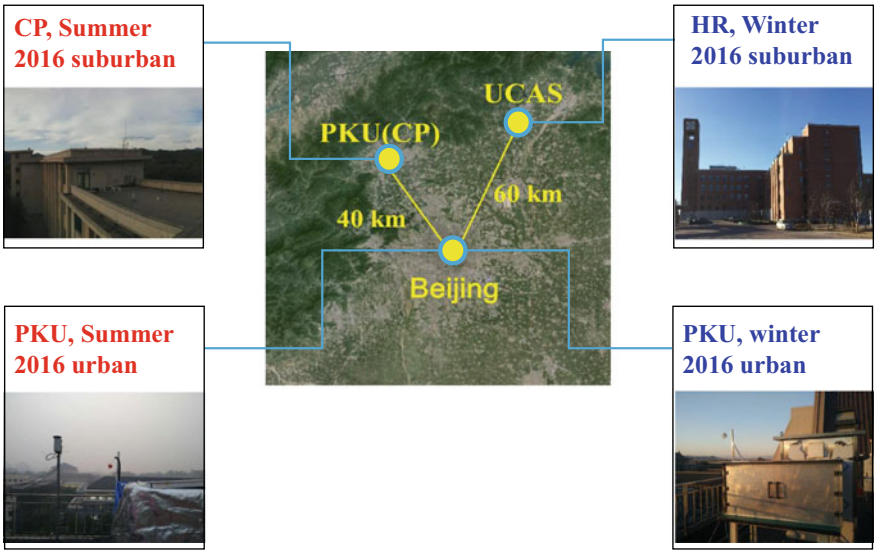

Fig. 3.1 The map of HR, CP, PKUS, and PKUW campaign sites

that affect the direct NO_3 removal process, such as NO, VOCs, RO_2; The parameters that affect the N_2O_5 uptake, such as PM concentration, number distribution, and chemical components. Based on the comprehensive experimental data collected in the field observation, we can describe the concentration level and variation of NO_3 and N_2O_5, and characterize its source and chemical removal processes. Combined with the simultaneous measurement of HO_x radicals, it is possible to analyze the NO_x removal process in winter. The parameters also include CO, SO_2, NH_3, HONO, HCHO, PAN, NO_y, meteorological, and photolysis parameters.

The relevant parameters of the synchronous measurement during the Huairou observation are summarized in Table 3.2. NO_x is measured by three measuring instruments at the same time. Two instruments from Peking University are based on the molybdenum conversion method and the photolysis conversion method, respectively. One NO_x measurement system based on the photolysis conversion method comes from Julich, Germany. O_3 is measured by ultraviolet spectrophotometry. VOCs are measured by the GC-MS/FID system, which measures 63 kinds of non-methane

Table 3.2 Lists of the observed gas and particle parameters used in this study during the HR campaign

Species	Time resolution	Limit of detection	Methods	Accuracy
N_2O_5	60 s	2.7 pptv	CEAS	±19%
NO_3 (calc)	60 s	–	Calculated	±19%
NO_2	60 s	50 pptv	Photolytic Conv. + CL	±10%
O_3	60 s	0.5 ppbv	UV	±10%
VOCs	1 h	5–70 pptv	GC-MS/FID	±10%
S_a	300 s	–	SMPS, APS	±30%
NO	60 s	50 pptv	CL	±10%
J-values	60 s	–	SR	±10%
Temperature	60 s	−50 °C–100 °C	Met One 083E	±0.1°C
HONO	300 s	10 pptv	LOPAP	±12%
HCHO	120 s	25 pptv	Hantzsch	±5%
PAN	300 s	50 pptv	GC-ECD	±10%
NH_3, SO_2, HCl, HNO_3 NH_4^+, Cl^-, NO_3^-, SO_4^{2-}	0.5 h	30–60 pptv	GAC	±10%
CO	60 s	40 ppbv	NDIR	±10%
SO_2	60 s	0.1 ppbv	UV-F	±10%
NOy	60 s	50 pptv	Mo Conv. + CL	±1%
$PM_{2.5}$	60 s	0.1 μg m^{-3}	TEOM	±5%
$PM_{1.0}$ component	300 s	0.005–0.424 μg m^{-3}	HR-ToF-AMS	±30%
OH	30 s	0.8 × 106 cm^{-3}	LIF	±11%
HO_2	30 s	0.2 × 108 cm^{-3}	LIF	±13%
RO_2	30 s	0.1 × 108 cm^{-3}	LIF	±11%
k_{OH}	90 s	0.3 s^{-1}	LP-LIF	±5–20%
Pressure	60 s	600–1100 hPa	Met One 092	±0.35 hPa
RH	60 s	0–100%	Met One 083E	±2.0%

hydrocarbon carbons in C_2-C_{12}. GAC measures soluble ionic components in particles, including NH_4^+, NO_3^-, SO_4^{2-}, Cl^- and gaseous NH_3, HCl, HNO_3, HONO [4]. AMS measures NH_4^+, NO_3^-, SO_4^{2-}, Cl^- and organic matter in $PM_{1.0}$ [3]. The mass concentration of $PM_{2.5}$ was measured using an oscillating balance method. The number size distribution of the particulate matter is measured by a combination of SMPS and APS, where SMPS measures the PM in the range of 10–700 nm, and APS measures the PM in the range of 700 nm–10 μm. The aerosol surface area is calculated from the range of 10 nm–2.5 μm and then corrected to the wet aerosol

surface area under actual atmospheric conditions by the growth factor. The measurement of HO_x, RO_2, and OH reactivity (k_{OH}) based on the LIF technique was described in detail in previous studies [10, 11]. HONO measured by a long-path absorption photometer (LOPAP) technique [9]. HCHO measured by a Hantzsch fluorescence analysis method (AL4021, Aerolaser GmbH, Germany). The photolysis reaction rate constant is calculated based on the solar flux measured by the spectro-radiometer, the absorption cross-section of the reaction molecule, and the quantum yield. Meteorological parameters (wind direction, wind speed, temperature, humidity, and atmospheric pressure) are measured using Met One's sensor meteorological measurement system.

The Changping campaign is conducted from May to June 2016. The site is selected on the roof of the teaching building of the Peking University Changping Campus in Changping District, Beijing, about 40 km from Beijing. The site is located in the northwest of Beijing and is a typical suburban site. There is no large industrial zone around the site, surrounded by mountains on both sides in the northwest, Beijing-Xinjiang Expressway at 600 m on both sides in the southwest, and Xishankou Village in the northeast. Similar to the Huairou station, when the wind direction is west or north, a typical background air mass is sampled. When the wind direction is south or southwest, the air mass mainly comes from the air masses in the North China Plain or the urban area of Beijing. The site is occasionally affected by local loose coal, biomass combustion emissions, and traffic emission. The main experimental instruments at this site are installed in the room on the fourth floor of the teaching building. The measured parameters include NO_x, O_3, CO, SO_2, NO_y, and particle number size distribution and $PM_{2.5}$ mass concentration. The soluble components of $PM_{1.0}$ are measured by AMS. The measurement methods of the key parameters during the four observation periods are summarized in Table 3.3. NO and NO_2 were

Table 3.3 Lists of the key parameters of the NO_3–N_2O_5 chemistry during the four field campaigns

	Parameters	HR-summer	CP-summer	PKU-summer	PKU-winter
Species	N_2O_5	√	√	√	√
	NO_3 (Calc)	√	√	√	√
Sources	NO_2	√	√	√	√
	O_3	√	√	√	√
Sink	VOCs (GC-MS)	√			√
	VOCs (PTR-MS)	√	√		
	NO	√	√	√	√
	S_a (SMPS)	√	√	√	√
	S_a (APS)	√	√	√	√
Others	TP	√	√	√	√
	PM (AMS)	√	√		√
	PM (ACSM)			√	
	PM (GAC)	√		√	√

only measured by the molybdenum conversion instrument; this observation has no measurement of HO_x radical parameters. The VOCs are measured using PTR-MS, including isoprene, monoterpene, styrene, benzene, etc. Besides, the I-FIGAERO-ToF-CIMS (Filter Inlet for Gas and AEROsols-Time of Flight-Chemical Ionization Mass Spectrometer) of Gothenburg University was used to simultaneously measure N_2O_5 and $ClNO_2$ [8]. The sampling tube of the experimental instrument is mainly placed on the top of the building, 15–20 m above the ground. The sampling line of PKU-CEAS is on the south side. The FIGAERO sampling line is located on the east side.

Peking University's summer campaign was carried out in September–October 2016. The site is located on the campus of Peking University, which is next to the Fourth Ring Road in Beijing. It is a typical urban site. The air mass represents the typical situation of the Beijing urban area, which is convenient for the measurement of the atmospheric chemical composition of the urban air mass. The instruments are installed in three laboratories, including two laboratories set on the sixth floor of Peking University Science Building No. 1 and one laboratory on the eighth floor. The sampling height of the sampling lines of the instruments are all higher than 20 m, and the sampling height of the eighth-floor laboratory is slightly higher than that of the sixth-floor laboratory. The measurement parameters during the summer observations of Peking University and the Huairou winter observations are similar, including the measurement of HO_x. NO, and NO_2 were measured using the molybdenum conversion method and photolysis conversion method, respectively; VOCs were measured using GC-MS/FID measurement system, measuring a total of 63 non-methane hydrocarbon molecules C_2–C_{12}.

PKU winter campaign is from November to December 2017. The site is the same as those of PKU in the summer campaign. It is worth mentioning that during the observation process, the North China region implemented strict emission reduction policies and sustained strong northerly wind weather. Compared to the same period in the past five years, air quality in the Beijing area is better during the measurement period, and $PM_{2.5}$ mass concentration level is low.

In order to facilitate a comparison of the parameters measured by the chemical analysis of NO_3 and N_2O_5 in the four campaigns, Table 3.3 summarizes the sources of NO_3 and N_2O_5, the key parameters of the removal processes, and other related auxiliary parameters. In general, the measurement of key parameters is covered in all four observations. Only the VOCs data observed in PKU (summer) campaign have not yet been finalized.

3.2 Overview of Meteorological and Chemical Conditions

The four campaigns cover summer and winter on the time scale and cover the urban and suburban areas on the spatial scale. Under different spatio-temporal conditions, there are great differences in meteorological and chemical conditions, which can provide a variety of research samples for NO_3 and N_2O_5 chemistry at night, help to

Table 3.4 The basic meteorological and chemical conditions in four filed campaigns (mean value ± standard deviation)

	HR-winter	CP-summer	PKU-summer	PKU-winter
T (°C)	−3 ± 6	23 ± 5	21 ± 3	2 ± 3
P (hPa)	1011 ± 7	–	1006 ± 4	1019 ± 5
RH (%)	35 ± 18	37 ± 15	71 ± 15	25 ± 14
NO_2 (ppbv)	11 ± 11	11 ± 9	32 ± 16	25 ± 17
O_3 (ppbv)	25 ± 13	57 ± 38	28 ± 30	15 ± 12
$PM_{2.5}$ (μg m^{-3})	27 ± 64	24 ± 20	69 ± 58	42 ± 47
Isoprene (pptv)	19 ± 20	293 ± 206	–	42 ± 36
CO (ppbv)	660 ± 860	490 ± 240	810 ± 330	650 ± 580
SO_2 (ppbv)	4 ± 5	3 ± 2	2 ± 2	4 ± 3

understand the concentration change and chemical reaction processes comprehensively. Table 3.4 summarizes the meteorological and chemical conditions during the four field observations. The differences in meteorological conditions are relatively small, but the seasonal differences are large. The average temperature of the Huairou campaign in winter is the lowest, only −3 °C, and the temperature level of Changping campaign in summer and Peking University campaign are similar. The relative humidity shows a trend of high in summer and low in winter, and the average relative humidity during the winter campaign of Huairou and Peking University is less than 40%. The average relative humidity observed in Changping in summer is 37%, while the average relative humidity observed in Peking University in summer is as high as 71%. Changping campaign is from May to June, and the summer campaign in Peking University is from September to October, with small seasonal differences.

In terms of chemical conditions, NO_2 and O_3 are the key precursors of NO_3 and N_2O_5. The average concentration of NO_2 and O_3 in the four observations is larger than 10 ppbv, which reflects the basic characteristics of high NO_x and O_3 in North China. The NO_2 concentration level has obvious NO_x emission source characteristics. No matter in summer or winter, the NO_2 concentration level in urban areas is more than double that in suburban areas. Affected by the difference in seasonal photochemical conditions, the concentration of O_3 in summer is significantly higher than that in winter. The level of O_3 in the Changping campaign is larger than the Huairou campaign.

The particle pollution from the southern air mass was occasionally observed in Huairou campaign. The average mass concentration of $PM_{2.5}$ during the entire observation period was low, with 27 μg m^{-3}. During the summer campaign in Changping, ozone was the mainly pollutants, and the average mass concentration of $PM_{2.5}$ was only 24 μg m^{-3}. The particulate matter pollution observed by Peking University in summer is serious, with an average $PM_{2.5}$ concentration level of 69 μg m^{-3}. During the winter observation at Peking University, a series of the most stringent emission limitation policies were implemented. At the same time, the meteorological conditions were a favor to flush the pollution. The cumulative effect of pollutants

is not obvious so that the particle concentration during the observation period is only 42 $\mu g\ m^{-3}$, which is much lower than the particle concentration level of winter in previous years. Isoprene is a typical biogenic VOCs, which is an indicator of biological source emissions. Due to the influence of temperature and light radiation intensity, the concentration level of summer is much higher than that of winter. The average concentration of isoprene was 293 pptv in the Changping campaign, while during Huairou campaign was only 19 pptv. CO and SO_2 mainly come from the primary emission process, including the process of burning loose coal and industrial production. Since 2013, China has implemented strict SO_2 emission control, resulting in a rapid decline in SO_2 emissions. The average concentration of SO_2 during the four observations was below 5 ppbv. The average concentration of CO observed in the summer of Peking University is 810 ppbv, which is greater than the measurement results of Huairou and Changping campaigns. Due to the impact of emission reduction, the winter observations at Peking University have an average CO concentration of 650 ppbv, which is equivalent to the average CO concentration measured by Huairou in 2016.

3.3 Overview of NO_3 and N_2O_5

3.3.1 Huairou Winter Campaign

The measurement of the Huairou campaign was divided into two parts. For N_2O_5, the effective measurement period for the first part is from January 13 to February 2, 2016. The second part is from February 19 to March 5, 2016. The gap is due to the holiday of the Spring Festival. Figures 3.2 and 3.3 shows the time series of N_2O_5 and related parameters in the two parts of the measurement period, respectively. The first part of the measurement process caused the data to be missing for three days due to the failure of the instrument's light source system, and the observed N_2O_5 for a total of 32 days is valid. The meteorological conditions were low temperature and low humidity throughout the observation period.

When the mass concentration of $PM_{2.5}$ is lower than 40 $\mu g\ m^{-3}$, the air masses usually dominated by northwest winds. At this time, O_3 often shows a background concentration level of about 40 ppbv. The nighttime N_2O_5 concentration peak of the background clean air mass is usually between 100 and 300 pptv. Under this condition, the N_2O_5 concentration level is usually affected by the low NO_2 concentration, which limits NO_3 production, such as the night of February 22 and February 23. When the mass concentration of $PM_{2.5}$ is higher than 40 $\mu g\ m^{-3}$, it is usually dominated by southerly or southwesterly winds, and the air masses from the south carry a large amount of primary and secondary pollutants, accompanied by high relative humidity. Because the observation site is far away from the urban area, the air mass has sufficient reaction time in the transport period. Under this wind direction, the concentration of N_2O_5 presents two situations, that is, a high concentration level of N_2O_5 under

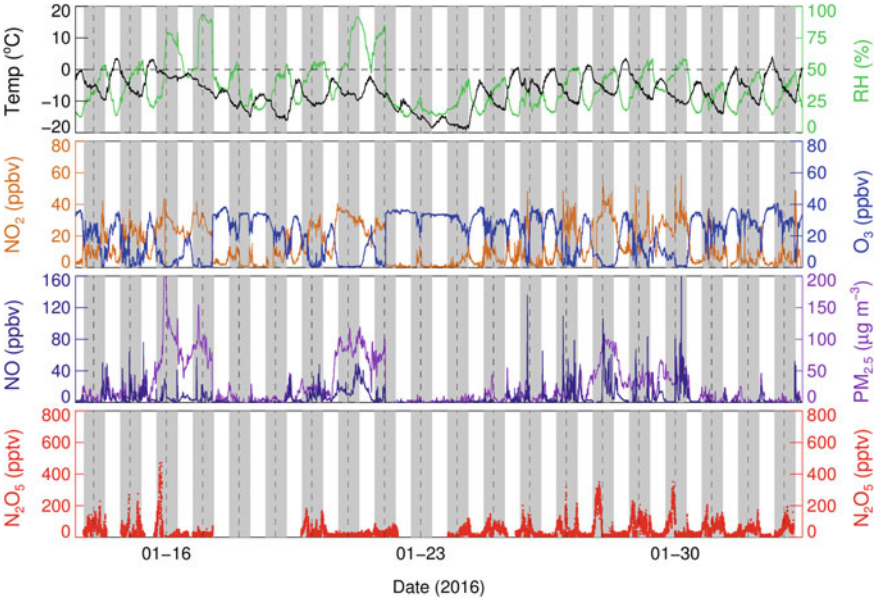

Fig. 3.2 Time series of N_2O_5 and other relevant parameters in the HR site (2016/01/13-2016/02/02)

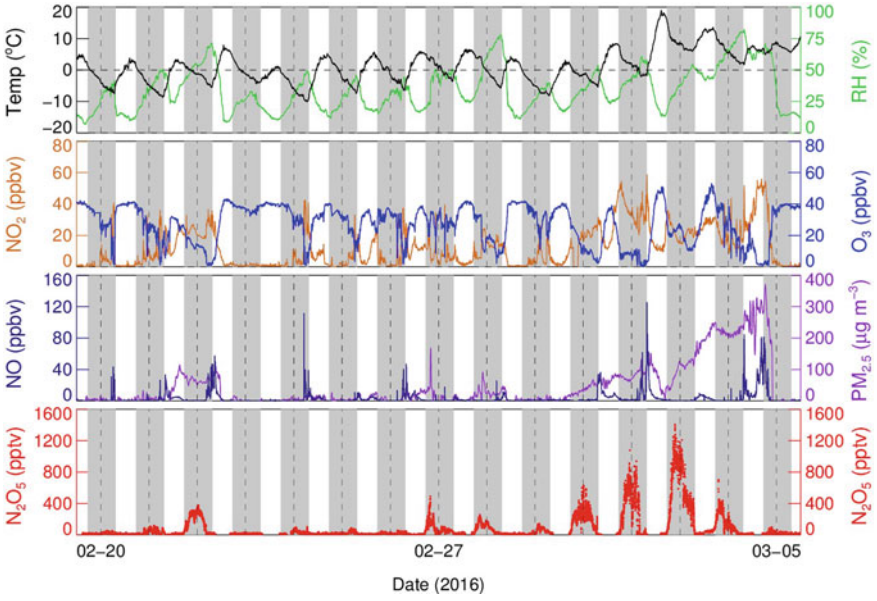

Fig. 3.3 Time series of N_2O_5 and other related parameters in the HR site (2016/02/19-2016/03/15)

low NO conditions (aged air masses); under high NO conditions, N_2O_5 is below the detection limit of the instrument (influenced by NO injection). When NO emitted from the urban area is completely oxidized by O_3 during the transport process, the high NO_2 is mixed with the O_3 in the background area, led to a fast production rate of NO_3. The concentration of N_2O_5 is much higher than the concentration level under the background air mass, such as the night of February 22, and the continuous pollution process from February 29 to March 5. When the NO concentration in the air mass is excessive, O_3 is depleted during the transport process. At this time, the formation of NO_3 is limited by low O_3, and the generated NO_3 suppressed by a high NO, resulting in the concentration of N_2O_5 being lower than the instrument detection limit. This situation occurred at night of January 16 and January 20. Some nights showed rapid switching between the two scenarios. For example, when O_3 suppresses NO in the first half of the night, higher N_2O_5 can be observed, but excessive NO exhausts O_3 in the middle of the night, the NO suppressed the NO_3 and N_2O_5 formation. High concentrations of N_2O_5 were observed in the first half of the night on January 15, January 27 and January 29. However, N_2O_5 suppressed by NO in the second half of the night, and the concentration was below the detection limit.

In the first part of the observation, the pollution process is often accompanied by the appearance of high concentrations of NO, and it has been observed many times that the short-term NO peak interferes with N_2O_5, which may come from the emission of traffic sources near the site. On the other hand, there was no continuous heavy pollution process in the first part of the stage. During the second-stage measurement process, there is less time to be interfered with by NO. February 29–March 4 is a long-term continuous pollution process. The continuous pollution process began at noon on February 29, and the concentration of particulate matter continued to rise, reaching 100 $\mu g\ m^{-3}$ at noon on March 2. On March 4, it reached a peak in the afternoon, with a maximum concentration of about 360 $\mu g\ m^{-3}$, and then the wind direction changed to the northwest wind to remove pollutants quickly. During this pollution, the concentration of N_2O_5 at night continued to be above 500 pptv, and the peak value could reach 1.4 ppbv.

3.3.2 Changping Summer Campaign

During the Changping campaign, the effective measurement time of N_2O_5 was from May 23 to June 5, 2016. Valid data have a total of 13 days. Figure 3.4 shows the time series of N_2O_5 and related measurement parameters during the observation period in Changping. From May 23 to May 27, the northwest wind is dominant, that is, the continuous cleaning process. Subsequent periods were dominated by southerly and southwesterly winds, and the air masses from southern urban areas were observed. The O_3 concentration of the background air mass is 60 ppbv, while the air mass from the urban area to the site presents serious O_3 pollution. The particle mass concentration is light with the $PM_{2.5}$ concentration is usually 30–80 $\mu g\ m^{-3}$.

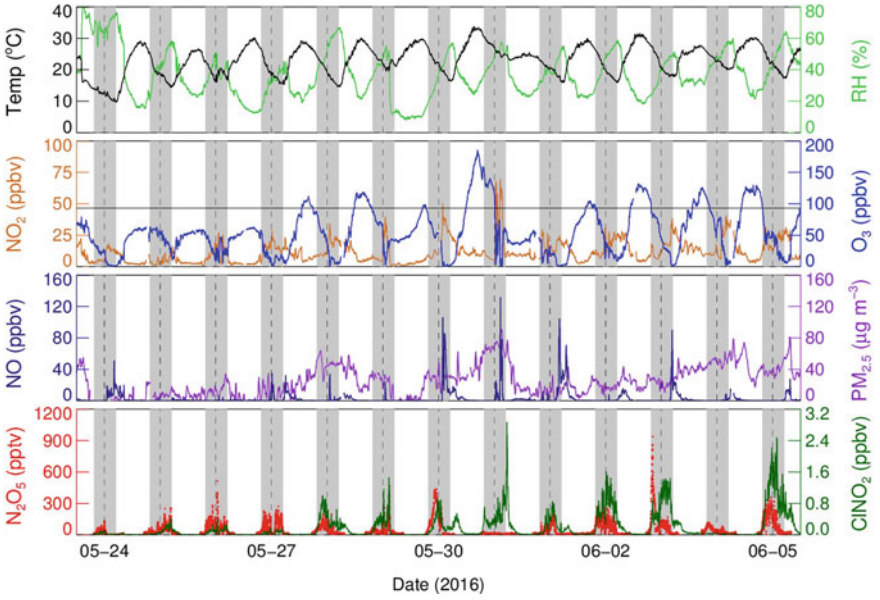

Fig. 3.4 Time series of N_2O_5, $ClNO_2$, and other related parameters in CP. The black line in the O_3 panel denotes Chinese national air quality standard for O_3 (ca. 93 ppbv)

The nighttime concentration of N_2O_5 in the background air mass is often lower than 300 pptv. It can be observed that NO injection in the night air mass causes the NO_2 concentration to continue to rise, causing an increase of N_2O_5. The concentration of NO_2 and O_3 in the urban polluted air mass transported in the south is higher than that of the background air mass, making the overall concentration of N_2O_5 higher than the background air mass. The N_2O_5 peak at night on June 2 was 937 pptv. During the observation period, the CIMS simultaneously observed significant $ClNO_2$ at night, which can reach a maximum of 2.9 ppbv, and the concentration of $ClNO_2$ in urban areas dominated by the south wind was significantly higher than that of the background air mass. It is worth mentioning that the phenomenon of $ClNO_2$ peaking after early sunrise was frequently observed, which can reach a maximum of 0.55 ppbv, which is consistent with the previous observations in London, Kansas, and Wangdu, China [1, 5, 13]. Due to the rapid photolysis of NO_3 and N_2O_5 after sunrise, the concentration of N_2O_5 is very low, and the near-ground $ClNO_2$ cannot be generated locally. Tham et al. found that a high concentration of $ClNO_2$ may come from the formation of a high-altitude residual layer at night. After the boundary layer is decoupled in the morning, it is transported vertically downward [13].

The molybdenum conversion (Mo) method measures NO_2 by using the following principle that NO_2 is converted to NO in a 325 °C molybdenum conversion furnace and then reacts with O_3 to generate chemiluminescence. Part of NO_z, such as PAN and HNO_3, will also be catalyzed when measuring NO_2 by Mo method. The interferences make the measured NO_2 by Mo method higher than the actual NO_2. Overall,

the photolysis method (chemiluminescence, CL) is relatively accurate. During the Changping campaign, NO_2 used molybdenum conversion measurement technology. As Changping is located in the downwind direction of urban areas, the air mass is relatively aging, and the NO_z content may be higher, so it may have a great interference with the NO_2 measurement. During the Wangdu observation period, NO_x was measured using molybdenum conversion and photolysis technology. Both the two observation periods are between May and July, and the chemical conditions are similar. As shown in Fig. 3.5b, O_3 at the two sites is relatively consistent in concentration level and change trend. In order to eliminate the interference of NO_z. The campaign of the Wangdu site was carried out in June 2014 in Wangdu, Hebei Province. This site is a typical regional pollution site in North China. It is located in the downwind direction of the southern urban pollution zone. It is similar to the Changping air mass. For details, please refer to [12]. In the Wangdu campaign, the ratio of NO_2 measured by the photolysis method to NO_2 measured by the molybdenum conversion method is stable at about 0.75 at night (Fig. 3.5a). There is a groove during the day, which corresponds to the peak value of O_3 during the day, indicating that O_3 oxidation promotes the formation and increase of NO_z and case interference of NO_2 measurement when using molybdenum conversion technology. At the same time, the NO_2 concentration during the day can also be estimated based

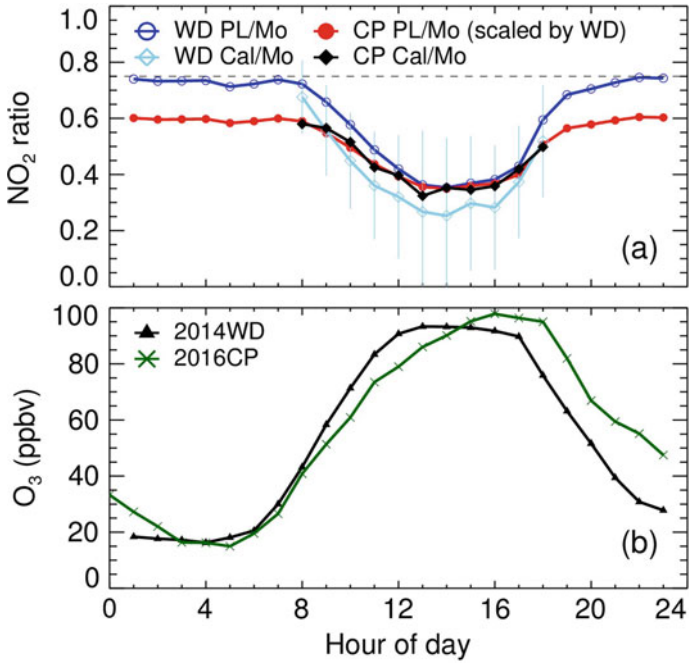

Fig. 3.5 **a** Shows the mean diurnal variation ratio of NO_2 measured by PL method or calculated by the steady-state method, to that measured by Mo convert method in Wangdu and Changping campaigns; **b** shows the mean diurnal variation of O_3 in Wangdu and Changping campaigns

on the measured NO and O_3 and $J(NO_2)$ based on the photo-chemical steady-state method (abbreviated as Cal), the calculation formula in Eq. (3.1).

$$[NO_2] = \frac{k_{NO+O3}[NO][O_3]}{J(NO_2)} \tag{3.1}$$

The ratio of Cal/Mo and PL/Mo of NO_2 in the Wangdu campaign has a good consistency, which shows that the daytime photo-steady state and photolysis method has a good consistency in NO_2 measurement. The result is reflecting the accuracy of photolysis measurement technology. The result indicates that the overestimation of NO_2 by the molybdenum conversion method is large. Since the photo-chemical steady-state is only valid during the day, it is impossible to correct the NO_2 measurement results at night. In order to evaluate the deviation of the Mo method measured in Changping, the PL/Mo diurnal variation was scaled and linearly fitted with Changping Cal/Mo during the daytime. The fitted Changping PL/Mo curve was extended in the nighttime. The scaled Cal/Mo is 0.6, indicating that the NO_2 measurement results at night in Changping are overestimated by 67%. Therefore, in the subsequent analysis, the nighttime NO_2 concentration is multiplied by 0.6 to correct the data (the NO_2 time series in Fig. 3.4 is the corrected result). As the air mass in the campaign is fluctuant, this correction may cause a large uncertainty. The error propagation shows that the uncertainty of NO_2 is 45%, and the uncertainty of the measurement of NO_2 is 20%. Therefore, the total uncertainty of NO_2 in the Changping summer campaign is 50%.

3.3.3 PKU Summer Campaign

During the PKU summer campaign, the measurement of N_2O_5 is from September 11 to October 3, 2016. Valid data has a total of 18 days. From September 25 to 29, the instrument was malfunctioning. Figure 3.6 shows the time series of N_2O_5 and related measurement parameters during the PKU summer campaign. The meteorological conditions were high temperature and high relative humidity, and there were scattered rainfall processes on September 17–19. The big difference from the observation of Changping is that the O_3 pollution process is often accompanied by simultaneous particulate matter pollution. During the observation period, the O_3 concentration reached 120 ppbv, and the $PM_{2.5}$ concentration can reach 240 $\mu g\ m^{-3}$. The daily variation of NO_2 and O_3 concentration is clear. The NO_2 concentration is low during the day and high at night. The O_3 concentration reaches the maximum in the afternoon and then starts to fall. After sunset, O_3 is quickly consumed by the impact of NO emissions and is usually runs out at midnight. NO suppressed by high O_3 in the first half of the night but began to accumulate a high value after O_3 exhausted in the middle of the night. The night-time NO–NO_2–O_3 chemical process with a strong diurnal variation pattern makes the N_2O_5 concentration in the Beijing urban area very regular. After sunset, the high precursor concentration level causes the N_2O_5 concentration

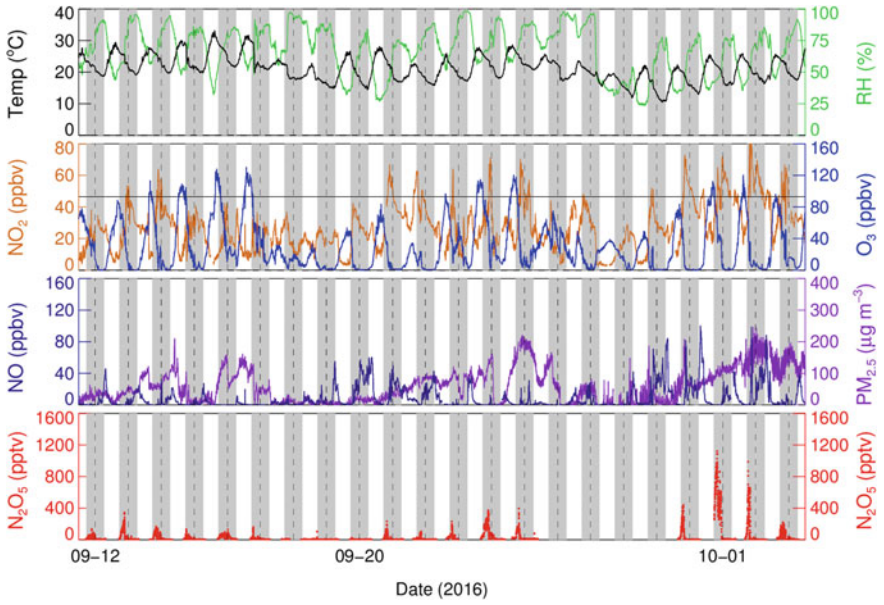

Fig. 3.6 Time series of N_2O_5 and other relevant parameters in the PKU summer campaign. The black line in the O_3 panel denotes Chinese national air quality standard for O_3

to rise rapidly and reach a peak within a few hours, subject to the removal process and the rapid NO_3 production rate. N_2O_5 drops rapidly after reaching the peak, and then quickly drops to 0 in the first half of the night. Similar to the Huairou campaign in winter, high N_2O_5 occurs during heavy pollution episodes. The maximum value is 1.3 ppbv under the 5 s integration time and 1.07 ppbv under the 5 min integration time.

3.3.4 PKU Winter Campaign

During the PKU winter observation period, the measurement N_2O_5 is from November 17 to January 3, 2017. The data is continuous, and the valid data totals 48 days. Figure 3.7 shows the time series of N_2O_5 and related measurement parameters during the PKU winter campaign. The meteorological conditions during the observation period are mainly manifested as low temperature and low humidity. The relative humidity is about 20% on clean day. The relative humidity accumulates during particulate matter pollution and rises quickly. This observation period coincides with the implications of the national air pollution control with a series of strict emission restriction policies. During the campaign, the $PM_{2.5}$ concentration level showed a very regular periodic change, that is, the process of cleaning-pollution-accumulation-cleaning. The concentration level and duration of heavy pollution have appeared a

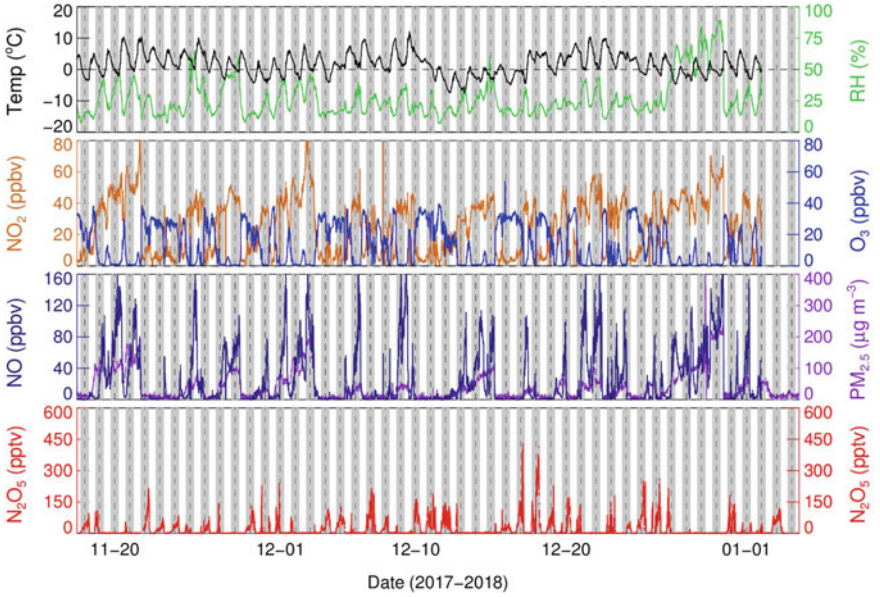

Fig. 3.7 Time series of N_2O_5 and other related parameters in PKU winter campaign

certain decline [7]. On the clean period, the concentration of O_3 is 40 ppbv, and the concentration of O_3 in the pollution process drops significantly. NO_x concentration is low in clean days and accumulation in polluted days. Affected by NO_x, the N_2O_5 concentration in the polluted days is suppressed by high NO, which is always lower than the detection limit of the instrument. In contrast, the NO_3 production rate is limited by the low NO_2 on a clean day. Therefore, the elevated N_2O_5 was observed in clean days. Due to the relatively small removal rate of NO_3 and N_2O_5 on a clean day, N_2O_5 will continue to accumulate throughout the night, thus appearing to peak before the next sunrise. The peak concentration of N_2O_5 during this observation period was relatively low, only 375 pptv.

3.4 Spatial and Temporal Variation

3.4.1 Diurnal Variation

Figure 3.8 shows the average daily change of N_2O_5 in four comprehensive field observation experiments. All the nocturnal N_2O_5 observed in Huairou, Changping, and PKU (summer) showed a single-peak distribution, and only PKU (winter) N_2O_5 showed a double-peak distribution. The diurnal variation of N_2O_5 in the two suburban sites of Huairou and Changping was the most consistent. N_2O_5 began to accumulate

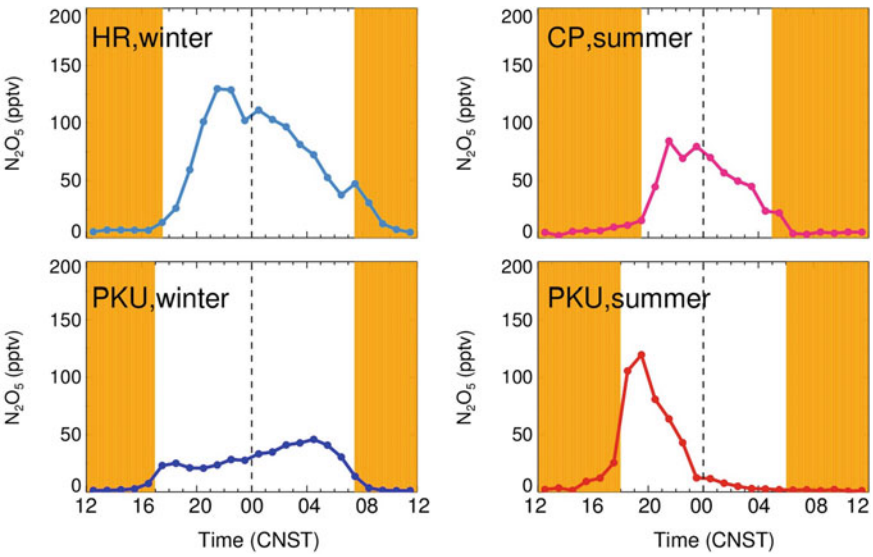

Fig. 3.8 Mean diurnal variations of N_2O_5 in four campaigns, the orange region represent daytime

gradually around sunset, and the concentration gradually increased, reaching a peak at night around 21:00. The average night peak observed by Huairou was 130 pptv, and the average peak observed by Changping was 84 pptv. Subsequently, N_2O_5 gradually decreased until sunrise, due to the photolysis reaction of N_2O_5 and NO_3, it rapidly decreased to below the detection limit of the instrument.

The summer and winter observations at PKU have their characteristics, and they are quite different from those in the suburbs. In the PKU winter campaign, the formation of a small peak of N_2O_5 around 18:00, the peak is 25 pptv. Then there was a weaker fall, and then it continued to accumulate from around 20:00 until it reached a peak around 05:00 the next day and began to decline. It was below the detection limit of the instrument after the beginning of the day. The average peak value at night was 46 pptv, mainly due to the continuous clean weather led to relatively good diffusion conditions, NO_2 concentration was difficult to accumulate to a high value, and N_2O_5 concentration accumulated overnight. The changes in the concentration of N_2O_5 observed at the PKU site in winter shows a typical clean atmospheric condition.

The summer N_2O_5 concentration at the PKU site showed a typical trend of N_2O_5 in highly polluted areas. After sunset, a high concentration of precursors caused N_2O_5 to rapidly generate and accumulate to a high value, with an average peak value of 120 pptv. Because O_3 is rapidly titrated by a large amount of NO, and due to the presence of reactive NO_3 and N_2O_5 removal pathways, N_2O_5 falls rapidly within the next four hours. It falls below the detection limit of the instrument around midnight. Although the relatively high concentration of N_2O_5 in urban areas in summer lasted a short time during the night than that in other seasons and regions, the rapid source

and removal flux make its impacts of atmospheric chemistry can not to be ignored (more details in Chaps. 4 and 5).

The NO_3 concentration at night can be calculated through the thermodynamic equilibrium between NO_2–NO_3–N_2O_5. Although the equilibrium of NO_3 and N_2O_5 is easily broken at the early sunset and after sunrise, the thermal equilibrium during most of the night is established and verified in field observations [2]. Under winter conditions, the time to reach equilibrium is long; the calculation uncertainty of NO_3 is relatively large. Figure 3.9 shows the average diurnal variation of NO_3 calculated from the four campaigns. NO_3 has a very obvious diurnal variation, similar to that of N_2O_5. The concentration level of NO_3 is much lower than N_2O_5. The peaks of NO_3 observed in Huairou, Changping, and PKU summer campaign appeared in the first half of the night. Only the NO_3 peak of the PKU winter campaign appeared in the second half of the night. The average peak NO_3 concentration in winter is less than 2 pptv, which limits the atmospheric chemical significance of NO_3 in winter. The NO_3 concentration calculated by Changping observation is the most significant, and the peak daily average night concentration can reach 20 pptv. The NO_3 concentration calculated in the PKU summer campaign is relatively low, with a peak average daily night of 6 pptv.

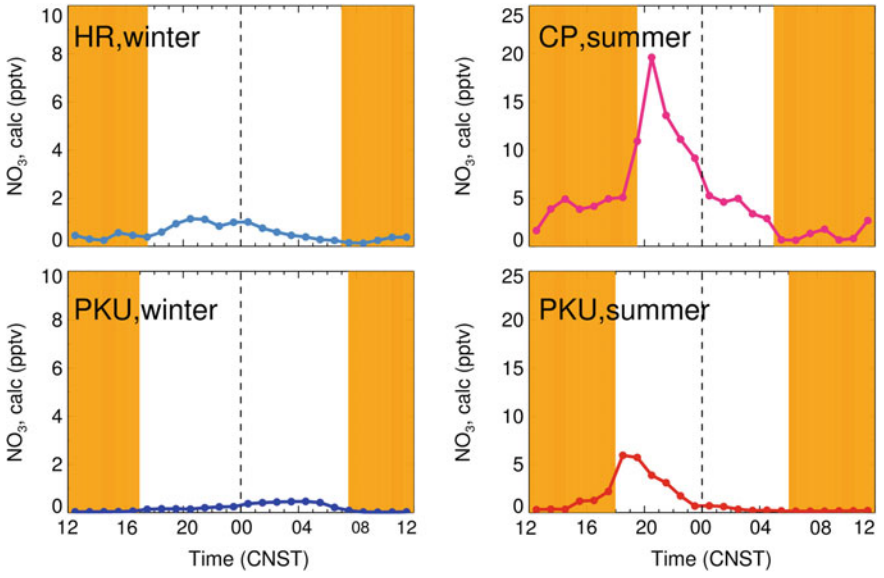

Fig. 3.9 Mean diurnal variations of calculated NO_3 based on the thermal equilibrium between NO_3 and N_2O_5 and the measured N_2O_5 in four field campaigns, the orange region represent daytime

Table 3.5 The campaign average of nocturnal N_2O_5 and calculated NO_3 based on thermal equilibrium (mean value ± standard deviation)

Campaign	NO_3 (pptv)	N_2O_5 (pptv)
CP	8.6 ± 12.7	69 ± 88
PKU-summer	2.1 ± 4.3	46 ± 116
HR	0.7 ± 1.7	89 ± 150
PKU-winter	0.3 ± 0.6	32 ± 43

3.4.2 Seasonal and Spatial Variation

Table 3.5 summarizes the nighttime average concentration levels of NO_3 and N_2O_5 from four campaigns. The average nighttime level of NO_3 is Changping > PKU Summer > Huairou > PKU Winter. The summer NO_3 concentration in Beijing is similar to the coastal areas in Greece and Lindenberg in the German mainland in summer [6, 14]. The NO_3 concentration level is high in summer and low in winter. From 2001 to 2003, the continuous observation of NO_3 free radicals in the Mediterranean area for two years found that the concentration levels in summer and winter were 5.6 pptv and 1.2 pptv, respectively. However, the seasonal differences reported in this article are large, and the NO_3 level in summer is about an order of magnitude higher than winter [15]. From a regional perspective, the suburbs are larger than the urban areas. More precisely, the downwind areas of the cities are larger than the urban areas. However, the magnitude of regional differences in NO_3 concentration is smaller than seasonal differences.

The concentration level of N_2O_5 is Huairou > Changping > PKU Summer > PKU Winter. There are certain differences between urban and suburban areas. As far as the suburbs are concerned, the N_2O_5 observed in Huairou in winter is higher than the N_2O_5 concentration in Changping in summer; in the case of PKU campaign, the concentration in summer is higher than that in winter. From a regional perspective, suburban N_2O_5 is significantly larger than urban areas. Overall, the seasonal difference of NO_3 is large, and the seasonal and regional variation of N_2O_5 is small.

Figure 3.10 shows the seasonal distribution of NO_3 and N_2O_5 in Beijing and the regional distribution of urban suburbs. Temperature levels are used to represent seasonal differences, and high temperatures represent summer, and low temperatures represent winter. The concentration level of NO_2 is used to represent the difference between urban and suburban areas. High NO_2 represents urban areas, and low NO_2 represents suburban areas. The radius indicates the average concentration of NO_3 and N_2O_5 at night during each observation. It shows that the NO_3 concentration level is dominated by seasonal changes, and summer is much higher than winter. N_2O_5 is a large difference between urban and suburban areas, with suburban areas being larger than urban areas. However, the seasonal difference of N_2O_5 is not obvious. In the suburbs, the N_2O_5 level in winter is greater than that in urban areas, and in urban areas, the N_2O_5 level in summer is greater than that in winter.

The concentration distribution of NO_3 and N_2O_5 is a manifestation of the relative changes in its source and sink, and it is also greatly affected by the thermodynamic

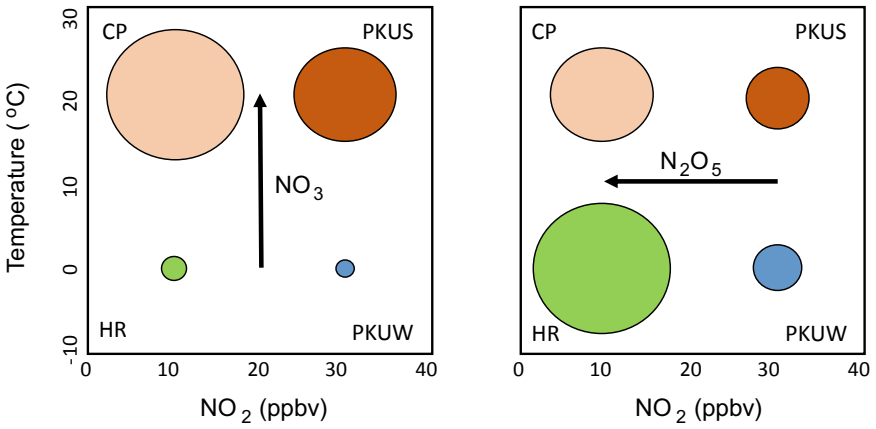

Fig. 3.10 The pictorial plot of seasonal and regional variations of calculated NO_3 and the measured N_2O_5 in Beijing, the radius represent the NO_3 or N_2O_5 concentration

equilibrium. In essence, seasonal differences are mainly reflected in temperature, and O_3 concentration levels and urban and suburban differences are reflected in NO_2 concentration levels. The common differences caused by the two dimensions also include seasonal changes in VOCs and changes in N_2O_5 heterogeneous reaction rate, and so on. Overall, temperature and NO_2 concentration levels are important indicators to describe the distribution of NO_3 and N_2O_5.

3.5 Summary

This chapter mainly introduces the basic situation of four comprehensive field observation experiments, including the introduction of campaign sites, parameters for simultaneous measurement, and instruments. The four field observations have comprehensive coverage from the two dimensions of regional scale and seasonal scale. The regional scale includes urban and suburban areas, and the seasonal scale includes summer and winter. PKU-CEAS was used to obtain high-quality N_2O_5 data in the above four campaigns, which were used to systematically describe the concentration levels and changes of NO_3 and N_2O_5. The measurement results show that the concentration of N_2O_5 is significant. The average night-time concentration in Beijing is 10–100 pptv, and the peak night-time level is usually between 100 and 1500 pptv. The difference between the suburbs and the suburbs is obvious, and the suburbs are significantly larger than the urban areas. The seasonal differences are not uniform. The urban area shows that the N_2O_5 concentration level is higher in summer than winter, and the suburbs show that N_2O_5 in winter is greater than that in summer. Concerning the average diurnal variation, most cases show a single-peak distribution. The peak usually appears about 2 h after sunset.

Based on thermodynamic equilibrium calculations, it is found that the average nighttime NO_3 concentration level is between 0.1 and 10 pptv, and the peak nighttime level is usually between 10 and 100 pptv. The concentration level has a large seasonal difference, NO_3 in summer is significantly higher than that in winter. The difference in the suburban scale is consistent with N_2O_5. That is, NO_3 in the suburbs is larger than that in the urban areas. The diurnal variation is relatively consistent with N_2O_5. The temperature in the second half of the night is low, and the concentration of NO_2 is high. The thermodynamic equilibrium favors N_2O_5, results in the difference of NO_3 between the first and the second half of the night. The seasonal and regional distribution of NO_3 and N_2O_5 are difficult to characterize with a certain factor, but NO_2 and temperature are important indicators that can describe such changes. N_2O_5 is more sensitive to NO_2 changes, while NO_3 is more sensitive to temperature changes.

References

1. Bannan TJ, Booth AM, Bacak A, Muller JBA, Leather KE, Le Breton M et al (2015) The first UK measurements of nitryl chloride using a chemical ionization mass spectrometer in central London in the summer of 2012, and an investigation of the role of Cl atom oxidation. J Geophys Res Atmos 120(11):5638–5657
2. Brown SS, Stark H, Ravishankara AR (2003) Applicability of the steady state approximation to the interpretation of atmospheric observations of NO_3 and N_2O_5. J Geophys Res-Atmos 108:Artn 4539
3. DeCarlo PF, Kimmel JR, Trimborn A, Northway MJ, Jayne JT, Aiken AC et al (2006) Field-deployable, high-resolution, time-of-flight aerosol mass spectrometer. Anal Chem 78(24):8281–8289
4. Dong HB, Zeng LM, Hu M, Wu YS, Zhang YH, Slanina J et al (2012) Technical Note: the application of an improved gas and aerosol collector for ambient air pollutants in China. Atmos Chem Phys 12(21):10519–10533
5. Faxon CB, Bean JK, Hildebrandt Ruiz L (2015) Inland concentrations of Cl-2 and $ClNO_2$ in Southeast Texas suggest chlorine chemistry significantly contributes to atmospheric reactivity. Atmosphere 6(10):1487–1506
6. Geyer A, Ackermann R, Dubois R, Lohrmann B, Muller T, Platt U (2001) Long-term observation of nitrate radicals in the continental boundary layer near Berlin. Atmos Environ 35:3619–3631
7. Guo S, Hu M, Zamora ML, Peng JF, Shang DJ, Zheng J et al (2014) Elucidating severe urban haze formation in China. P Natl Acad Sci USA 111:17373–17378
8. Le Breton M, Hallquist AM, Pathak RK, Simpson D, Wang YJ, Johansson J et al (2018) Chlorine oxidation of VOCs at a semi-rural site in Beijing: significant chlorine liberation from $ClNO_2$ and subsequent gas- and particle-phase Cl-VOC production. Atmos Chem Phys 18:13013–13030
9. Li X, Rohrer F, Hofzumahaus A, Brauers T, Haseler R, Bohn B et al (2014) Missing gas-phase source of HONO inferred from Zeppelin measurements in the troposphere. Science 344(6181):292–296
10. Lou S, Holland F, Rohrer F, Lu K, Bohn B, Brauers T et al (2010) Atmospheric OH reactivities in the Pearl River Delta—China in summer 2006: measurement and model results. Atmos Chem Phys 10(22):11243–11260
11. Lu KD, Rohrer F, Holland F, Fuchs H, Bohn B, Brauers T et al (2012) Observation and modelling of OH and HO_2 concentrations in the Pearl River Delta 2006: a missing OH source in a VOC rich atmosphere. Atmos Chem Phys 12(3):1541–1569

12. Tan Z, Fuchs H, Lu K, Hofzumahaus A, Bohn B, Broch S et al (2017) Radical chemistry at a rural site (Wangdu) in the North China Plain: observation and model calculations of OH, HO_2 and RO2 radicals. Atmos Chem Phys 17(1):663–690
13. Tham YJ, Wang Z, Li QY, Yun H, Wang WH, Wang XF et al (2016) Significant concentrations of nitryl chloride sustained in the morning: investigations of the causes and impacts on ozone production in a polluted region of northern China. Atmos Chem Phys 16(23):14959–14977
14. Vrekoussis M, Kanakidou M, Mihalopoulos N, Crutzen PJ, Lelieveld J, Perner D et al (2004) Role of the NO_3 radicals in oxidation processes in the eastern Mediterranean troposphere during the MINOS campaign. Atmos Chem Phys 4:169–182
15. Vrekoussis M, Mihalopoulos N, Gerasopoulos E, Kanakidou M, Crutzen PJ, Lelieveld J (2007) Two-years of NO_3 radical observations in the boundary layer over the Eastern Mediterranean. Atmos Chem Phys 7:315–327

Chapter 4
NO_3 Reactivity and N_2O_5 Uptake Coefficient

Abstract Here, ambient NO_3 reactivity is quantified and characterized, the biogenic VOCs dominates NO_3 reactivity during summertime. Ambient N_2O_5 heterogeneous uptake coefficient is derived and predicted by several parameterization schemes. Existing parameterizations are unable to fully predict the variation in N_2O_5 uptake coefficients in Beijing, the key control factors of N_2O_5 uptake processes are discussed.

4.1 NO_3 Production Rate

The formation pathways of NO_3 is summarized in Chap. 1. The night chemical reaction process of NO_3 and N_2O_5 mainly comes from the reaction of NO_2 and O_3. Other reaction channels are limited by the concentration levels of O^1D and OH radicals at night. The reaction rate constant of this reaction channel is greatly affected by temperature. At 298 K, the reaction rate constant of $NO_2 + O_3$ is 3.5×10^{-17} molecule^{-1} s^{-1}, while at 273 K, the reaction rate constant is only 1.6×10^{-17} molecule^{-1} s^{-1}. The concentration levels of NO_2 and O_3 affect the production rate largely. NO_2 and O_3 are the main pollutants in urban areas. The high intensity of emissions during the day and the accumulation of photochemical pollution of NO_2 and O_3 will make the NO_3 chemical reaction continue the fast oxidation removal process at night. The literature showed that the NO_3 production rate has a large regional difference, increasing from <0.01 ppbv h^{-1} in the background area to more than 10 ppbv h^{-1} in the urban area, spanning four orders of magnitude [13]. In the Los Angeles area, it was once observed that the NO_3 production rate was as high as 57 ppbv h^{-1}, and the NO_3 concentration level could be as high as 355 pptv. This difference in the production rate directly reflects the NO_x removal capacity of the NO_3 chemical process at night [22].

The high NO_x and O_3 in urban areas lead to a high NO_3 production rate. Figure 4.1 shows the comparison of the average production rates of these four campaigns and other large urban areas around the world. Among them, the Changping, PKU summer, Huairou, and PKU winter campaign observed the NO_3 production rates at night were 1.26, 1.92, 0.18, 0.20 ppbv h^{-1}, respectively. The production rate in summer is much

H. Wang, *The Chemistry of Nitrate Radical (NO_3) and Dinitrogen Pentoxide (N_2O_5) in Beijing*, Springer Theses, https://doi.org/10.1007/978-981-15-8795-5_4

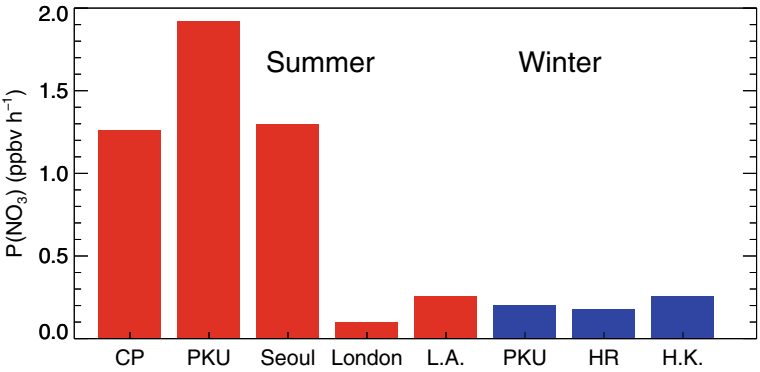

Fig. 4.1 Summary of nocturnal average NO_3 production rate, the red bar represents summer, and the blue bar represents winter

higher than that in winter in Beijing. The NO_3 production rate in Beijing in summer is the same level as that in Wangdu, where the average NO_3 production rate was 1.70 ppbv h^{-1} [25]. The average NO_3 production rate observed at the top of Mount Taishan in Shandong Province can also reach 0.45 ppbv h^{-1} [29]. The rate of NO_3 production in the Seoul area is comparable to the situation in the Beijing area of China and is 5–10 times higher than that in the London and Los Angeles areas (recently case). The winter NO_3 production rate in Beijing is slightly lower than that in Hong Kong, mainly due to the higher winter temperature in Hong Kong (>5 °C). However, the overall level is similar to that of London and Los Angeles in summer. The high NO_3 production rate in China potentially reflects the strong nighttime atmospheric oxidation capacity. Due to the large seasonal temperature difference, the ratio of N_2O_5/NO_3 in winter is more than 10 times higher than that in summer, and the difference in concentration distribution ratio leads to the N_2O_5 chemical process in winter more important.

4.2 NO_3 Reactivity

Despite the high NO_x and O_3 concentration levels lead to NO_3 production rate in urban China is much higher than that in large urban areas in Europe and America. However, from the measurement results of NO_3 and N_2O_5 in typical areas, the measured N_2O_5 and calculated NO_3 concentration levels in Beijing are not higher than those in other regions, indicating that the removal rate of NO_3 and N_2O_5 in China may be faster than those in abroad. The oxidation reaction of NO_3 and VOCs and the heterogeneous uptake reaction of N_2O_5 are the key NO_3 loss pathways. Therefore, the reaction rates of the above two need to be characterized quantitatively. Due to the fast thermodynamic equilibrium between NO_3 and N_2O_5, it is difficult to analyze the budget of NO_3 or N_2O_5 separately, so the two species are considered as a united

system. For the direct removal of NO_3, the reaction of NO_3 and NO, and the reaction of NO_3 and VOCs are the most important reaction pathways. In the downwind area far away from the city, the NO emitted from the urban area is effectively oxidized by O_3, so it is usually not considered the reaction of NO to NO_3.

The effective quantification of NO_3 reactivity can help to conduct the closure study of NO_3 and N_2O_5. During the observation period in Huairou, the measured data parameters of VOCs are relatively complete, and the NO_3 reactivity can be calculated from the measured VOCs concentration. Table 4.1 summarizes the rate constants of some VOC species reacting with NO_3, mainly referring to [4, 5]. Some of the measured VOC species have no laboratory quantitative reaction rate constants and estimated by the reaction rate constant of similar structure species.

Here the VOCs species are divided into alkanes, anthropogenic emissions of olefins (AVOCs), aromatic hydrocarbons, and olefins emitted by biogenic sources (BVOCs). The contribution of the measured VOC species to NO_3 reactivity is shown in Fig. 4.2. Combined with the time series of pollutant concentrations observed in Huairou, it is found that the k_{NO3} on clean days is low, at 2.0×10^{-3}–1.0×10^{-2} s^{-1}. The k_{NO3} in polluted days is high, and the maximum can reach 2.5×10^{-2} s^{-1}. Figure 4.3a is the average daily change of k_{NO3} during the Huairou observation period, showing a trend of low daytime and high nighttime. The activity of k_{NO3} is inversely correlated with solar radiation. The level of k_{NO3} is the lowest at noon, only 6.0×10^{-3} s^{-1}. The removal of VOCs by the photochemical process during the day is relatively significant, resulting in a low concentration of VOCs during the day. The average level of k_{NO3} at night is 6.6×10^{-3} s^{-1} (see Fig. 4.3b). The anthropogenic sources dominate and account for 95.0% NO_3 reactivity. The contribution of isoprene to NO_3 reactivity is 4.7%, and the contribution of aromatic hydrocarbons and alkanes to NO_3 reactivity is only 0.3%. The top 3 VOCs are all olefin species with the double bond in the middle of the carbon chain (lumped as OLI in RACM2), which are 2-methyl-2-pentene, *trans*-2-butene, 2-methyl-2-butene. The concentration level of the top 3 VOCs and the average contribution to k_{NO3} are summarized in Table 4.2.

The measured VOC species in the 2017 PKU winter campaign are the same as the Huairou winter campaign. The time series of the measured contribution of VOC species to NO_3 reactivity is shown in Fig. 4.4. The pollution days featured high k_{NO3}, which can reach a maximum of 0.08 s^{-1}, and the k_{NO3} during the clean day is relatively stable, with the range of 2.0×10^{-3}–1.0×10^{-2} s^{-1}. The anthropogenic emissions of olefins dominate the NO_3 reactivity at night with the contribution of 85.3%. The contribution of isoprene to NO_3 reactivity was 13.7%, while the contribution of aromatic hydrocarbons and alkanes to NO_3 activity accounted for only 1.0%. The composition of k_{NO3} was consistent with the results observed in Huairou in winter. Figure 4.5a is the average daily change of k_{NO3} during the winter observation period of Peking University. The NO_3 activity in the first half of the day is relatively stable, maintaining at 6.0×10^{-3} s^{-1}, and there is a trough in the second half of the day, the minimum is about 2.0×10^{-3} s^{-1}. The change of k_{NO3} at night is small, with an average level of 3.7×10^{-3} s^{-1} (Fig. 4.5b), in which olefins anthropogenic emission sources are the main contributors. The top 3 VOCs that contributed to k_{NO3} in this winter observation are also OLI, namely styrene, *cis*-2-butene, and *trans*-2-butene.

Table 4.1 The rate constants of the reaction of NO_3 and VOCs

VOCs	A, × 10^{14} (cm^3 s^{-1})	Ea/R (K)	Ref.	VOCs	A, × 10^{14} (cm^3 s^{-1})	Ea/R (K)	Ref.
AVOCs, alkane				AVOCs, alkene			
Ethane	0.001	0	AA03	Ethylene	0.00049	2282	AA03
Propane	0.001	0	AA03	Propylene	45.9	1156	AA03
iso-Butane	305	3060	AA03	*trans*-2-Butene	39	0	AA03
n-Butane	276	3279	AA03	1-Butene	31.4	938	AA03
Cyclopentane	0.014	0	Estimated	*cis*-2-Butene	35	0	AA03
iso-Pentane	299	2927	AA03	1-Pentene	1.5	0	AA03
n-Pentane	0.0087	0	AA03	*trans*-2-Pentene	39	0	AA03
2,2-Dimethylbutane	0.044	0	AA03	*cis*-2-Pentene	35	0	AA03
2,3-Dimethylbutane	0.044	0	AA03	1-Hexene	1.8	0	AA03
2-Methylpentane	0.018	0	AA03	iso-Butene	33	0	Geyer01
3-Methylpentane	0.022	0	AA03	3-methyl-1-butene	1.4	0	NIST
n-Hexane	0.11	0	AA03	2-methyl-1-butene	52	0	NIST
2,4-Dimethylpentane	0.015	0	AA03	2-methyl-2-butene	320	0	NIST
2-Methylhexane	0.018	0	Estimated	4-methyl-1-pentene	1.4	0	Estimated
2,3-Dimethylpentane	0.015	0	Estimated	2-methyl-1-pentene	52	0	Estimated
Cyclohexane	0.014	0	AA03	2-methyl-2-pentene	320	0	Estimated
3-Methylhexane	0.018	0	Estimated				
2,2,4-Trimethylpentane	0.009	0	AA03				
n-Heptane	0.015	0	AA03	AVOCs, aromatic			
2,3,4-Trimethylpentane	0.009	0	Estimated	Benzene	0.003	0	Geyer01

(continued)

Table 4.1 (continued)

VOCs	A, × 10^{14} (cm^3 s^{-1})	Ea/R (K)	Ref.	VOCs	A, × 10^{14} (cm^3 s^{-1})	Ea/R (K)	Ref.
2-Methylheptane	0.018	0	Estimated	Toluene	0.007	0	AA03
3-Methylheptane	0.022	0	Estimated	Ethylbenzene	0.06	0	AA03
n-Octane	0.019	0	AA03	*m/p*-Xylene	0.05	0	AA03
Nonane	0.023	0	Estimated	*o*-Xylene	0.041	0	AA03
n-Decane	0.028	0	AA03	Styrene	150	0	AA03
n-Undecane	0.028	0	Estimated	Isopropylbenzene	0.1	0	Estimated
n-Dodecane	0.028	0	Estimated	*n*-Propylbenzene	0.1	0	Estimated
Methylcyclopentane	0.014	0	Estimated	3-Ethyltoluene	0.09	0	Estimated
Methylcyclohexane	0.014	0	Estimated	4-Ethyltoluene	0.09	0	Estimated
BVOCs				1,3,5-Trimethylbenzene	0.088	0	AA03
Isoprene	315	450	AA03	2-Ethyltoluene	0.09	0	Estimated
α-pinene*	119	−490	AA03	1,2,4-Trimethylbenzene	0.18	0	AA03
β-pinene*	251	0	AA03	1,2,3-Trimethylbenzene	0.19	0	AA03
Sabinene*	1100	0	AA03	1,3-Diethylbenzene	0.1	0	Estimated
Limonene*	1220	0	AA03	1,4-Diethylbenzene	0.1	0	Estimated

[a]Rate coefficients calculated according to $k = A \exp(-Ea/RT)$
[b]NIST is available at http://webbook.nist.gov/chemistry/
[c]*A* zero value for *Ea/R* indicates no experimental temperature dependence available
These species are not available during the four campaigns

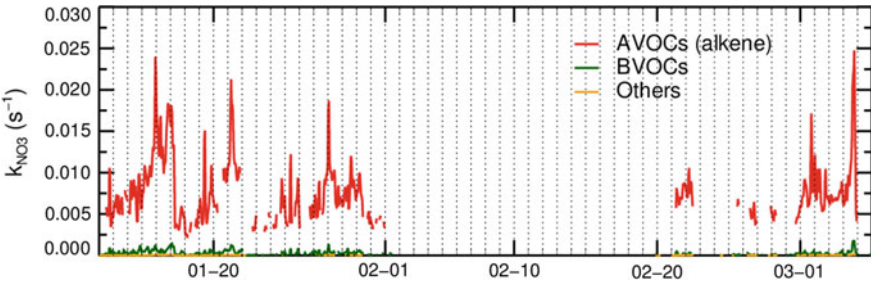

Fig. 4.2 Time series of NO_3 reactivity to VOCs in HR campaign

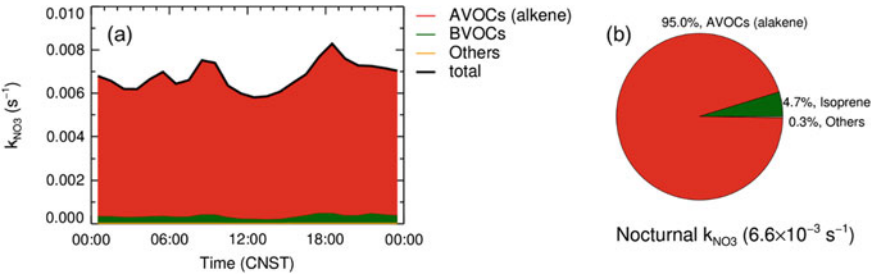

Fig. 4.3 **a** Shows the mean diurnal variation of k_{NO3} in HR campaign; **b** shows the average contribution of different VOCs to k_{NO3}

Table 4.2 The mixing ratio and percentage of the top five VOCs species in nocturnal k_{NO3} during HR campaign

Species	Mixing ratio (pptv)	k_{NO3} (s^{-1})
2-methyl-2-pentene	19	1.5×10^{-3}
trans-2-butene	125	1.2×10^{-3}
2-methyl-2-butene	14	1.1×10^{-3}

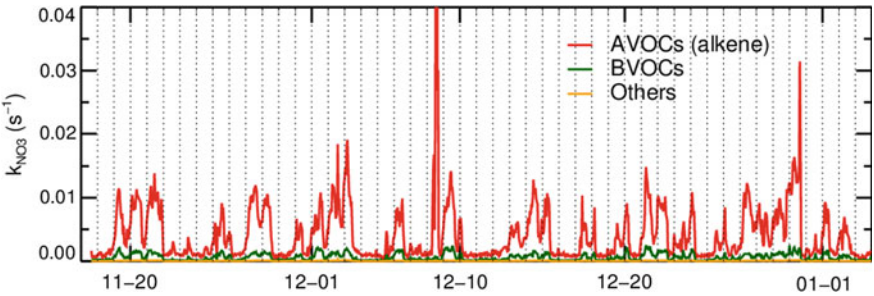

Fig. 4.4 Time series of NO_3 reactivity to VOCs in PKU winter campaign

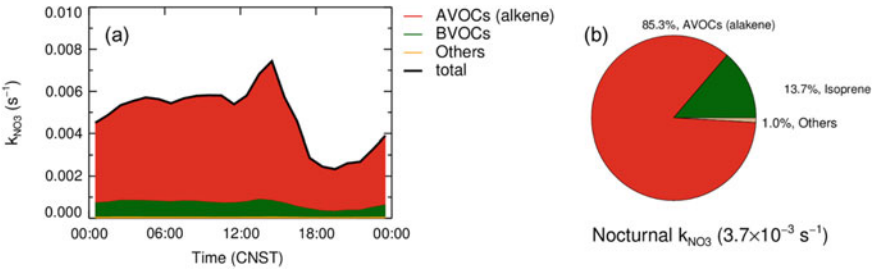

Fig. 4.5 **a** Shows the mean diurnal variation of k_{NO3} to VOCs in PKU winter campaign; **b** shows the average contribution of different VOCs to k_{NO3}

Table 4.3 The mixing ratio and percentage of the top three VOC species in nocturnal k_{NO3} during the PKU winter campaign

Species	Mixing ratio (pptv)	k_{NO3} (s^{-1})
Styrene	56	2.1×10^{-3}
trans-2-butene	39	3.7×10^{-4}
cis-2-butene	83	0.8×10^{-4}

The concentration level and the average contribution to k_{NO3} are summarized in Table 4.3.

According to the above results, the k_{NO3} observed in two winters is usually 2.0×10^{-3}–2.0×10^{-2} s^{-1}. The level in pollution days is greater than that of clean days, and the average level at night is around 5.0×10^{-3} s^{-1}. The anthropogenic olefins in the measured VOCs dominate the NO_3 reactivity. The corresponding NO_3 atmospheric lifetime in winter Beijing is about 200 s. The tower measurement in the winter in Denver area, United States showed the k_{NO3} was at 10^{-4}–10^{-2} s^{-1} with an average level less than 10^{-3} s^{-1}, which was much lower than the results of this study [26].

During the summer campaign in Changping, VOCs were measured using PTR-MS. The measured components were significantly different from those observed in the two winters. Only monoterpenes, isoprene, styrene, benzene, and toluene were observed in the Changping campaign. In the classification, AVOCs only considered styrene. BVOCs considered isoprene and monoterpenes. The PTR-MS measurement of monoterpenes cannot distinguish isomers. Since the main component of monoterpenes in the summer observation of southern Beijing in 2006 is α-pinene. Therefore, in the Changping campaign, it is assumed that all the monoterpene is α-pinene. According to Table 4.1, the reaction rate constant of α-pinene is 6.15×10^{-12} cm^3 s^{-1} at 298 K. The reaction rate constant is at a medium level compared to other monoterpenes (see Table 4.1). Relative to the uncertainty of the measurement technique, the uncertainty of the reaction rate constant caused by the uncertainty of the composition of the monoterpene may be large. Figure 4.6 shows the time series of k_{NO3} during the observation period in Changping. The contribution of benzene and toluene to NO_3 reactivity is almost negligible, and the contribution of BVOCs

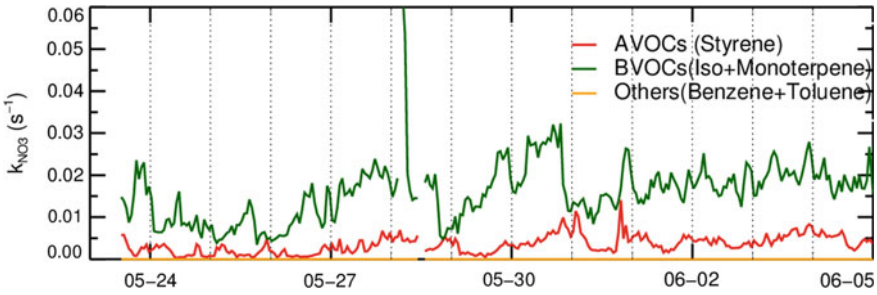

Fig. 4.6 Time series of NO_3 reactivity to VOCs in CP summer campaign

is the largest, followed by AVOCs. The average daily variation of NO_3 reactivity is unapparent (Fig. 4.7a). Figure 4.7b shows the composition of NO_3 reactivity at night. The average reactivity at night is 1.9×10^{-2} s^{-1}. The top 3 VOCs that contributed to NO_3 reactivity are monoterpene, styrene, isoprene, and in Table 4.4.

In general, in summer, the dominant factor for NO_3 reactivity in North China is monoterpenes. Anthropogenic emissions of olefins are also at a relatively high level compared with Europe and the United States. The species of VOCs measured during the Changping observation period are not comprehensive. The calculated NO_3 reaction activity value only represents a lower limit, but its NO_3 reaction activity is already much higher than that in the two winter campaigns. It shows that there is a high NO_3 reactivity in the suburbs of Beijing in summer, and BVOCs are the main contributing source of NO_3 reactivity. In the 2014 Wangdu campaign, both PTR-MS and GC-MS were used to measure VOCs. The average k_{NO3} without considering

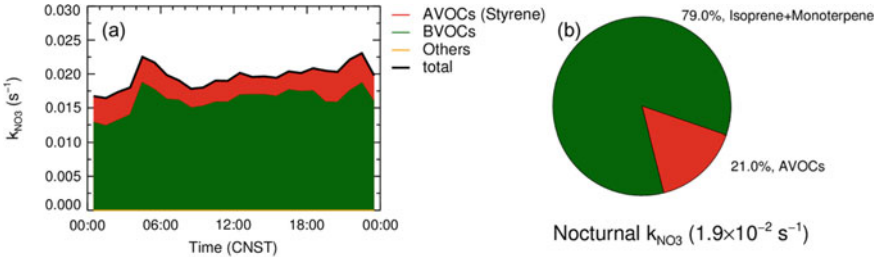

Fig. 4.7 **a** Shows the mean diurnal variation of k_{NO3} to VOCs in CP summer campaign; **b** shows the average contribution of different VOCs to k_{NO3}

Table 4.4 The mixing ratio and percentage of the top three VOCs species in nocturnal k_{NO3} during the CP summer campaign

Species	Mixing ratio (pptv)	k_{NO3} (s^{-1})
Monoterpene	88	1.3×10^{-2}
Styrene	113	4.0×10^{-3}
Isoprene	141	2.0×10^{-3}

monoterpenes was 8.9×10^{-3} s^{-1}, of which isoprene contributed 4.1×10^{-3} s^{-1}, and anthropogenic emissions of olefins contributed 4.8×10^{-3} s^{-1}, the contribution of aromatics and other species is almost negligible. If the measurement result of monoterpene is included, and assuming the representative of α-pinene, the average NO_3 reactivity at night can be as high as 7.0×10^{-2} s^{-1}. Table 4.5 summarizes the composition of NO_3 reactivity measured in other field studies. Due to the high temperature in summer, the emissions of BVOCs are large, and the NO_3 activity in most areas is dominated by BVOCs. Since BVOCs are small in winter, the AVOCs account for a large proportion of NO_3 reactivity.

The results highlight the importance of the accurate measurement of the classification of monoterpenes in quantifying NO_3 reactivity. The total NO_3 reactivity is helpful to understand the oxidation process of NO_3. Recently, the Crowley group of Max Planck Institute, Germany, firstly developed a measurement device of total NO_3 reactivity, and successfully carried out k_{NO3} measurement in the forest area of northern Finland. They found that the missing k_{NO3} can be as high as 30% at night and up to 60% during the day [17, 18]. The manifestation reflects the possibility of unknown oxidation mechanisms, such as the reaction with the intermediate from oxidized VOCs. The NO_3 reactivity in this study is much lower than the direct measurement results in the forest area, which may be because some BVOCs are not measured in urban areas. At present, there is still a lack of research on NO_3 and reactive intermediate substances. Due to the lack of online measurement studies of total reactivity, the importance of this process cannot be conducted. In Chap. 3, it is pointed out NO_3 in summer is also much higher than that in winter. The combination fully shows that the gas phase oxidation of NO_3 in summer on VOCs may be significantly higher than that in winter. The impacts on atmospheric oxidation capacity will be introduced in Chap. 5.

Table 4.5 Summary of the NO_3 reactivity observed in a different region

	Location	Region	k_{NO3} (10^{-3} s^{-1})	Dominant	References
Summer	Houston, USA	Urban	<1	AVOCs	[9]
	Houston, USA	Rural	<4	BVOCs	[9]
	Houston, USA	Urban	5–50	BVOCs	[24]
	Maine, USA	Coastal	1–60	BVOCs	[2]
	East coast, UK	Coastal	1–40	BVOCs	[1]
	Hong Kong, CN	Coastal	6	BVOCs	[10]
	Wangdu, CN	Suburban	70	BVOCs	This study
	Beijing, CN	Rural	19	BVOCs	This study
Winter	Boulder, USA	Rural	<1	–	[26]
	Beijing, CN	Urban	3	AVOCs	This study
	Beijing, CN	Rural	7	AVOCs	This study

4.3 The Derivation of N_2O_5 Uptake Coefficient

There are few field studies on the quantification of N_2O_5 uptake coefficient. The quantitive methods for deriving N_2O_5 uptake coefficient in field studies include pseudo-steady state [12], iterative box model method [26], products growth fitting method [21], and the flow tube measurement method [7]. The first three methods are indirect quantitative methods, mainly based on the measurement of N_2O_5 and related parameters, the flow tube method is a direct measurement method.

The pseudo-steady state method is based on the field measurement of trace gases such as NO_3 or N_2O_5 [12], and is currently the most widely used field quantitative method for the N_2O_5 uptake coefficient. NO_3, N_2O_5, NO_2, and ambient temperature measured by aircraft measurement to calculate the steady-state lifetime of N_2O_5 and NO_3. Then established the relationship between the loss terms of NO_3/N_2O_5 and lifetime [11], where $\tau_{ss}(NO_3)$ and $\tau_{ss}(N_2O_5)$ represent the atmospheric lifetime of NO_3 and N_2O_5 respectively, and k_{NO3} and k_{N2O5} represent the loss term of NO_3 and N_2O_5, respectively. The loss term of N_2O_5 can be fitted by any of the following formulas (Eqs 4.1, 4.2), and then the uptake coefficient of N_2O_5 can be calculated by Eq 1.10. For example, by linearly fitting K_{eq} $[NO_2]$ and $[\tau_{ss}(NO_3)]^{-1}$ (using Eq. 4.1), the slope is the reaction rate constant of N_2O_5, and the uptake coefficient can be obtained, while the intercept represents the removal rate constant of NO_3.

$$\tau_{ss}(NO_3) = \frac{[NO_3]}{k_{NO2+O3}[NO_2][O_3]} = \left(k_{NO3} + K_{eq}[NO_2]k_{N2O5}\right)^{-1} \tag{4.1}$$

$$\tau_{ss}(N_2O_5) = \frac{[N_2O_5]}{k_{NO2+O3}[NO_2][O_3]} = \left(k_{N2O5} + \frac{k_{NO3}}{K_{eq}[NO_2]}\right)^{-1} \tag{4.2}$$

Here an assumption is that a pseudo-steady state is reached between NO_3 and N_2O_5. The pseudo-steady-state conditions are difficult to achieve in the following three situations. Firstly, the removal rates of NO_3 and N_2O_5 are very small, leading to a failure to reach steady-state; Secondary, the mixing time scale of the air mass is close to the time scale of the chemical reactions. Besides, the covariance between the independent variable, $K_{eq}[NO_2]$, k_{NO3} and k_{N2O5} is one of the uncertain factors. Strong correlation between the aerosol surface area and $K_{eq}[NO_2]$ suggests the existence of covariance [8].

The product growth fitting method was first proposed by [21]. This method assumes that the growth processes of $ClNO_2$ and pNO_3^- observed at night attributes to the heterogeneous reaction of N_2O_5, and requires the air mass to be relatively stable, without the influences of physical processes such as deposition and transportation, other chemical sources and removal routes are negligible. In addition, it is assumed that the N_2O_5 uptake coefficient and $ClNO_2$ yield are independent of the particle size. In order to achieve the prerequisites for calculation as much as possible, the following two characteristics need to be met in the data selection process: (1) The trend of the concentration of $ClNO_2$ and pNO_3^- at night is a continuous increase,

and there is a correlation between the two species, which implies the growth of the two species are dominated by the heterogeneous hydrolysis of N_2O_5, and the effect of the heterogeneous uptake process of HNO_3 on the pNO_3^- can be ignored; (2) The increase of ammonium is equivalent or even higher than the increasing rate of pNO_3^-, indicating that excess NH_3 effectively suppresses the degas of pNO_3^- to generate HNO_3 through the gas-particle partition. The limitation of this method is that it can only be used to analyze the simultaneous growth episodes of pNO_3^- and $ClNO_2$.

The iterative box model method assumes that each set of observed data represents an independent air mass. The model's starting time usually set to the sunset time. The air mass moves from sunset time until transport to the measurement site at the measurement time point. After that, the air mass moves to the downwind area subsequently. The whole process of the emission injection does not consider during the transmission [26]. This model only considers the formation and dominating loss of NO_3 and N_2O_5. NO_3 removal only considers oxidation with VOCs, and N_2O_5 only considers heterogeneous reactions. It is assumed that the air mass is not affected by other physical processes such as transport, deposition, and diffusion. The concentration changes of NO_2 and O_3 only come from the chemical processes of NO_3 and N_2O_5. The model time step is set to 1 min. Based on the NO_2 and O_3 concentrations measured at night, the integration formulas of Eqs (4.3) and (4.4) are used to calculate the NO_2 and O_3 concentrations at sunset (the zero point). $s(t)$ represents the removal coefficient of NO_2, which is between 0 and 1. When the removal process of the NO_3–N_2O_5 is dominated by NO_3 oxidation, $s(t)$ approaches 0. When the N_2O_5 heterogeneous uptake is the main removal pathway, $s(t)$ approaches 1, the calculation of $s(t)$ is shown as Eq (4.7). Taking the calculated NO_2 and O_3 at the zero point and the other initial input (Sa and k_{NO3}), the total concentration of NO_3 and N_2O_5 is calculated by Eq (4.5). Assuming that NO_3 and N_2O_5 are in thermodynamic equilibrium, the ratio distributes the concentration of NO_3 and N_2O_5 by Eq (4.6).

The model calculation has two steps. The first step is to infer the NO_2 and O_3 concentrations at the initial time point of the model by measuring the NO_2 and O_3 concentrations at the time point (the modeling end), and derive the NO_3 and N_2O_5 through the initial NO_2, O_3, k_{NO3}, and k_{N2O5}, simulate the concentration of N_2O_5 and then calculate $s(t)$. The second step will iterates the k_{N2O5}, recalculate the zero time NO_2 and O_3 by the updated $s(t)$, and simulate N_2O_5 until the difference between the simulated and measured N_2O_5 level is within 1%. The advantage of the iterative model is that it does not need to consider whether NO_3 and N_2O_5 have reached pseudo-steady-state conditions. However, the stability of the air mass is highly required. The injection of trace gas under actual conditions may lead to inaccurate iterative calculation results. For example, the injection of NO emissions will lead to the update of the model start time. Overall, this method is more suitable for remote areas away from emission source.

$$\frac{\mathrm{d}\,[O_3]}{\mathrm{d}t} = -k_{NO2+O3}[O_3][NO_2] \tag{4.3}$$

$$\frac{\mathrm{d}\,[NO_2]}{\mathrm{d}t} = -(1 + s(t)) \times k_{NO2+O3}[O_3][NO_2] \tag{4.4}$$

$$\frac{\mathrm{d}\,[NO_3 + N_2O_5]}{\mathrm{d}t} = k_{NO2+O3}[O_3][NO_2] - k_{N2O5}[N_2O_5] - k_{NO3}[NO_3] \tag{4.5}$$

$$\frac{[N_2O_5]}{[NO_3]} = K_{eq}[NO_2] \tag{4.6}$$

$$s(t) = \frac{\int_0^t k_{N2O5} \cdot [N_2O_5]dt + [N_2O_5]_t}{[O_3](0) - [O_3](t)} \tag{4.7}$$

4.3.1 N_2O_5 Uptake in Changping Campaign

The calculation of the N_2O_5 uptake coefficient during the Changping campaign is suitable by using the pseudo-steady state method. The summer temperature is high, and the pseudo-steady state condition can be reached quickly after sunset. Compared with urban areas, it is less affected by anthropogenic emissions. However, this method requires a higher measurement accuracy of NO_2, since the measurement error of NO_2 has a great impact on the calculation results. In this campaign, NO_2 is corrected by the photo-stationary state and is relatively reliable at the concentration level, but still has large uncertainty. Since this observation has the simultaneous measurement of N_2O_5, pNO_3^- and $ClNO_2$, the product growth fitting method can be used to fit the N_2O_5 uptake coefficient and $ClNO_2$ yield. The growth rate of NH_4^+ in the particle phase is consistent or even faster than that of pNO_3^-, indicating that the growth of nitrate at night mainly comes from the heterogeneous reaction of N_2O_5, and the gaseous NH_3 can effectively suppress the gaseous phase emission of NO_3^-. During the campaign, a total of 5 nights of measurement data meet the requirements. The fitted $ClNO_2$ and pNO_3^- concentration is obtained by adding the initial γ and f. The iterative γ and f are conducted until both the fitted $ClNO_2$ and pNO_3^- increasing is consistent with the actual measurement results. Here all data are synchronized to a time resolution of 5 min. Figure 4.8 is an example of optimized fitting at night on May 28. The fitted $ClNO_2$ and pNO_3^- can reproduce the growth process well, and the obtained γ and f take the values of 0.017 and 1.0, respectively. The fitting results of during the five nights are summarized in Table 4.6. γ is between 0.012 and 0.055, with an average of 0.034 ± 0.018; f takes the value of 0.5–1.0, with an average of 0.73 ± 0.25. The main sources of uncertainty in this method are the measurement of N_2O_5, S_a, $ClNO_2$, and pNO_3^-. According to error propagation, the accumulated uncertainty is more than 50%.

The N_2O_5 uptake coefficient calculated during the observation period in Changping is comparable to the results in the suburbs of Germany [21]. This result is higher than the observations in the United Kingdom and the United States, although

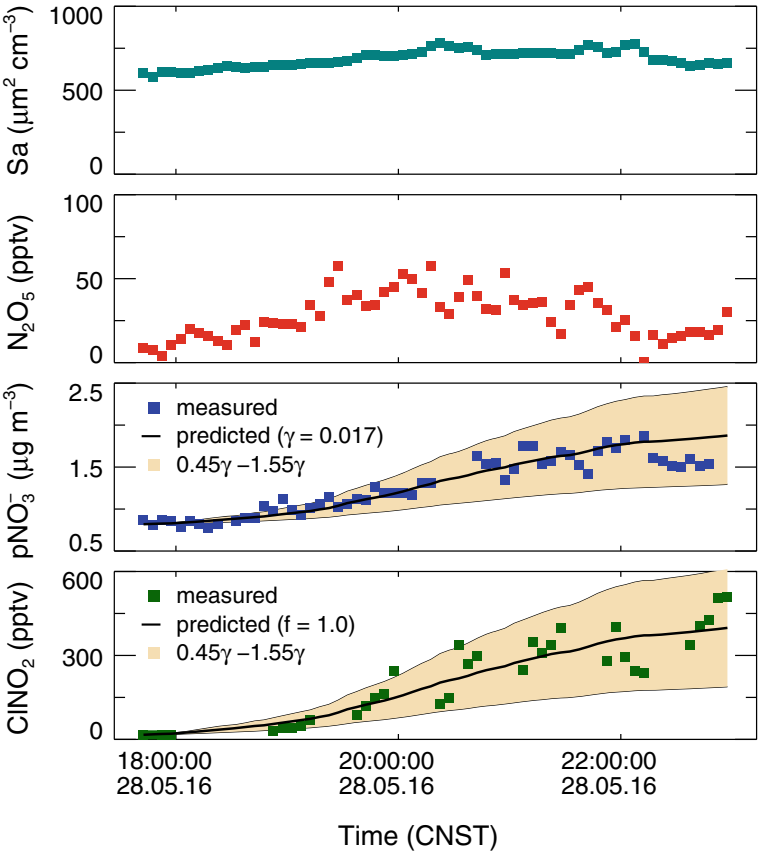

Fig. 4.8 The optimized fitting of γ and f to reproduce the observed $ClNO_2$ and pNO_3^- with an offset on May 28. The black lines are the predicted results of the integrated pNO_3^- and $ClNO_2$ by using the observed S_a and N_2O_5. Reproduced from with Permission [27]; link to the original file https://www.atmos-chem-phys.net/18/9705/2018/acp-18-9705-2018.pdf

Table 4.6 List of the N_2O_5 uptake coefficients and $ClNO_2$ yield in the CP campaign

Start time	End time	γ	f
05/25 00:00	05/25 05:00	0.047	0.60
05/25 18:30	05/25 23:00	0.012	1.0
05/27 19:00	05/27 20:40	0.040	0.50
05/28 19:00	05/28 23:00	0.017	1.0
05/30 21:00	05/31 00:00	0.055	0.55

there are some differences in measurement and calculation methods [8, 11, 19, 23]. The results of Changping observations are in good agreement with the studies in North China [28, 29], although their research method is a pseudo-steady-state analysis method. It is reflected that the relatively high uptake coefficient is relatively common in North China. In this observation, the concentration of sulfate in the particles exceeds 30%, which may be one of the reasons for the high uptake coefficient [11]. Although the content of chlorine in the particles observed this time is very low (<0.1 $\mu g\ m^{-3}$), the $ClNO_2$ yield is relatively high, even comparable to the $ClNO_2$ yield of the chlorine-rich air mass that emitted from coal-fired power plants [29].

4.3.2 N_2O_5 Uptake in PKU Summer Campaign

During the PKU summer campaign, the measurement of NO_2 is carried out by the method of photolysis conversion, so the steady-state calculation method is applicable to calculate the N_2O_5 uptake coefficient. In order to estimate the time required to reach steady-state after sunset under typical conditions in this campaign, a box model was used for checking this assumption. Here NO_2 is set to 20 ppbv. Ozone is 100 ppbv, S_a is set to 1500 $\mu m^2\ cm^{-3}$, the temperature is 25 °C, the NO_3 loss rate constant is set to 0.024 s^{-1}, N_2O_5 uptake coefficient is set to 0.02, the corresponding N_2O_5 removal rate is about 0.002 s^{-1}. Figure 4.9 shows the modeled steady-state and actual lifetime, and its relative ratio of NO_3 and N_2O_5, respectively. In general, the modeled

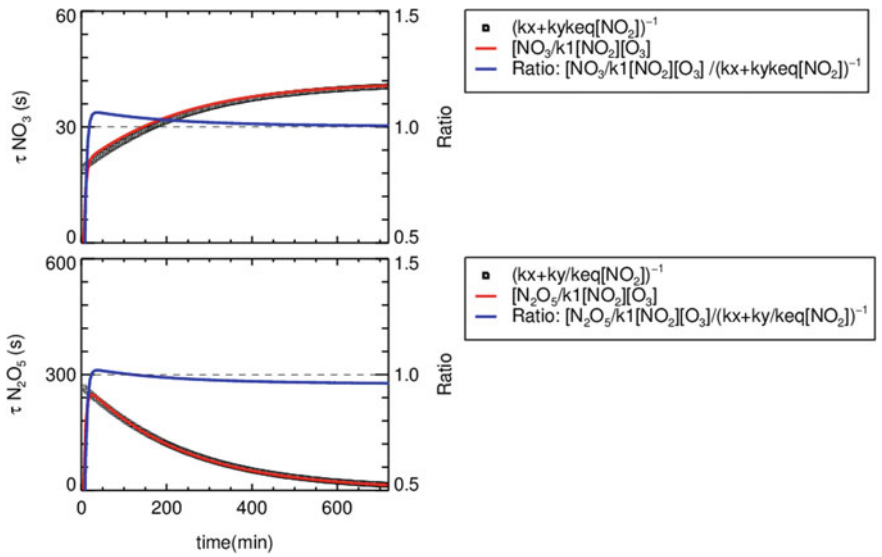

Fig. 4.9 The estimated steady-state time of NO_3 and N_2O_5 based on the box model simulation. The k_x and k_y denotes the loss rate constant of NO_3 and N_2O_5, respectively

steady-state lifetime can be consistent with the real value within 30 min; that is, the steady-state is established. Therefore, in the subsequent analysis, the data within 30 min of the sunset are excluded.

Figure 4.10 shows the fitting results on September 23, 24, 29, and 30. The overall fitting result is reasonable. Table 4.7 summarizes the fitting results of these four days, as well as the S_a, NO_2 concentration, and RH. The NO_2 and relative humidity during this period are very high. The data selection during the fitting process is that NO is less than 0.1 ppbv. The N_2O_5 uptake coefficients for these four days ranged from 0.025 to 0.072, which was slightly higher than the results in Changping campaign, with an average level of 0.048. The uncertainties include S_a (30%), the measurement

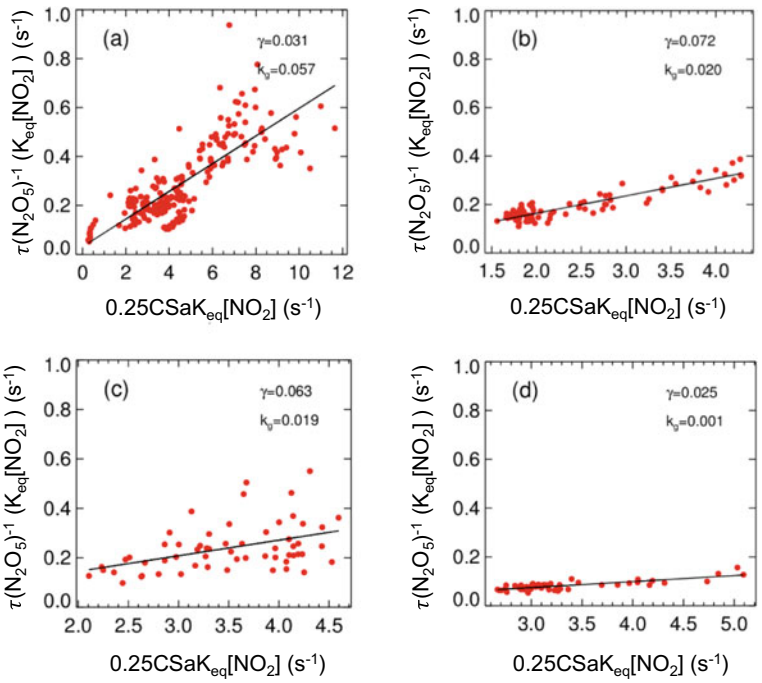

Fig. 4.10 Derivation of γ via analysis of N_2O_5 steady-state lifetime variation with NO_2 and S_a, plots **a–d** denote the results of the nights on Sept 23, 24, 29, and 30, respectively

Table 4.7 Details of the derived γ, NO_3 reactivity, and the observed S_a, NO_2, RH in PKU summer campaign

Time	γ	k_{NO3} (s^{-1})	S_a (μm^2 cm^{-3})	NO_2 (ppbv)	RH (%)
23/09–24/09	0.031	0.057	3061	39.1	72.6
24/09–25/09	0.072	0.020	3101	25.2	68.1
29/09–30/09	0.063	0.019	1270	42.5	37.4
30/09–01/10	0.025	0.001	1624	41.0	43.9

of N_2O_5 (19%), the measurement of NO_2 (20%). Propagated uncertainty is less than 50%. The intercept in the fitting process represents the direct removal rate of NO_3, which is generally considered to be the removal rate constant of NO_3 to VOCs, in the range of 0.001–0.057 s^{-1}, which is comparable to the NO_3 reactivity calculated during the summer observation in Changping. When analyzing the data in the other days, the fitted k_{NO3} is negative occasionally, or the N_2O_5 uptake coefficient over 0.1. The unrealistic fitting results show that the pseudo-steady state analysis method has certain limitations and is not suitable for all the cases.

The high N_2O_5 uptake coefficient in the Peking University summer campaign may be related to the high aerosol water content. The ISORRPIA-II thermodynamic model is used to estimate aerosol water content. The mode is selected as the forward mode. Since the high RH during the observation period, the particle phase state set to metastable. The input data includes ACSM measured soluble components, including NO_3^-, SO_4^{2-}, NH_4^+, Cl^- and GAC gaseous pollutant components NH_3, HNO_3, HCl. It is calculated that the average aerosol water content in these four days is 50.8 $\mu g\ m^{-3}$, accounting for about 50% of the mass concentration of wet $PM_{2.5}$. The high water content in the polluted particles is a typical feature of the particulate matter component in Beijing. Compared with the conditions of Europe and the United States, the water content is high [20, 30]. The elevated water content can effectively promote the formation of $NO_2HO_2^+$ in the particle phase, and promote the heterogeneous uptake of N_2O_5.

4.3.3 N_2O_5 Uptake in Huairou Campaign

Due to the low temperature during the winter campaign in Huairou, it takes a long time to establish the steady-state of NO_3 and N_2O_5, so it is not suitable to use the steady-state method to calculate the uptake coefficient. Similar to the case in the downwind area of the Denver urban area, the N_2O_5 uptake coefficient can be quantified using an iterative model calculation method based on the measurement of N_2O_5. The N_2O_5 concentration at the measurement time point is optimized by iterating the N_2O_5 uptake coefficient until the difference between the simulated N_2O_5 concentration and the measured N_2O_5 concentration is less than 1%. On the clean day, S_a, the concentration of NO_2, the temperature, and RH are low. Assuming that the NO_3 reactivity is $6 \times 10^{-3}\ s^{-1}$, the uptake coefficient of N_2O_5 is 0.003, and S_a is assumed to be 200 $\mu m^2\ cm^{-3}$. The calculated removal rate of N_2O_5 is only $4 \times 10^{-4}\ s^{-1}$. Under this condition, the thermal equilibrium time of NO_3 and N_2O_5 needs nearly 3 h. The slow N_2O_5 uptake led to k_{NO3} has a large interference on the results, indicating that in clean days, the iterative box model may have larger uncertainties than that in polluted days.

In the model simulation, the determination of the time zero of the model is very important. If the air mass is not influenced by anthropogenic emissions during transportation, it is usually assumed that the starting time of the model is sunset time. If influenced by regional NO emissions, the accumulated NO_3 and N_2O_5 will be titrated

until NO is consumed by O_3, and the chemical process of N_2O_5 uptake continues, that is, the model start time is reset to zero. The period from zero time to the measurement point is the air mass age (t_{plume}). A simple calculation method to estimate the t_{plume} was shown in Eq. (4.8) [11].

$$t_{plume} = \frac{\mathrm{In}(1 - S(1 + m))}{S k_{NO2+O3} \overline{O_3}} \tag{4.8}$$

Here $\overline{O_3}$ is the average concentration of O_3 in the calculation period, m represents the slope of O_3 to NO_2. A strong correlation between O_3 and NO_2 with the slope less than -1.0, indicating O_3 loss not only caused by the injected NO but also by the chemical processes of NO_3 and N_2O_5 at night. If $m > -1.0$, the sunset time is used as the starting point of the model simulation. If the calculated air mass age is less than the period from the measurement time point to the sunset time, the air mass age and the measurement time point are used to calculate the time zero of the model simulation. If the air mass age is greater than the measurement time point to the sunset time, the sunset time is used as the time zero point.

The aerosol surface area in the model is calculated using the <2.5 μm number size distribution data measured by SMPS and APS. The inorganic content is measured by AMS and input to the ISORRPIA-II model to calculate the aerosol water content. It is assuming that there is no significant difference in the density of dry particulate matter and wet particulate matter. The hygroscopic growth factor of the wet particulate matter can be calculated according to the mass change, and the surface area of the wet particulate matter is corrected. The NO_3 activity input data simulated by the model uses the average value calculated from VOCs measured at each night. Due to the great influence of NO on the model, in the process of model simulation, the data of NO less than 0.1 ppbv was selected for subsequent analysis. The S_a is calculated at the time point. Although the iterative model method can be used to calculate the N_2O_5 uptake coefficient, the overall uncertainty of this method is relatively large, and it has many assumptions.

The selection of time zero in the process of model simulation is one of the important sources of uncertainty. Besides, during the air mass change, it is assumed that there is no change in S_a, and N_2O_5 uptake coefficient. Due to the low temperature in winter, the chemical equilibrium tends to the chemical process of N_2O_5, and the change of NO_3 reactivity has relatively little effect on the N_2O_5 uptake coefficient. However, when the air mass comes from the background air mass in the north, the aerosol surface area of the particulate matter is small. The change of NO_3 reactivity during the model simulation process has a great impact on the estimation of the N_2O_5 uptake coefficient. In order to minimize the uncertainty of the model estimation, only the period when S_a is greater than 1000 $\mu m^2\ cm^{-3}$ is selected for further estimation.

Taking the calculation on February 21 as an example, Fig. 4.11 shows the derived N_2O_5 uptake coefficient value. There is a clear anti-correlation between NO_2 and O_3 in 20:00–23:30, and the air mass age during this period is about 100 min, indicates the reaction time length was 100 min. After 23:30, both NO_2 and O_3 show a downward

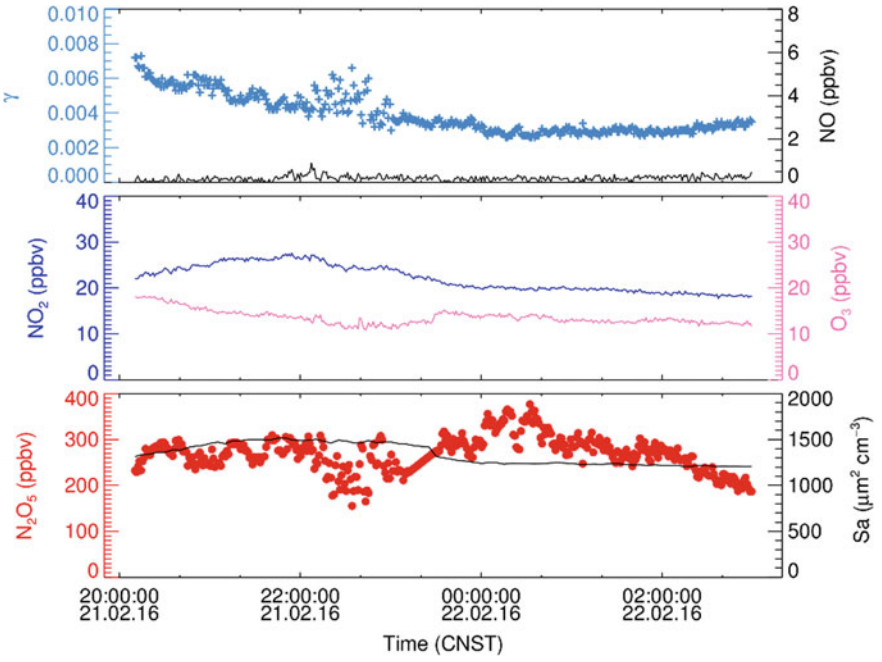

Fig. 4.11 The N_2O_5 uptake coefficient determined on the night of February 21, 2016 in the HR winter campaign

trend. A positive correlation between NO_2 and O_3 presented, so the sunset time is adopted as the starting time of the model. Despite the varying air mass age, the uptake coefficient of N_2O_5 reflects the essential properties of particulate matter. It can be found that the uptake coefficient of N_2O_5 does not change quickly throughout the night. It was also found that the shear of the air mass will cause a large change in the N_2O_5 uptake coefficient in other nights, which also shows that the N_2O_5 uptake coefficient is affected by aerosol type.

During the observation period in the Huairou campaign, the nights of February 21–22, February 27–28, February 29–March 1, March 1–2, March 2–3, and March 3–4 were selected. A total of six nights of measurement data were used to deduce the N_2O_5 uptake coefficient, and the relevant parameters are summarized in Table 4.8. Except for the night of February 27–28, the average of the N_2O_5 uptake coefficients for the other five nights was lower than 0.005. The average uptake coefficient at the night of February 27–28 could reach 0.013, and the highest value could reach 0.02. By comparison, it was found that the uptake coefficients of three nights with RH greater than 50% were higher than those of the other three nights with relative humidity less than 50% (Fig. 4.12a), which is similar to the previous laboratory experiments results [16].

Previous works proved that the uptake of N_2O_5 is promoted by H_2O and inhibited by pNO_3^-, so the N_2O_5 uptake coefficient is greatly affected by the molar ratio of

Table 4.8 The derived N_2O_5 uptake coefficient and relevant parameters in the HR winter campaign

Time	γ	RH (%)	T (°C)	H_2O ($\mu g\ m^{-3}$)	NO_3^- ($\mu g\ m^{-3}$)	Mole (H_2O/NO_3^-)
21/02–22/02	0.0039 ± 0.0011	53.2 ± 2.3	-1.0 ± 0.6	24.3 ± 3.4	23.9 ± 3.5	3.5 ± 0.2
27/02–28/02	0.013 ± 0.0026	54.9 ± 9.1	0.8 ± 2.2	10.2 ± 5.2	6.8 ± 2.1	4.9 ± 1.9
29/02–01/03	0.0031 ± 0.0009	40.2 ± 5.1	-2.8 ± 1.9	6.0 ± 2.1	9.0 ± 0.8	2.3 ± 0.7
01/03–02/03	0.0017 ± 0.0006	43.4 ± 1.8	1.7 ± 0.5	11.3 ± 1.6	20.8 ± 1.0	1.7 ± 0.2
02/03–03/03	0.0019 ± 0.0008	38.8 ± 6.4	7.9 ± 1.1	10.7 ± 4.9	22.4 ± 2.8	1.6 ± 0.7
03/03–04/03	0.0050 ± 0.0016	65.2 ± 5.3	5.8 ± 1.6	84.2 ± 25.4	67.1 ± 10.5	4.2 ± 0.7

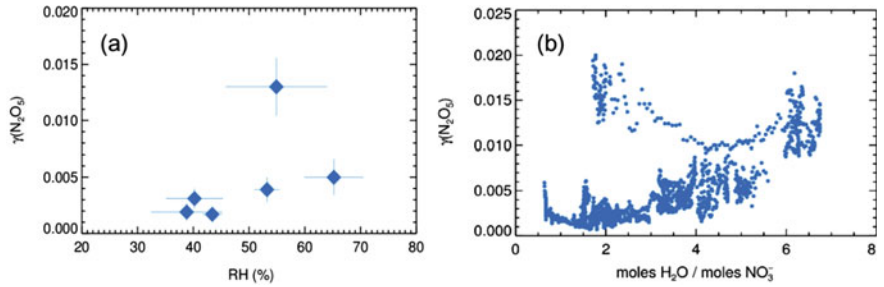

Fig. 4.12 **a** Shows the dependence of N_2O_5 uptake coefficient on RH in HR winter campaign; **b** shows the mole ratio of H_2O/NO_3^-

H_2O/NO_3^- [6, 15]. As shown in Fig. 4.12b, the N_2O_5 uptake coefficient during the Huairou campaign has a significant positive correlation with H_2O/NO_3^-, except that some data points derived on February 27 were higher and not follow this trend. When the H_2O/NO_3^- ratio is increased from 1 to 7, the uptake coefficient can be increased from 0.002 to nearly 0.015, indicating that the water content and nitrate in the particles may have a very important role in the N_2O_5 uptake process. The disobedience of some data on the H_2O/NO_3^- constraint on February 27 shows that the influencing factors of the heterogeneous uptake process of N_2O_5 are very complex and may be affected by other parameters. We further explored the relationship between the N_2O_5 uptake coefficient and Org/SO_4^{2-}. Except for February 27, the overall N_2O_5 uptake coefficient decreased slightly when Org/SO_4^{2-} increased, but the trend was not notable. In addition, when calculating the N_2O_5 uptake coefficient, some clean air masses were selected for evaluation. It is found that the calculated uptake coefficient is usually unrealistically large. On the one hand, the source may be much larger than the removal path due to the low removal rate. On the other hand, the thermal equilibrium between NO_3 and N_2O_5 is not established, then resulting in the overestimation.

4.4 Modeling of N_2O_5 Uptake Coefficient

The BT09 parameterization scheme is based on the aqueous reaction mechanism and proposed by laboratory studies. The specific reaction process is listed below (Eqs. 4.9–4.13). Assuming that the aerosol phase is aqueous, N_2O_5 diffuses into the particles through adsorption and then dissociates to form $H_2ONO_2^+$, part of which reacts with aerosol liquid water to produce nitric acid, and partly reacts with halogen ions X^- (referring to Cl^-, Br^-, etc.) and produces XNO_2, such as $ClNO_2$. In this mechanism, it is assumed that there is no difference in particle size, aerosol phases are internal mixed, and the reaction mechanism is a bulk reaction. The mechanisms of aerosol water content, NO_3^- and Cl^- on N_2O_5 uptake are considered. Both the promotion of H_2O and Cl^- on N_2O_5 uptake, and there is competition with each other. NO_3^- has an inhibitory effect on N_2O_5 uptake. The formula for the parameterized

N_2O_5 uptake coefficient in Eq (4.14). Where V is the total particle volume concentration ($m^3\ m^{-3}$), and ω is the average molecular velocity ($m\ s^{-1}$) of N_2O_5. K_H is the dimensionless Henry coefficient of N_2O_5. Where k_{2f}' is the dissociation coefficient of N_2O_5, which is a function of the aerosol water content (Eq. 4.15). β and δ were quantitatively parameterized by laboratory experiments, namely $1.15 \times 10^6 \pm 3 \times 10^5\ s^{-1}$ and $1.3 \times 10^{-1} \pm 5 \times 10^{-2}\ M^{-1}$. k_{2b}, k_3, and k_4 correspond to the reaction rate constants of Reactions (4.11)–(4.13), respectively.

$$N_2O_5(gas) \leftrightarrow N_2O_5(aq) \tag{4.9}$$

$$N_2O_5(aq) + H_2O\ (l) \rightarrow H_2ONO_2^+(aq) + NO_3^-(aq)k_{2f} \tag{4.10}$$

$$H_2ONO_2^+(aq) + NO_3^-(aq) \rightarrow N_2O_5(aq) + H_2O\ (l)k_{2b} \tag{4.11}$$

$$H_2ONO_2^+(aq) + H_2O\ (aq) \rightarrow HNO_3(aq) + H_3O^+(aq) \tag{4.12}$$

$$H_2ONO_2^+(aq) + X^-(aq) \rightarrow XNO_2 + H_2O\ (l) \tag{4.13}$$

$$\gamma = \frac{4V}{\omega S_a} K_H k_{2f}^{,} \left(1 - \frac{1}{\frac{k_3[H_2O(l)]}{k_{2b}[NO_3^-]} + 1 + \frac{k_4[Cl^-]}{k_{2b}[NO_3^-]}} \right) \tag{4.14}$$

$$k_{2f}^{,} = \beta - \beta e^{(-\delta[H_2O](l))} \tag{4.15}$$

The parameterization of DV08 was established based on the laboratory research results of N_2O_5 uptake on the surface of ammonium sulfate and nitrate aerosols. The parameterized model scheme established by a weighted regression method considered temperature and pressure, particulate inorganic compositions, and particle-phase state. The aerosol divided into $(NH_4)_2SO_4$, NH_4HSO_4, and NH_4NO_3 (named as AB, AS, and AN). The phase states are divided into solid and liquid. Regression of different aerosol uptake coefficients using temperature and humidity to parameterize N_2O_5 uptake coefficients of different aerosol types (Eqs. 4.16–4.19). For liquid-phase aerosols, the uptake coefficient is equal to the sum of the molar weights of different types of aerosols, where x represents the weighting coefficient of different types of aerosols.

$$\gamma_{AB}* = \min\left(\gamma_{AB,} 0.08585\right) \tag{4.16}$$

$$\gamma_{AS}* = \min\left(\gamma_{AB,} 0.053\right) \tag{4.17}$$

$$\gamma_{AN}* = \min\left(\gamma_{AB,} 0.0124\right) \tag{4.18}$$

$$\gamma_{aq} = x_{AB} \times \gamma_{AB} * + x_{AS} \times \gamma_{AS} * + x_{AN} \times \gamma_{AN} * \tag{4.19}$$

$$x_{AB} = 1 - (x_{AS} + x_{AN}) \tag{4.20}$$

$$xAS = \max(0, \min(1 - xAN), \frac{[NH_4^+]}{[NO_3^-] + [SO_4^{2-}]} - 1) \tag{4.21}$$

$$xAN = \frac{[NH_4^+]}{[NO_3^-] + [SO_4^{2-}]} \tag{4.22}$$

The limitation of the above two parameterization schemes is that only for inorganic aerosols. Anttila et al. proposed an organic coating model. The basic assumption is that organic aerosols are organic coatings on the surface of particles to form a uniform coating [3]. The core is a liquid-phase inorganic substance, and the shell is an organic film (as shown in Fig. 4.13). The thin film will affect N_2O_5 uptake indirectly via the effect on liquid water content and their surface activity by acting as an uptake barrier. In this parameterization, the role of inorganics and organics is considered simultaneously. A resistance model to comprehensively consider the uptake coefficient of the two parts; the expression is Eq. (4.23). The parameterization method of the uptake coefficient of the organic part is Eq. (4.24), where D_{org} and H_{org} represent the diffusion coefficient and Henry's equilibrium constant on the organic film, respectively. Assuming that there is no significant difference between Henry's equilibrium constant and the inorganic aerosol surface, that is, $H_{org} = H_{aq}$, and D_{org} is assumed to be 3% of D_{aq}, that is, $D_{org}H_{org} = 0.03H_{aq}D_{aq}$. Here H_{aq} is 5000 mol m^{-1} atm^{-1}, and D_{aq} recommends 10^{-9} m^2 s^{-1}. R_p, R_c, and l represent the radius of the particulate matter, the radius of the inorganic core, and the thickness of the organic coating film. This parameterization of the inorganic core can carry a variety of different parameterization schemes of the liquid phase core of the inorganic substance.

$$\frac{1}{\gamma} = \frac{1}{\gamma_{coat}} + \frac{1}{\gamma_{core}} \tag{4.23}$$

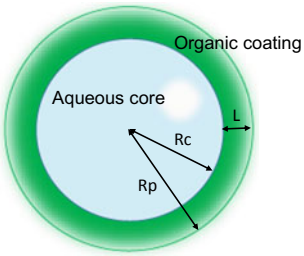

Fig. 4.13 Schematic of the heterogeneous reaction of N_2O_5 with organic coating aerosol particles

$$\gamma_{coat} = \frac{4\mathrm{RT}D_{org}H_{org}R_c}{cl\,R_p} \tag{4.24}$$

During the PKU summer campaign, a total of four N_2O_5 uptake coefficients were obtained by the pseudo-steady state analysis method. In the subsequent Changping campaign, only five N_2O_5 uptake coefficients were obtained. The dataset was limited to carry out the intercomparison. Figure 4.14 shows the BT09 and DV08 parameterization results, and the field derived results in Changping. It is found that only two of the data points have a certain degree of agreement with the model, and the measurement results of the other three data points are much higher than those predicted by the BT09 and DV08 models. Although the changes between the two parameterizations are indeed very consistent, the simulated maximum is only 0.03, which is lower than the quantitative N_2O_5 uptake coefficient. If the inhibitory effect of organic coatings is considered, the predicted uptake coefficient value will be further decreased.

During the Huairou winter campaign, we derived 2289 N_2O_5 uptake coefficients. Several parameterizations were used to estimate the N_2O_5 uptake coefficients. The influence mechanism of Cl^- was considered in the original BT09 model. In this study, the inclusion of the Cl^- mechanism led to the parameterized scheme overestimating the uptake coefficient by 5–10 times. When the Cl^- mechanism is excluded, the prediction effect of this model will be greatly improved, as shown in Fig. 4.15. The BT09 method was significantly underestimated on February 27–28, but had a reasonable agreement after 22:00. The best simulation performance occured from the night of February 29 to March 01, which accurately captures the changing process of the N_2O_5 uptake coefficient from 02:00 to 06:00. The simulation results of the other four days are higher than the measured values. We found the BT09 program seriously underestimated the N_2O_5 uptake coefficient on February 21 and March

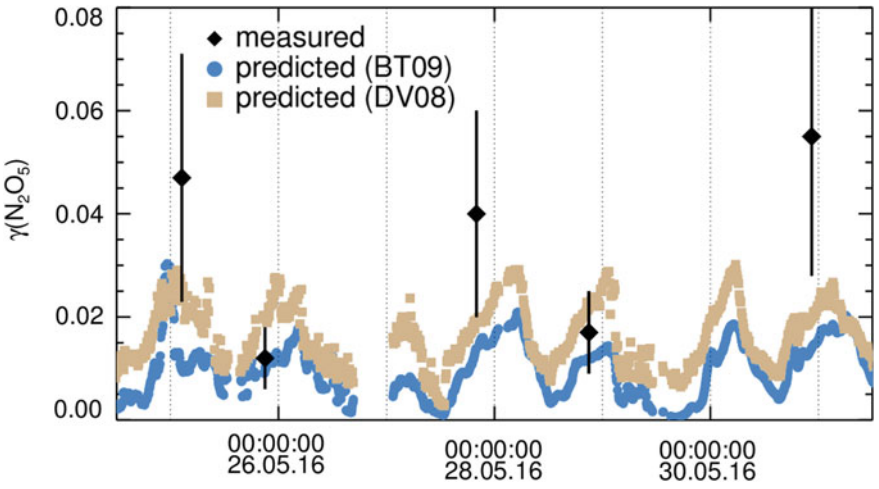

Fig. 4.14 Intercomparison of the N_2O_5 uptake coefficient by field determination and parameterization of BT09 and DV08

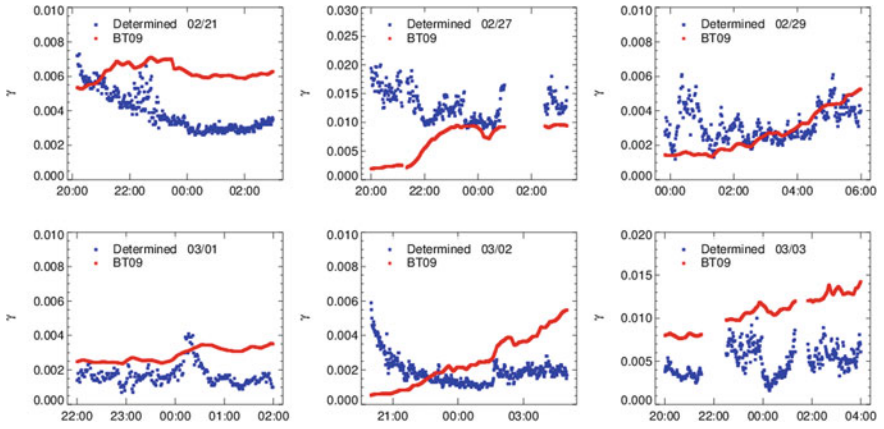

Fig. 4.15 Intercomparison of the N_2O_5 uptake coefficient by field determination and BT09 parameterization method in the HR winter campaign

02. Mainly due to the low relative humidity in the first half of the night, the water content calculated by the thermodynamic model is 0, which caused large uncertainty. In other periods, BT09 parameterization scheme generally has an overestimation with 50–150%.

Figure 4.16a shows the functional dependence of the ratio between the BT09 parameterization scheme and the observation results on RH (except February 27). When the RH is less than 35%, the BT09 method is significantly lower than the observed value. When the RH is larger than 35%, the ratio starts to be greater than 1. It increases with the increase of RH, indicating that the overestimation of BT09 has a clear dependence on RH humidity. When RH > 65%, the overestimation of BT09 reaches 100–150%. There are three possible reasons that caused overestimation. Firstly, the role of water content in BT09 is overestimated. Secondary, the estimated aerosol water content by ISORRPIA-II may have a systematic overestimation. At last,

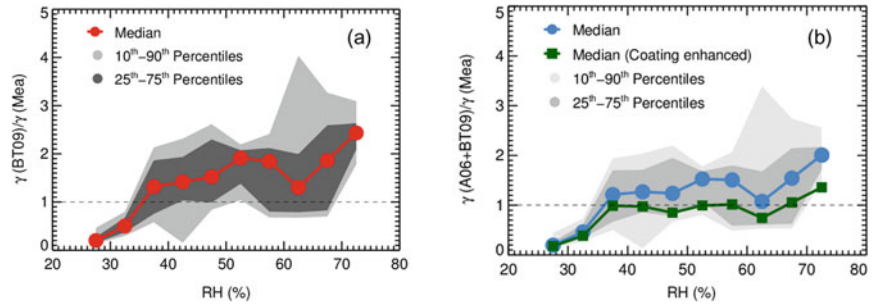

Fig. 4.16 The dependence of the ratio of the parameterized to the determined N_2O_5 uptake coefficient on RH in the HR winter campaign (excluded 02/27), **a** shows the BT09 result, **b** shows the A06 + BT09 (dodger blue) and the coating enhanced A06 + BT09 (dark green)

the organic coating effect is not considered. The first two possibilities are difficult to verify, and the third one can be verified or assessed by using the A06 organic coating model.

The parameterization scheme of organic coatings recommended by Anttila et al., is used to consider the uptake coefficient of organic coatings, and the BT09 scheme is used to calculate the uptake coefficient of the inorganic aerosol core, namely the A06 + BT09 scheme. Figure 4.16b shows the result of the A06 + BT09 scheme. After considering the organic coating, the predicted value is reduced by 20%, which effectively reduces the gap between the observation and prediction. However, under high relative humidity, there is still an overestimation of nearly 100%.

Recent studies indicate that low O:C organic-coated aerosols have a greater inhibitory effect on N_2O_5 heterogeneous uptake. Even when the organic content is less than 20%, it may still reduce N_2O_5 uptake by more than 80% [14]. During the last pollution episode in the Huairou campaign, the average O:C ratio of aerosol organics was 0.44. The case met the typical low O:C conditions, reflecting that during the campaign, low-oxidized organics were more likely to exist as a core-shell structure. The parameterization scheme recommended by [14] suggests that under low relative humidity conditions, D_{org} is low and can be replaced by 0.008 D_{aq}. Here we called this scheme as organic coating enhanced model (Coating enhanced). As shown in Fig. 4.17b, when RH over 35%, this coating enhanced parameterized model can well simulate the change of N_2O_5 uptake coefficient. Although there is no direct evidence on the value of D_{org}, it also shows that under winter conditions in Beijing, the inhibitory effect of organic matter on N_2O_5 uptake may be underestimated.

Figure 4.17 shows the comparison of the DV08 parameterization and observed results. The N_2O_5 uptake coefficient calculated by DV08 is higher than the observation result overall, and the degree of overestimation can be up to 4 times. Only on February 27 to 28 matches well. Besides, although the N_2O_5 uptake coefficient value

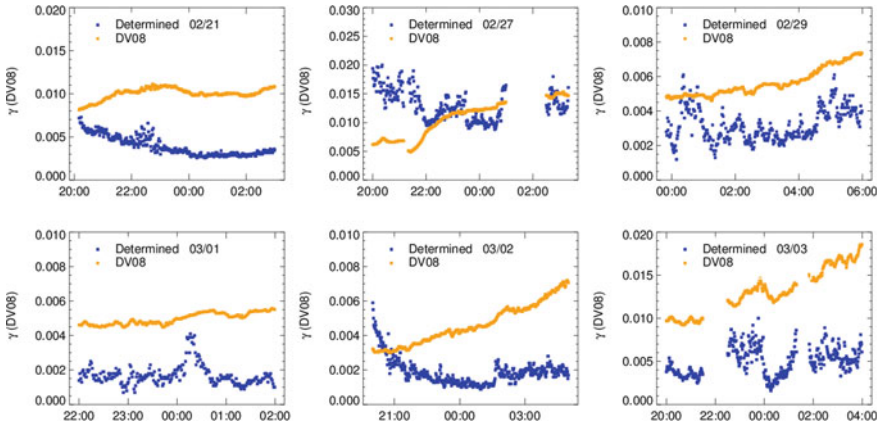

Fig. 4.17 Intercomparison of the N_2O_5 uptake coefficient by field determination and DV08 parameterization method in the HR winter campaign

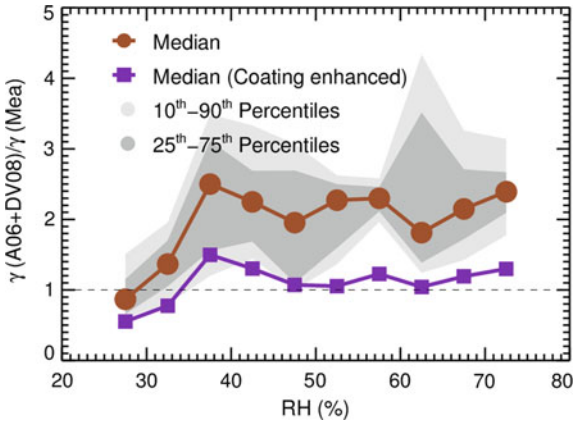

Fig. 4.18 The dependence of the ratio of the N_2O_5 uptake coefficient calculated by parameterization method to field determination on RH in the HR winter campaign (excluded February 27), shows the A06 + DV08 (dodger blue) and the coating enhanced A06 + DV08 (purple)

simulated by the DV08 scheme is much higher than the observation results on the night of February 29 and March 03, the intercomparison depicted a good agreement from the trend during the two nights.

Figure 4.18 shows that the A06 + DV08 parameterization scheme still generally overestimate more than 100% under the condition that the organic coating effect is not enhanced. With the enhancement of the organic coating effect, the predicted uptake coefficient value can better match the measured value. This result shows that the inhibition of organic coatings may play a significant role. In summary, BT09 and DV08 have a certain degree of overestimation in the prediction of the N_2O_5 uptake coefficient in Beijing winter. The heterogeneous reaction of N_2O_5 in Beijing winter may have a significant organic coating inhibition effect, and this inhibition effect has a higher suppression effect than the previous classic organic coating model. However, it needs to be further verified by field and laboratory experiments.

4.5 NO_3 and N_2O_5 Loss Rates

Based on the steady-state method, the steady-state lifetimes of NO_3 and N_2O_5 can be calculated, and the removal capacity of NO_3 and N_2O_5 at the measuring site can be evaluated. This method has been widely used in the study of nocturnal NO_3 and N_2O_5 chemistry. The calculations show that the N_2O_5 steady-state lifetime in summer campaign at PKU is below 1278 s, with an average value of 80 ± 110 s. The N_2O_5 steady-state lifetime in the Changping summer campaign ranged from <5 to 1140 s, with an average of 310 ± 240 s. It shows that the removal process of N_2O_5 in urban areas is very fast. Due to the limitation of the VOCs measurement during the PKU summer campaign, the direct quantification of k_{NO3} cannot be achieved. Based on the steady-state calculation, not only the N_2O_5 uptake coefficient can be calculated, but the linear fitting intercept can also indicate the reaction activity of NO_3. The NO_3 and N_2O_5 removal rates of the four polluted days observed at the PKU campaign were

calculated. The N_2O_5 heterogeneous removal rate was calculated using the average daily N_2O_5 uptake coefficient. The comparison found that the N_2O_5 heterogeneous reaction contributed 70–100% to the removal of NO_3–N_2O_5 on four polluted days (September 23, September 24, September 29, and September 30), which completely dominated the loss of NO_3 and N_2O_5. While in clean days, the removal process of N_2O_5 contributes minor, even if the uptake coefficient is kept above 0.05. It shows during nighttime, in addition to the level of N_2O_5 uptake coefficient, the proportion of NO_3 and N_2O_5 removal processes will be strongly affected by the level of particulate matter.

Figure 4.19 shows the comparison results of the N_2O_5 total removal rate calculated based on two different methods during the Changping campaign. Here the steady-state loss rate constant ($L_{ss}(N_2O_5)$) is the reciprocal of the steady-state lifetime, and k_{N2O5} represents the contribution of N_2O_5 heterogeneous to the loss term. The contribution to k_{NO3} is unified by chemical equilibrium conversion, where the heterogeneous uptake of N_2O_5 is 8.1×10^{-4} s^{-1}, and the NO_3 + VOCs is 1.63×10^{-3} s^{-1}, NO_3 oxidation dominates the removal process of NO_3–N_2O_5 during the Changping campaign, accounting for more than 65%. Besides, through comparison, it is found that the loss rate constant calculated by the steady-state method is slightly higher than the calculated sum from NO_3 oxidation and N_2O_5 uptake. This difference may be caused by two aspects. On the one hand, the species of VOCs measured by PTR-MS are limited and not comprehensive; a large number of VOCs did not include in the calculation. On the other hand, although all the data filtering in the calculation was a period with NO less than 0.1 ppbv, the NO concentration below 0.1 ppbv can still make a certain contribution. Some unmeasured VOCs and lower concentrations of NO were not included in the calculation of k_{NO3}, which resulted in a low loss rate constant of 1.63×10^{-3} s^{-1}.

During the Huairou winter campaign, the steady-state analysis method is difficult to apply. The uncertainty of the lifetime calculated by the steady-state method is large. If the clean day is dominated by the VOCs reaction of NO_3, the reaction activity is about 0.005 s^{-1}, and the nocturnal life of NO_3 is about 3 min. Assuming that the uptake coefficient is 0.003, and the aerosol surface area is 1000 μm^2 cm^{-3}

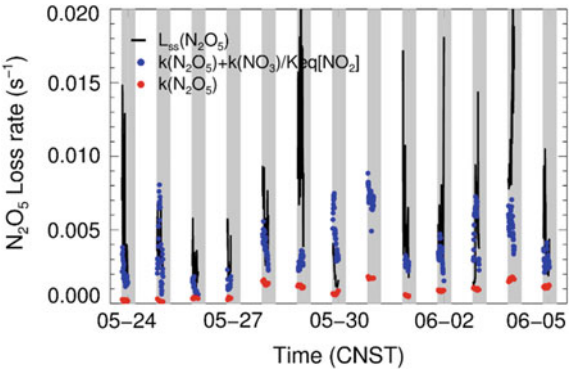

Fig. 4.19 Time series of the individual N_2O_5 loss terms and the loss rate constant of N_2O_5 in steady-state (named as $L_{ss}(N_2O_5)$) in CP summer campaign

in polluted days. It is estimated that the atmospheric lifetime of N_2O_5 is about 1.5 h, which is much longer than the summer atmospheric lifetime. In general, NO_3 and N_2O_5 are more reactive in summer, and the atmospheric life in summer is short; the reaction in winter is relatively slow, and the corresponding atmospheric timelife is relatively long.

4.6 Summary

This chapter mainly introduces the sources and sink of NO_3 and N_2O_5. The NO_3 production rate is as high as 1–2 ppbv h^{-1}, which is about an order of magnitude higher than that in winter. The NO_3 reactivity in summer is much higher than that in winter. The k_{NO3} observed in PKU and Huairou winter campaign is 6.6×10^{-3} s^{-1} and 3.7×10^{-3} s^{-1}, respectively, while the average value in Changping summer campaign can reach 1.9×10^{-2} s^{-1}, in which BVOCs dominate the NO_3 oxidation removal processes.

Based on the quantification of the N_2O_5 uptake coefficient, it is found that there are generally high uptake coefficients in the summer in Beijing, with the values ranging from 0.012 to 0.072, and an average value of 0.04, which is much higher than the field measurement results in Europe and America. The N_2O_5 uptake coefficient in winter is low, with an average of 0.005, which increases with the increase of RH, and has a significant positive correlation with H_2O/NO_3^- in the particles, indicating that the importance of aerosol water content and the particles nitrate in the N_2O_5 uptake processes. The parameterized model of inorganic aerosols generally overestimates the N_2O_5 uptake coefficient. Even considering the organic coating model proposed by Anttila et al. [3], it is still overestimated, we proposed that it may underestimate the inhibitory effect of organic matter on N_2O_5 uptake in Beijing winter.

Analysis of the removal process revealed that the removal rate in summer is much higher than that in winter. The atmospheric lifetime of N_2O_5 in summer is short, on the scale of minutes, and the atmospheric lifetime of N_2O_5 in winter can reach the order of hours. Regardless of whether it is summer or winter, the N_2O_5 heterogeneous reaction on the PM polluted day dominates the removal process of NO_3 and N_2O_5.

References

1. Aldener M, Brown SS, Stark H, Williams EJ, Lerner BM, Kuster WC et al (2006) Reactivity and loss mechanisms of NO_3 and N_2O_5 in a polluted marine environment: results from in situ measurements during New England air quality study 2002. J Geophys Res Atmos 111(D23)
2. Ambrose JL, Mao H, Mayne HR, Stutz J, Talbot R, Sive BC (2007) Nighttime nitrate radical chemistry at Appledore island, Maine during the 2004 international consortium for atmospheric research on transport and transformation. J Geophys Res Atmos 112(D21)

3. Anttila T, Kiendler-Scharr A, Tillmann R, Mentel TF (2006) On the reactive uptake of gaseous compounds by organic-coated aqueous aerosols: theoretical analysis and application to the heterogeneous hydrolysis of N_2O_5. J Phys Chem A 110(35):10435–10443
4. Atkinson R, Arey J (2003) Atmospheric degradation of volatile organic compounds. Chem Rev 103(12):4605–4638
5. Atkinson R, Baulch DL, Cox RA, Crowley JN, Hampson RF, Hynes RG et al (2006) Evaluated kinetic and photochemical data for atmospheric chemistry: volume II—gas phase reactions of organic species. Atmos Chem Phys 6:3625–4055
6. Bertram TH, Thornton JA (2009) Toward a general parameterization of N2O5 reactivity on aqueous particles: the competing effects of particle liquid water, nitrate and chloride. Atmos Chem Phys 9(21):8351–8363
7. Bertram TH, Thornton JA, Riedel TP (2009) An experimental technique for the direct measurement of N_2O_5 reactivity on ambient particles. Atmos Measur Tech 2(1):231–242
8. Brown SS, Dube WP, Fuchs H, Ryerson TB, Wollny AG, Brock CA et al (2009) Reactive uptake coefficients for N_2O_5 determined from aircraft measurements during the Second Texas air quality study: comparison to current model parameterizations. J Geophys Res Atmos 114
9. Brown SS, Dube WP, Peischl J, Ryerson TB, Atlas E, Warneke C et al (2011) Budgets for nocturnal VOC oxidation by nitrate radicals aloft during the 2006 Texas air quality study. J Geophys Res Atmos 116
10. Brown SS, Dube WP, Tham YJ, Zha QZ, Xue LK, Poon S et al (2016) Nighttime chemistry at a high altitude site above Hong Kong. J Geophys Res Atmos 121(5):2457–2475
11. Brown SS, Ryerson TB, Wollny AG, Brock CA, Peltier R, Sullivan AP et al (2006) Variability in nocturnal nitrogen oxide processing and its role in regional air quality. Science 311(5757):67–70
12. Brown SS, Stark H, Ryerson TB, Williams EJ, Nicks DK, Trainer M et al (2003) Nitrogen oxides in the nocturnal boundary layer: simultaneous in situ measurements of NO_3, N_2O_5, NO_2, NO, and O-3. J Geophys Res Atmos 108(D9): ACH18
13. Brown SS, Stutz J (2012) Nighttime radical observations and chemistry. Chem Soc Rev 41(19):6405–6447
14. Gaston CJ, Thornton JA, Ng NL (2014) Reactive uptake of N_2O_5 to internally mixed inorganic and organic particles: the role of organic carbon oxidation state and inferred organic phase separations. Atmos Chem Phys 14(11):5693–5707
15. Griffiths PT, Cox RA (2009) Temperature dependence of heterogeneous uptake of N_2O_5 by ammonium sulfate aerosol. Atmos Sci Lett 10(3):159–163
16. Hallquist M, Stewart DJ, Stephenson SK, Cox RA (2003) Hydrolysis of N_2O_5 on sub-micron sulfate aerosols. Phys Chem Chem Phys 5(16):3453–3463
17. Liebmann J, Karu E, Sobanski N, Schuladen J, Ehn M, Schallhart S et al (2018) Direct measurement of NO_3 radical reactivity in a boreal forest. Atmos Chem Phys 18(5):3799–3815
18. Liebmann JM, Schuster G, Schuladen JB, Sobanski N, Lelieveld J, Crowley JN (2017) Measurement of ambient NO_3 reactivity: design, characterization and first deployment of a new instrument. Atmos Measur Tech 10(3):1241–1258
19. Morgan WT, Ouyang B, Allan JD, Aruffo E, Di Carlo P, Kennedy OJ et al (2015) Influence of aerosol chemical composition on N_2O_5 uptake: airborne regional measurements in northwestern Europe. Atmos Chem Phys 15(2):973–990
20. Nguyen TKV, Zhang Q, Jimenez JL, Pike M, Carlton AG (2016) Liquid water: ubiquitous contributor to aerosol mass. Environ Sci Technol Lett 3(7):257–263
21. Phillips GJ, Thieser J, Tang MJ, Sobanski N, Schuster G, Fachinger J et al (2016) Estimating N_2O_5 uptake coefficients using ambient measurements of NO_3, N_2O_5, $ClNO_2$ and particle-phase nitrate. Atmos Chem Phys 16(20):13231–13249
22. Platt U, Perner D, Winer AM, Harris GW, Pitts JN (1980) Detection of NO_3 in the polluted troposphere by differential optical-absorption. Geophys Res Lett 7(1):89–92
23. Riedel TP, Bertram TH, Ryder OS, Liu S, Day DA, Russell LM et al (2012) Direct N_2O_5 reactivity measurements at a polluted coastal site. Atmos Chem Phys 12(6):2959–2968

24. Stutz J, Wong KW, Lawrence L, Ziemba L, Flynn JH, Rappengluck B et al (2010) Nocturnal NO_3 radical chemistry in Houston, TX. Atmos Environ 44(33):4099–4106
25. Tham YJ, Wang Z, Li QY, Yun H, Wang WH, Wang XF et al (2016) Significant concentrations of nitryl chloride sustained in the morning: investigations of the causes and impacts on ozone production in a polluted region of northern China. Atmos Chem Phys 16(23):14959–14977
26. Wagner NL, Riedel TP, Young CJ, Bahreini R, Brock CA, Dube WP et al (2013) N2O5 uptake coefficients and nocturnal NO_2 removal rates determined from ambient wintertime measurements. J Geophys Res Atmos 118(16):9331–9350
27. Wang H, Lu K, Guo S, Wu Z, Shang D, Tan Z et al (2018) Efficient N_2O_5 uptake and NO_3 oxidation in the outflow of urban Beijing. Atmos Chem Phys 18(13):9705–9721
28. Wang XF, Wang H, Xue LK, Wang T, Wang LW, Gu RR et al (2017) Observations of N_2O_5 and $ClNO_2$ at a polluted urban surface site in North China: high N_2O_5 uptake coefficients and low $ClNO_2$ product yields. Atmos Environ 156:125–134
29. Wang Z, Wang WH, Tham YJ, Li QY, Wang H, Wen L et al (2017) Fast heterogeneous N_2O_5 uptake and $ClNO_2$ production in power plant and industrial plumes observed in the nocturnal residual layer over the North China Plain. Atmos Chem Phys 17(20):12361–12378
30. Wu Z, Wang Y, Tan T, Zhu Y, Li M, Shang D et al (2018) Aerosol liquid water driven by anthropogenic inorganic salts: implying its key role in haze formation over the North China plain. Environ Sci Technol Lett

Chapter 5
Atmospheric Impacts

Abstract This chapter introduces the atmospheric impacts of NO_3 and N_2O_5 chemistry in Beijing. It includes three aspects: (1) It was estimating the NO_3 oxidation and the contribution to atmospheric oxidation. (2) Based on the existing chemical reaction mechanism, quantifying the contribution of each nitrate production pathways by constraining the key parameters, and assessing the effect of N_2O_5 heterogeneous hydrolysis on the formation of particulate nitrate. (3) Evaluating the production of $ClNO_2$ in winter and look insight into the role of $ClNO_2$ in photochemistry.

5.1 Nocturnal Atmospheric Oxidation

The main oxidants in the atmosphere are OH, O_3, and NO_3. OH is mainly driven by photochemical reactions and dominates the atmospheric oxidation process during the day, NO_3 oxidation is concentrated at night, and the oxidation process of O_3 covers the entire time range. To systematically characterize the contribution of NO_3 chemistry to atmospheric oxidation, a comparative analysis of the chemical reaction process of OH, NO_3, and O_3 on a 24-h time scale is required.

During the summer Changping campaign, there is a lack of OH radical measurement. However, the OH radical concentration is controlled by the photochemical process. It has a good correlation with $j(O^1D)$ [17], so the OH can be estimated based on the observation of $j(O^1D)$. Under different environmental conditions, the slopes of OH radicals and $j(O^1D)$ have a certain difference. The air mass of the Wangdu campaign (June) in summer 2014 is similar to that of the Changping campaign. In the Wangdu campaign, we observed a slope of OH and $j(O^1D)$ with 4.5×10^{11} cm^{-3} s^{-1} and an intercept of 1×10^6 cm^{-3} [20]. The average concentration level of OH radicals estimated in the Changping campaign by applying this slope (without considering the intercept). The average OH level is 2.6×10^6 cm^{-3}, and the peak daytime concentration level is 4.0×10^6–1.2×10^7 cm^{-3}.

The measured VOCs in Changping is not comprehensive, but isoprene and monoterpene are valid. Isoprene and monoterpene are the two species with the largest emissions of natural source VOCs, so these two species are used to represent BVOCs. Figure 5.1 shows the oxidation rate of BVOCs by the three atmospheric oxidants. The

H. Wang, *The Chemistry of Nitrate Radical (NO_3) and Dinitrogen Pentoxide (N_2O_5) in Beijing*, Springer Theses, https://doi.org/10.1007/978-981-15-8795-5_5

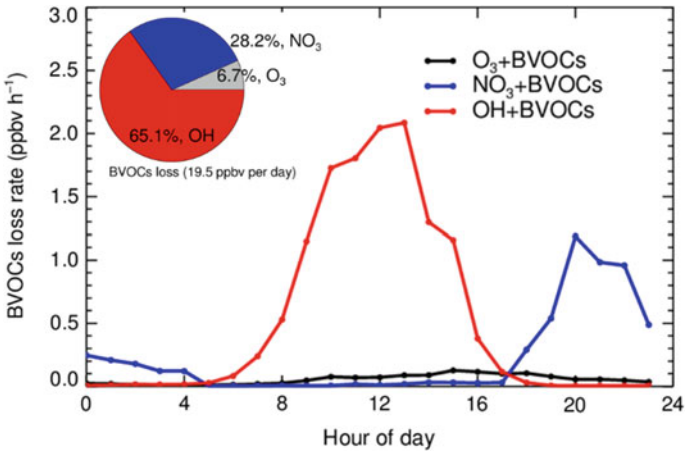

Fig. 5.1 The mean diurnal variation of the loss rate of BVOCs by oxidation reaction in the CP summer campaign, the red, blue, and black lines represent the contribution of OH, NO_3, and O_3; the insert pie chart showed the distribution of the three oxidants

degradation trend of BVOCs by OH is consistent with the daily change of OH. The removal rate reaches a maximum value of 2.1 ppbv h^{-1} at noon, the daily removal of BVOCs by OH reached 12.7 ppbv. The average daily removal of BVOCs by NO_3 is 5.5 ppbv, and the removal rate is consistent with the daily variation of NO_3 mixing ratio. The daily removal of BVOCs by O_3 was the smallest, only 1.3 ppbv. The pie chart inserted in Fig. 5.1 shows the contribution of three oxidants to the removal of BVOCs on the 24-h scale. On the 24-h scale, OH is still the main oxidant for the removal of BVOCs, but only dominates the daytime process, and the contribution of NO_3 radicals is 28%, which is similar to the results reported in German forest areas [6]. In addition, the calculation indicates that NO_3 dominates the oxidative degradation of more than 90% of BVOCs throughout the night, and is the most important oxidant at night in suburban Beijing. The reaction rates of different types of VOC species and the above three oxidants are different. For example, the reaction rate of NO_3, O_3 with alkane is slow, OH radical is the most important oxidant of alkane. An aircraft measurement in North America shows that NO_x emission has an important effect on NO_3 oxidation at night. When the ratio of NO_x/isoprene at sunset is larger than 0.6, NO_3 dominates the oxidation process at night. When the ratio increases, the leading role of NO_3 is further strengthened, and the oxidation contribution can exceed 90% [4]. During the Changping campaign, the ratio of NO_x/isoprene keep above 10, and excessive NO_x as a precursor of NO_3 ensured the dominant of NO_3 in the nighttime oxidation. In general, NO_3 in summer is a very important oxidant and has an important role in the oxidation of VOCs.

Although OH and BVOCs have a fast reaction rate, the yield of organic nitrate is lower than that of NO_3 oxidation. A model simulation study based on the constrained measurement data of Yufa (suburban Beijing) in 2006 found that the NO_3 oxidation and OH oxidation processes during summer nights contributed equally to the

production of organic nitrate, and the production rate of organic nitrate at night was 0.06 ppbv h^{-1} [24]. In order to estimate the contribution of NO_3 oxidation of BVOCs to the organic nitrate formation, the yield of organic nitrate produced by the reaction of NO_3 with isoprene was set to 0.7 [18]. The yield of organic nitrate produced by NO_3 with monoterpenes was set to 0.15 [19]. Here we assume that all the monoterpenes are α-pinene. The calculated rate of NO_3 oxidation of BVOCs at night was 0.11 ± 0.09 ppbv h^{-1}. Since organic nitrate may be an important precursor of SOA, the NO_3 oxidation process at night in the Changping campaign may have a very important contribution to the formation of SOA.

During the winter campaign in Huairou, the OH radicals measurement is available, but the lack of simultaneous measurement of monoterpenes. In order to systematically evaluate the atmospheric oxidation in winter, a box model is used to simulate the atmospheric oxidation process. In this model, the RACM2 mechanism is used, and OH, N_2O_5, O_3, and merged VOCs are constrained [9]. The constrain of N_2O_5 can better simulate the NO_3 concentration level, and the N_2O_5 uptake coefficient is set to 0.005, and the $ClNO_2$ yield is set to the unit.

Figure 5.2 shows the average diurnal variation of the oxidation rate of VOCs by OH, NO_3, and O_3 during the winter campaign in Huairou. The overall oxidation capacity is about an order of magnitude lower than that in summer (Yufa in 2006 and PKU in 2008, the daytime peak value obtained by using the same model simulation can reach 15 ppbv h^{-1}). OH still dominates the entire winter oxidation removal processes, and the pattern of OH-dominated atmospheric oxidation process has not changed with the seasonal changes. Unlike that in summer, the O_3 oxidation rate in winter is higher than that of NO_3 at night, which reflects NO_3 oxidation capacity in winter is significantly reduced and not important. The average oxidation rate of NO_3 at night is only 0.05 ppbv h^{-1}, which is even lower than the nocturnal OH oxidation rate. A significant concentration of OH radicals ($0.5–3 \times 10^6$ cm^{-3}) was once observed at night in summer [10]. Compared with the daytime, the night OH concentration level is low, and the measurement values near the detection limit, with a certain degree of uncertainty, but in the case where the overall oxidation capacity is weak at night, OH may play an important role in nocturnal atmospheric oxidation.

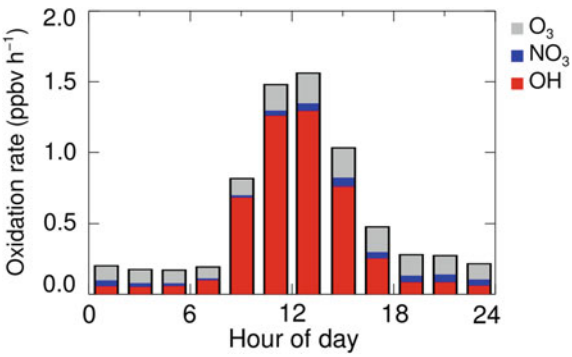

Fig. 5.2 The mean diurnal variation of the oxidation rate in the HR winter campaign

In summary, the winter OH in Beijing is the most important source of atmospheric oxidization. NO_3 has a weak and limited oxidation contribution.

5.2 Nitrate Formation

Nitrate acid is an important part of the particulate matter composition. High particulate nitrate fraction of $PM_{2.5}$ has been reported in Beijing. The nocturnal growth of nitrate at night may relate to the N_2O_5 heterogeneous chemical process [14, 15]. However, due to the lack of determining N_2O_5 and N_2O_5 uptake coefficient, the nitrate produced by N_2O_5 heterogeneous reaction cannot be well quantified. In this study, the nitrate production rate during the N_2O_5 heterogeneous reaction can be calculated based on the constrain of observed N_2O_5 and its uptake coefficient. During the PKU summer campaign, the nitrate production rate within the effective time range of the N_2O_5 uptake coefficient (September 23, 24, 29, 30) was quantified. The $ClNO_2$ yield was set to 1 to calculate a lower limit of nitrate formation.

Figure 5.3 shows the average diurnal change of nitrate production rate contributed by the N_2O_5 heterogeneous reaction in the above four days. The rate of the first half of the night is fast and has a large change. The peak is concentrated around 20:00, which is usually accompanied by the peak of N_2O_5 concentration appears, and the nitrate production rate at this time can reach a maximum of 27 $\mu g\ m^{-3}\ h^{-1}$. Table 5.1 summarizes the total amount of nitrate produced per day calculated from the N_2O_5 uptake, ranging from 23.8 to 84.6 $\mu g\ m^{-3}$, and the daily nitrate production is mainly concentrated in the first half of the night. The four-day average production was 56.8 $\pm$ 27.6 $\mu g\ m^{-3}$. Previous studies in Taishan, Shandong province indicated that the N_2O_5 heterogeneous reaction at night could contribute 17 $\mu g\ m^{-3}$ nitrate, which is

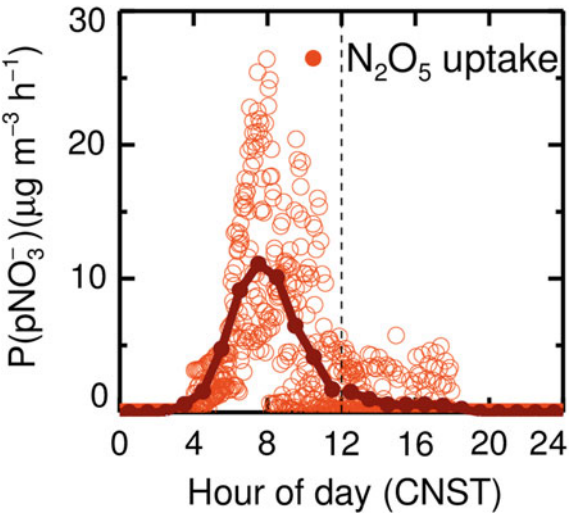

Fig. 5.3 The mean diurnal variation of the particulate nitrate formation rate via N_2O_5 heterogeneous uptake in the PKU summer campaign. Reproduced with permission [24]. Copyright (2017) American Chemical Society

Table 5.1 Daily integrated pNO_3^- formation potential from N_2O_5 hydrolysis reaction in PKU summer campaign

Time (CNST)	γ	S_a (μm^2 cm^{-3})	pNO_3^- formation potential (before 24:00) (μg m^{-3})	pNO_3^- formation potential (all night) (μg m^{-3})
23/09–24/09	0.031	3061	40.5	45.1
24/09–25/09	0.072	3101	64.7	84.6
29/09–30/09	0.063	1270	23.8	23.8
30/09–01/10	0.025	1624	72.2	73.5
Average ± SD	0.048 ± 0.023	2264 ± 955	50.3 ± 22.3	56.8 ± 27.6

Table 5.2 The average HNO_3 production rate from the gas-phase chemical reactions during the PKU summer campaign

Reactions	Reaction rate constants (298 K, cm^3 $molecule^{-1}$ s^{-1})	HNO_3 production rate (ppbv h^{-1})
$HCHO + NO_3 \rightarrow HNO_3 + CO + HO_2$	5.56×10^{-16}	8.0×10^{-4}
$HO_2 + NO_3 \rightarrow 0.3HNO_3 + 0.7 NO_2 + 0.7OH$	4.0×10^{-12}	2.3×10^{-3}
$N_2O_5 + H_2O \rightarrow 2HNO_3$	2.5×10^{-22}	5.0×10^{-2}
$HO_2 + NO \rightarrow HNO_3$	4.56×10^{-15}	2.2×10^{-3}
$OH + NO_2 \rightarrow HNO_3$	9.41×10^{-12}	1.3

much lower than the results in this study [27]. The main difference is that the NO_3 production rate of Taishan is much lower than that of Beijing's urban sites.

In addition to the N_2O_5 heterogeneous reaction, the particulate nitrate may also come from other reactions. Table 5.2 summarizes the reaction pathways for the gas phase reaction to generate HNO_3, the reaction rate constant, and the average during the summer observation period. It can be found that the main reaction pathway is the reaction of $OH + NO_2$, and its production rate is 1.3 ppbv h^{-1}, which occupies more than 95% of the gas-phase formation of HNO_3. The reaction is mainly concentrated in the process of high OH concentration during the day. Therefore, it can be considered that there are two main ways to generate particulate nitrate. The first one is the heterogeneous reaction of N_2O_5, and the second is the gas phase reaction of OH and NO_2 and the subsequent partitioning in the presence of NH_3. In order to quantitatively compare the contribution of the two reaction pathways, the ISORRPIA-II model was used to estimate the gas-particle partition coefficient of nitrate. It was found that the air masses in the Beijing area features high temperature, high humidity, and high NH_3; the entire distribution is inclined to the particle phase. Figure 5.4 shows the average daily change in the partition coefficient estimated by the above four-day model, with an average coefficient value of 0.79. Assuming that 79% of the HNO_3 generated in the gas phase enters the particle phase and forms particulate

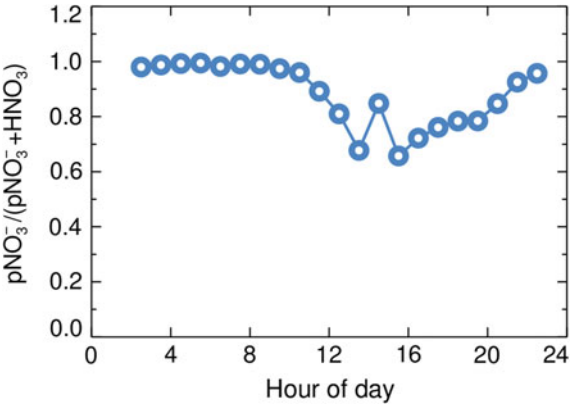

Fig. 5.4 Mean diurnal profile of the calculated partition of HNO_3 to particle phase represented by $pNO_3^-/(pNO_3^- + HNO_3)$ during the four polluted days (September 23, 24, 29, 30)

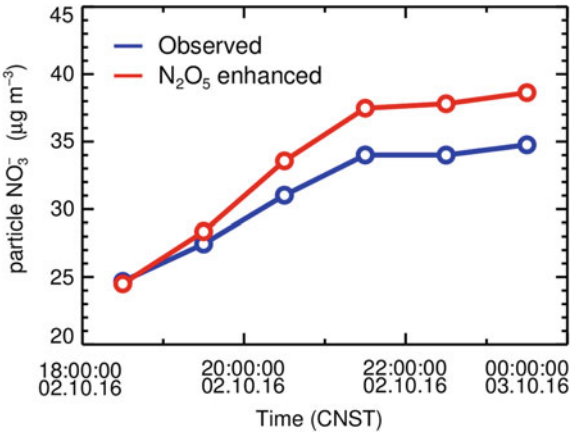

Fig. 5.5 A case of nocturnal particulate nitrate enhancement happened on the night of October 2, and the red curve shows the integrated particulate nitrate with an offset for comparison with the observation

nitrate, the daily production contribution can be 52.0 ± 11.0 μg m^{-3}, indicating that the contribution of gas reaction process to nitrate is lower than that of the N_2O_5 heterogeneous process.

The above analysis shows that N_2O_5 heterogeneous uptake is the key formation pathway of particulate nitrate during the accumulation of particulate matter in the summertime. The increase of particulate nitrate concentration will change the physical and chemical properties of particulate matter, such as particle optical absorption, scatting, and hygroscopicity [28], thereby further aggravating particulate pollution. The average daily total nitrate production rate during the pollution episodes in urban Beijing in summer can reach hundreds of μg m^{-3}. However, the actual atmospheric nitrate concentration level is around 20 μg m^{-3}, which is much lower than the total production, which may be related to regional transportation and the process of atmospheric deposition.

Figure 5.5 shows the accumulated nitrate produced by the N_2O_5 heterogeneous reaction at night on October 2 and the actual observed nitrate growth process during

the night. An initial nitrate value is added for better intercomparison of nocturnal increase. The value of the uptake coefficient is set to an average of 0.048. We found that the nitrate enhancement caused by N_2O_5 uptake has a good synchronization with the actual measurement results, and the accumulated amount caused by the N_2O_5 heterogeneous process is larger than the actual nitrate growth. The gap is proposed to be the nitrate removal processes. This synchronization indicates that the nitrate growth observed at night likely attributed to the N_2O_5 heterogeneous reaction.

During the Changping campaign, the N_2O_5 uptake coefficient is calculated by the product growth fitting method. Therefore, it is quite self-consistent if using the uptake coefficient to calculate the nitrate production rate. The N_2O_5 uptake coefficient during the winter campaign in Huairou was well quantified, so the particulate nitrate formation can also be estimated, too. The average of the N_2O_5 uptake coefficient of the day was interpolated by the same night value when the uptake coefficient was available, and the IUPAC recommended 0.02 was used for other periods without the derived N_2O_5 uptake coefficients. The concentrations of OH and NO_2 were measured by LIF and PL methods, respectively. The yield of $ClNO_2$ is calculated based on the parameterization scheme proposed by [3]. The calculated yield is high, with an average value greater than 0.95. A unit yield is used for the calculation to keep the calculation principle consistent with that of the PKU summer campaign. The partition coefficient of the clean days calculated by HNO_3 and NO_3^- simultaneously measured by GAC is low. However, the partition coefficient of the polluted days is significantly increased. In the last continuous pollution process, almost all the soluble nitrate is in the particulate phase (Fig. 5.6). The ratio result of ISORROPIA-II estimation is much lower than the result of GAC measurement. Here we decided to use the result of GAC measurement to constrain the pNO_3^- production rate synchronously. In the last pollution process, the partition coefficient is almost equal to 1. The cleaning process shows the characteristics of large at daytime and small at nighttime. The nighttime distribution coefficient during clean days is about 0.6, while during polluted days, it is over 0.95.

As shown in Fig. 5.7, at a time resolution of 4 h, the contribution of N_2O_5 heterogeneous uptake on clean days to the nitrate production rate is almost negligible, and there is a certain contribution to pollution days, the total amount of nitrate produced

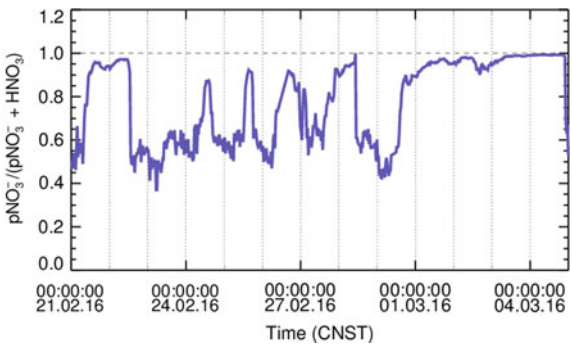

Fig. 5.6 The time series of the partition coefficient based on GAC data

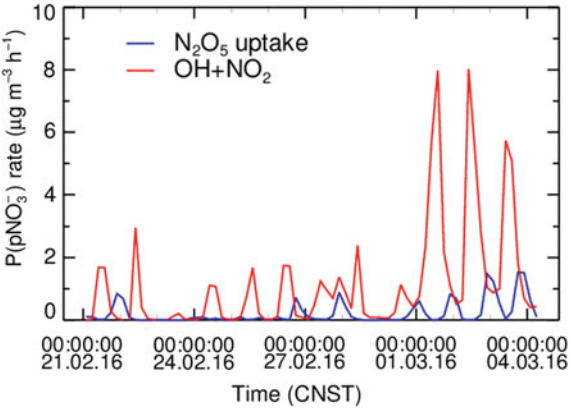

Fig. 5.7 The particulate nitrate formation rate via N_2O_5 uptake and OH + NO_2 from February 21 to March 04, 2016, during the HR winter campaign

by the N_2O_5 heterogeneous process at night is between 5 and 20 $\mu g\ m^{-3}$. The contribution of the OH + NO_2 channel is quite different. During the clean day, the contribution is relatively stable, the daytime peak of the production rate is usually around 2 $\mu g\ m^{-3}\ h^{-1}$, while the daytime peak of the polluted day is 1-8 $\mu g\ m^{-3}\ h^{-1}$, which was caused by the difference in the concentration of OH radicals. The daytime peak value of OH during cleaning before February 27 is only 3–6 $\times\ 10^6\ cm^{-3}$, while after February 27, the peak daily OH radical concentration after day is 4–12 $\times\ 10^6\ cm^{-3}$. The contribution of OH + NO_2 on clean days is small at night. However, during the polluted days, such as the last heavy pollution episode, the night-time formation from the gas-phase reaction channel can be comparable to the contribution of N_2O_5 uptake. Although the night OH is 5 $\times\ 10^5\ cm^{-3}$, the high concentration of NO_2 during pollution night enhanced the OH + NO_2. If the nitrate produced by the OH + NO_2 reaction at night is not considered, the N_2O_5 heterogeneous reaction accounts for 10–40% of the average daily nitrate production contribution during polluted days.

In the last stage of the heavy pollution process from February 29 to March 4, the N_2O_5 heterogeneous reaction produced a total of 42 $\mu g\ m^{-3}$ nitrate, while the OH + NO_2 reaction produced 212 $\mu g\ m^{-3}$ nitrate. The cumulative amount of nitrate in its two pathways is shown in Fig. 5.8. The contribution of the N_2O_5 heterogeneous reaction is 17%, which is much lower than the results observed in summer. Nevertheless, the contribution of N_2O_5 heterogeneous to nitrate should not be ignored. By comparison, it was found that except for the air mass change between March 2 and March 3, which caused a trough in the measured nitrate, the trend between the calculated value and the actual measured value in other periods was very consistent. On the one hand, the contribution of the above two nitrate formation pathways has the potential to explain the currently measured high nitrate concentration levels. On the other hand, the consistent trend shows the accuracy of the nitrate formation mechanism. Due to the lack of quantification of the removal rate of HNO_3 and particulate nitrate, it is impossible to conduct a closure budget experiment of particulate nitrate. From the perspective of the concentration trend, it may be possible to make

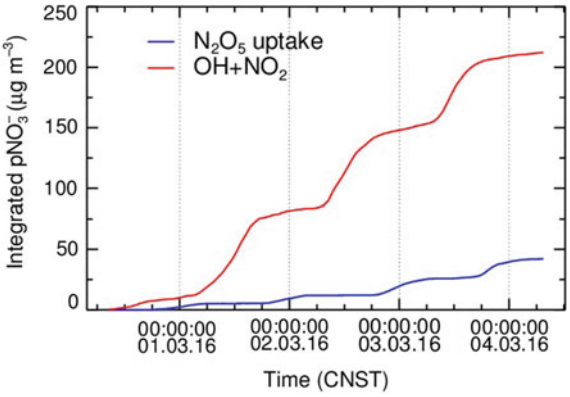

Fig. 5.8 The integrated particulate nitrate formed via N_2O_5 uptake and OH + NO_2 from February 29 to March 04, 2016, during the HR winter campaign

a better relationship between observed nitrate and nitrate formation potential after adding a reasonable removal rate constraint. Therefore, the measurement of relevant parameters in future studies may be able to predict the concentration level of nitrate accurately.

From 20:00 on February 28 to 4:00 on March 1, the weather conditions are relatively stable, assuming that there is no obvious regional transportation and air mass change. That is, only chemical processes exist. The calculated nitrate formation potential value between 20:00 on February 28 and 04:00 on March 1 is found to be slightly greater than the measured nitrate growth. When assuming the lifetime of nitrate is 48 h, and the initial concentration of nitrate set to 0.7 μg m^{-3}, the predicted growth of nitrate can well reproduce the observation results, as shown in Fig. 5.9a, there is a very good correlation between the observation and calculation. The correlation coefficient reaches 0.98 (as shown in Fig. 5.9b). Figure 5.10 shows the case from 06:00 on March 3 to 06:00 on March 4, which is consistent with the above one. The cumulative amount calculated based on the precursor is also higher

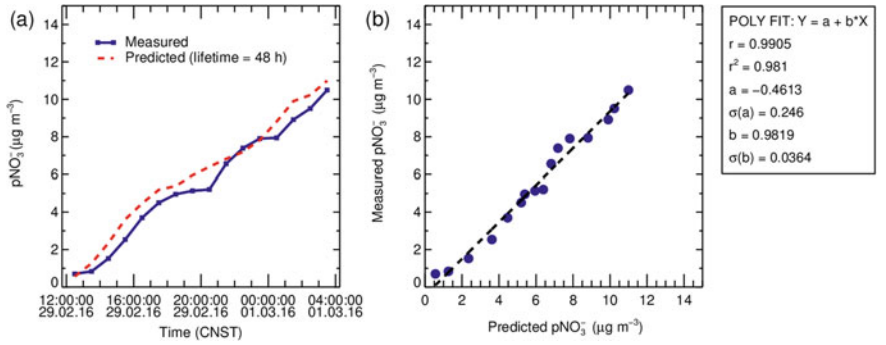

Fig. 5.9 **a** Shows intercomparison of the integrated particulate nitrate formed via N_2O_5 uptake and OH + NO_2 with the measured value from 02-28 to 03-01, 2016, during the HR winter campaign; **b** shows the correction of measurement and integration result

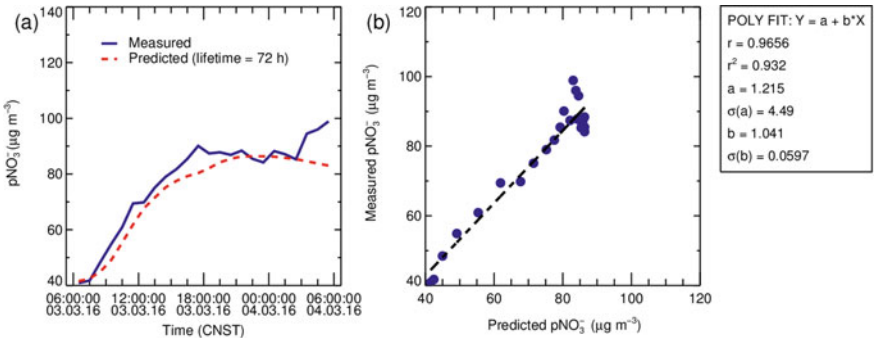

Fig. 5.10 **a** Shows the intercomparison of the integrated particulate nitrate formed via N_2O_5 uptake and OH + NO_2 with the measured value from 03-03 to 03-04, 2016, during the HR winter campaign; **b** shows the correction of measurement and integration result

than the measured value, the initial value set to 40.9 μg m^{-3}, and the atmospheric lifetime of nitrate set to 72 h, the model can predict the observation results with the correlation coefficient of 0.93. Early literature shows that the atmospheric life of fine particles is about seven days, and the results of this study show that when the atmospheric lifetime of particulate nitrate set 2–3 days, the simulation greatly improved. The partition between HNO_3 and particulate nitrate may accelerate the removal of nitrate as HNO_3 has a fast deposition rate. It may also be that there are other ways to remove particulate nitrate, resulting in a short atmospheric lifetime. Recent studies have pointed out that the photolysis of particulate nitrate may be an important way to generate HONO [29, 30]. Although this issue remains controversial, it may be pointed out for the possible removal pathway of particulate nitrate.

5.3 Nitryl Chloride Formation

In the four campaigns mentioned above, the synchronized $ClNO_2$ measurements are only available in the Changping campaign. The measurement results show that there is significant $ClNO_2$ production during the night. The calculated that the $ClNO_2$ yield in Beijing in summer was higher, between 0.5 and 1.0. Particle Cl^- is a key precursor for $ClNO_2$ production, but the Cl^- concentration level measured by AMS is always very low, with an average value lower than 40 pptv (see Fig. 5.11). The simultaneous analysis showed that the concentration of Cl^- in the particles has a good correlation with CO and SO_2, indicating that the source of Cl^- may be due to the biomass combustion processes [8]. However, even so, it is difficult to explain the source of Cl^- to produce $ClNO_2$. Based on the backward trajectory analysis, the air mass hardly comes from the coastal area, indicating that NaCl will not be an important source of Cl^-. During the PKU summer campaign, HCl up to 10 ppbv was once observed, which promote the speculation that a large amount of HCl continuously

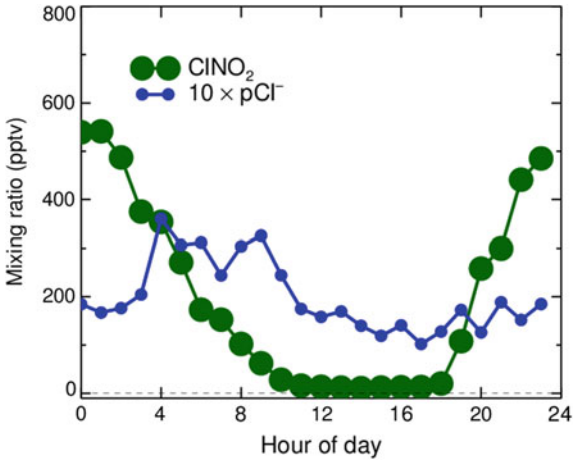

Fig. 5.11 The mean diurnal variation of $ClNO_2$ and particulate chloride times ten during the CP summer campaign

supplied Cl^- into the particle phase by the acid replacement reaction, and observed large HCl could be the precursors of $ClNO_2$. This speculation was also proposed in previous studies [21]. Subsequent analysis of the average daily change of chlorinated inorganics based on CIMS measurements found that only the daily change of HCl showed a clear anti-correlation relationship with $ClNO_2$, which may make the above speculation more convincing.

The calculated daily peak photolysis rate of $ClNO_2$, referred from the latest version of JPL dataset (Jet Propulsion Laboratory) is between 1.2 and 3.2×10^{-4} s^{-1} during the day. Based on the measured $ClNO_2$ and the parameterized photolysis rate constant, the production rate of Cl radicals can be determined (Fig. 5.11). In general, the production rate of Cl radicals is small, with a peak of around 1×10^5 cm^{-3} s^{-1}. In the early morning, the phenomenon that the concentration of $ClNO_2$ rises and reaches a peak appears to be mainly suspected to be caused by vertical transport [21]. When vertical transportation occurs, the calculated rate of Cl radical production rate can reach nearly 2.0×10^6 cm^{-3} s^{-1}, which is much higher than the results in other periods, such as the case on May 30 and June 5 (Fig. 5.12). Figure 5.13 shows the average daily change of the Cl radical production rate. The peak of the average Cl radical production rate appears around 08:00 in the morning. The peak can reach 5.2×10^5 cm^{-3} s^{-1}, which is more than ten times higher than the calculation results in the UK [1, 2], but compared with the results of Wangdu in China, the peak of Cl radical production rate in Changping is about one-third of that in Wangdu. Figure 5.13 shows the formation rate of Cl began to decrease rapidly after 08:00 in the morning, and the formation rate could be maintained at 1.0×10^5 cm^{-3} s^{-1} around noon, indicating that the oxidation process of Cl radicals was covered about half of the daytime. The long persisting period promotes $ClNO_2$ chemistry have a great contribution to the atmospheric oxidation during the day.

$$j(\mathrm{ClNO_2}) = 3.6 \times j\left(\mathrm{O^1D}\right) - 18,920 \times j\left(\mathrm{O^1D}\right)^2 + 0.027 \times j(\mathrm{NO_2}) + 0.094 \times j(\mathrm{NO_2})^2 \tag{5.1}$$

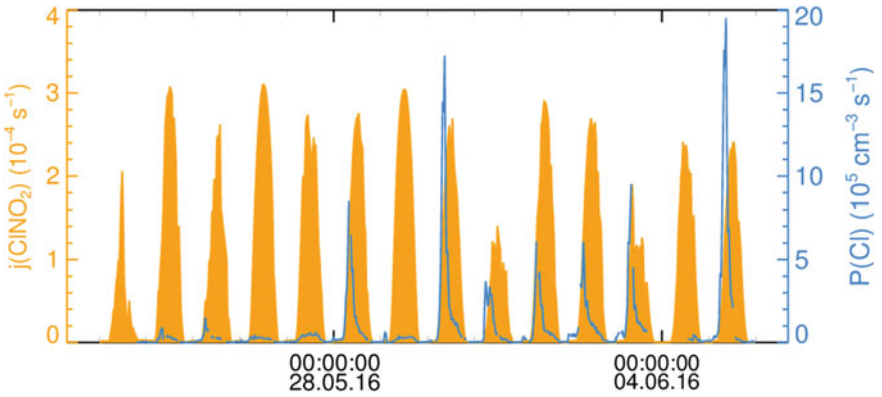

Fig. 5.12 Time series of the production rate of chloride radical via $ClNO_2$ photolysis during the CP summer campaign

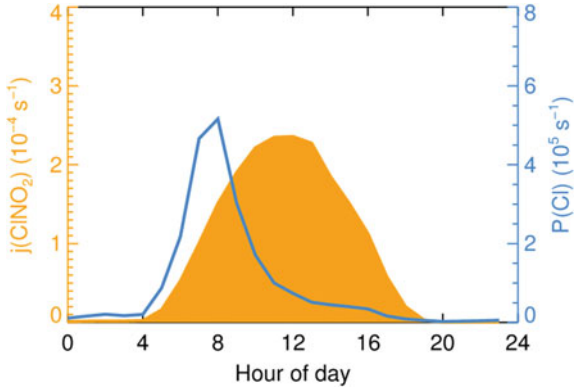

Fig. 5.13 The mean diurnal variation of the production rate of chloride radical via $ClNO_2$ photolysis during the CP summer campaign

Many field observations have been carried out to measure $ClNO_2$. Based on the measurement, the contribution of $ClNO_2$ photolysis to the production of Cl radicals is estimated. Table 5.3 summarizes the mean daily peak level of the Cl radical production rate based on $ClNO_2$ photolysis reported in the existing literature, which can represent the contribution of $ClNO_2$ to atmospheric oxidation to a certain extent. The production rate of Cl radicals is between 1 and 25 $\times$ 10^5 cm^{-3} s^{-1}. The production rate calculated based on the Changping campaign is at a medium level, while the production rate based on Wangdu is relatively high. It is worth mentioning that the observed $ClNO_2$ up to 4.7 ppbv at the high mountain site in Hong Kong, but there are also has a low case of 280 pptv, indicating that the $ClNO_2$ concentration varies greatly between different air masses. Under high $ClNO_2$ conditions, an additional 77% of OH and 106% of HO_2 may be produced by $ClNO_2$ chemistry, indicating that $ClNO_2$ may have a significant contribution to the photochemical process of the next day. However, the day-to-day difference in $ClNO_2$ concentration level may bring large

Table 5.3 Summary of the campaign average daily peak of the chloride radical via $ClNO_2$ photolysis reported in previously filed campaigns

Location	Region	P(Cl) ($\times 10^5$ cm^{-3} s^{-1}) Mean diurnal peak	References
Beijing, China	Rural	5.2	This study
Wangdu, China	Suburban	16.3	[21]
Hong Kong, China	Coastal	3.1	[22]
North Norfolk Coast, UK	Coastal	<1.0	[1]
London, UK	Urban	2.5	[2]
Hessen, Germany	Rural	12	[16]
Calgary, Canada	Rural	7 (Campaign peak)	[11]
Houston, USA	Urban	3.4 (Estimated)	[5]
Houston, USA	Urban	8.0	[13]
Boulder, USA	Rural	2.5 (Estimated)	[23]
Los Angeles, USA	Urban	25	[31]

variation to atmospheric oxidation at the next day [26]. Due to the lack of measurement of a large amount of VOCs during the Changping campaign, it is difficult to evaluate the possible impact of the $ClNO_2$ photolysis process on the formation of RO_x and O_3.

During the PKU summer campaign, it was found that the N_2O_5 heterogeneous process contributed a lot to the nitrate formation on polluted days, with an average daily contribution of 56 $\mu g\ m^{-3}$, or 20 ppbv. In order to restrict the amount of nitrate produced during the calculation, the yield of $ClNO_2$ is assumed to be 1. Based on this assumption, the accumulated $ClNO_2$ may reach 20 ppbv. In this case, the Cl^- content may be the main limiting factor. The GAC data observed the highest value of $HCl + Cl^-$ from September 23 to September 30 was only 3 ppbv, which shows that in the process of N_2O_5 heterogeneous uptake reaction to generate $ClNO_2$ if the yield can be greater than 0.15. The limiting factor for $ClNO_2$ may be the source of Cl.

To evaluate the effect of $ClNO_2$ photolysis processes on daytime photochemistry in winter, it is assumed that the yield of $ClNO_2$ is 1 to represent the maximum value of $ClNO_2$ daytime photochemistry. The box model is used to simulate the chemical process of $ClNO_2$ in the last continuous pollution process. The mechanism used is the RACM2 mechanism [7]. The Cl chemical mechanism module has been added in the previous literature, mainly refer to the MCM3.2 mechanism [20]. The N_2O_5 heterogeneous reaction mechanism module and Cl chemical coupling reaction and the VOCs merge mechanism can be found in [25]. In order to accurately describe the production of $ClNO_2$ and subsequent reactions, there is no constraint on NO in the model, but constraints on N_2O_5, NO_2, O_3, VOCs and S_a. The photolysis rate constant of $ClNO_2$ is obtained based on Eq. (5.1). Figure 5.14a shows the time series of $ClNO_2$ concentration simulated in the last pollution process. The simulated peak

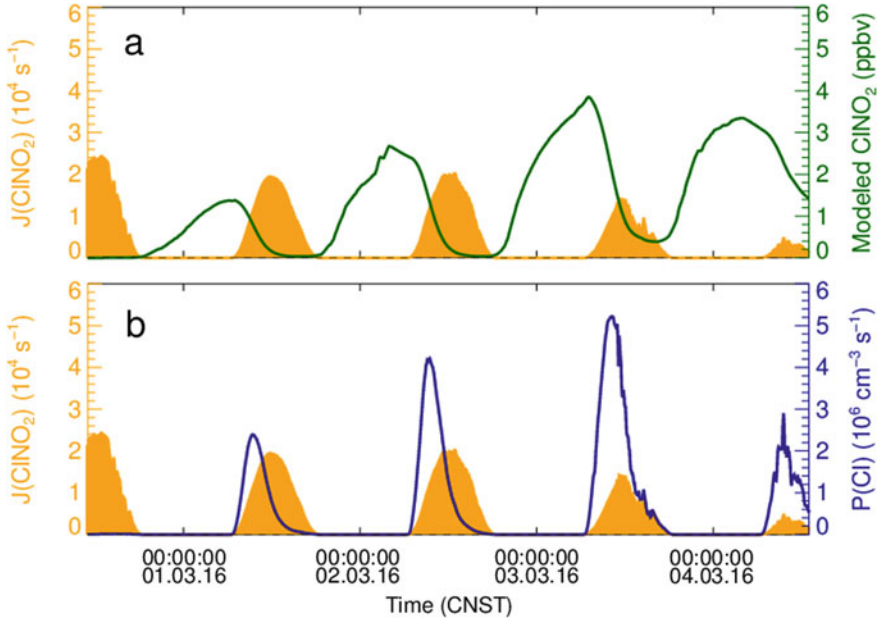

Fig. 5.14 The time series of **a** the modeled $ClNO_2$ concentration and **b** the production rate of chloride radical via $ClNO_2$ photolysis during the HR winter campaign

concentration of $ClNO_2$ is 1.5–4.0 ppbv, which is similar to the $ClNO_2$ concentration observed in Changping and Wangdu in summer [21]. Compared with the Changping campaign, the photolysis rate constant of $ClNO_2$ has largely decreased with a peak value of 0.5–2.5 $\times$ 10^4 s^{-1}. Figure 5.14b shows the modeled Cl radical production rate of $ClNO_2$ photolysis. The peak of Cl radical production rate appears at around 09:00 in the morning as in the summer observation, compared with the peak value of Cl radical production rate in Table 5.3. The model results during the wintertime are obviously higher, with a peak value of 2.5–5.5 $\times$ 10^6 cm^{-3} s^{-1}.

Two simulation cases that including and excluding the $ClNO_2$ mechanism are compared. Figure 5.15a shows that the addition of $ClNO_2$ mechanism can effectively increase the net production rate of O_3, especially between 08:00 a.m. and 02:00 p.m., the enhancement effect on O_3 formation can reach 1.55 ppbv h^{-1}. The average daily increase in the amount of O_3 generated due to the $ClNO_2$ chemical process can reach 7 ppbv, and the contribution to the primary source of O_3 is 21%, as shown in Fig. 5.15b.

In terms of RO_x, $ClNO_2$ chemistry also has a certain contribution. If the $ClNO_2$ reaction mechanism is not considered, the total primary formation of RO_x during the day is 14 ppbv. The most important primary source is the photolysis of HONO in this campaign, which contributed more than 50% of the total primary source (Fig. 5.16a). After considering the $ClNO_2$ mechanism into the model, the calculated total RO_x primary production amount reaches 16 ppbv, as shown in Fig. 5.16b, the

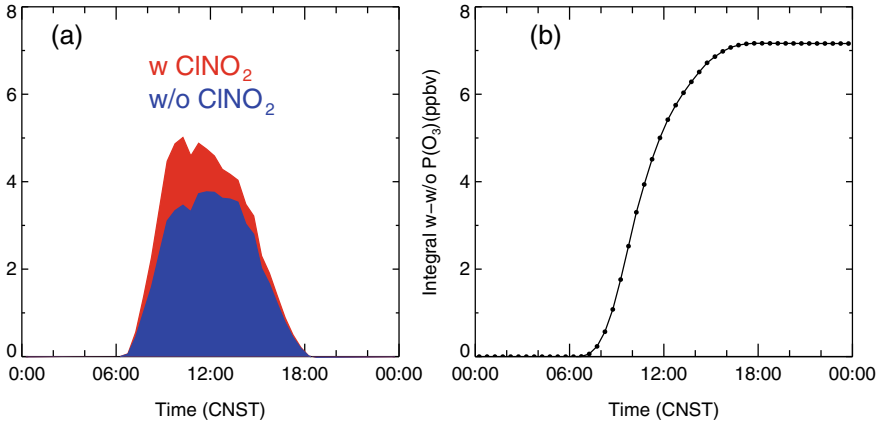

Fig. 5.15 **a** The diurnal variation of the modeled net O_3 production rate when the model running with (w) and without (w/o) $ClNO_2$ mechanism; **b** the integral of the differential between the two cases during the HR winter campaign (February 29 to March 04)

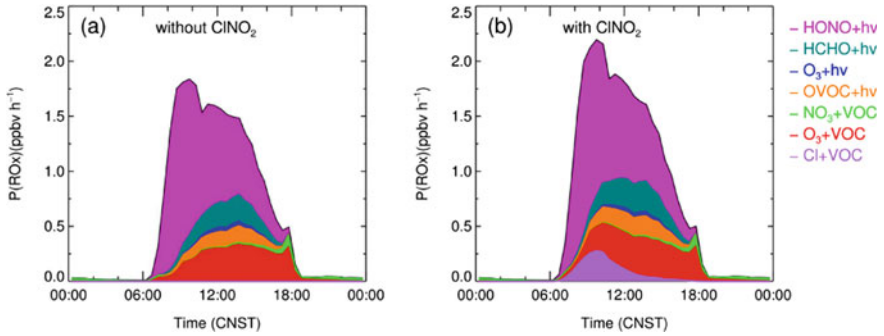

Fig. 5.16 The diurnal variation of the modeled primary RO_x production rate when the model running with (**a**) and without $ClNO_2$ mechanism (**b**) during the HR winter campaign (February 29 to March 04)

rate of $ClNO_2$ chemistry on the primary source of RO_x appears around 10:00 in the morning and can reach a maximum of 0.34 ppbv h^{-1}. The average contribution of $ClNO_2$ photolysis and subsequent reaction process to RO_x growth enhancement can reach 13%.

Although the concentration of $ClNO_2$ may not be as high as simulated in the actual atmosphere, it illustrates the potential importance of $ClNO_2$ to contribute to the atmospheric oxidation in winter, at least. In this model, the greatest uncertainty in the $ClNO_2$ concentration simulation is the $ClNO_2$ yield during the N_2O_5 heterogeneous reaction. The parameterized scheme based on the relationship between the particle Cl^- and the water content [3], still difficult to accurately predict the $ClNO_2$ yield [12, 27]. Therefore, the follow-up study on the yield of $ClNO_2$ in winter will help to

improve the accuracy of the winter oxidation assessment and optimize the simulation of its impacts on other radical chemistry.

5.4 Summary

This chapter mainly studies the atmospheric impacts of NO_3 and N_2O_5 chemical removal pathways. It includes the following three results:

1. NO_3 oxidation is significant in summer but weak in winter. Based on summer observations in Changping, it was found that the daily removal of BVOCs by NO_3 was 5.5 ppbv h^{-1}, and the maximum value was 1.2 ppbv h^{-1}. NO_3 dominates the nocturnal BVOCs degradation, with more than 90% of BVOCs removed by NO_3 throughout the night. This result suggests that NO_3 chemistry is the most important oxidant at night during summer in Beijing. On the 24-h scale, NO_3 contributes 28.2% to the oxidation of BVOCs, rank only second to OH radicals. The oxidation rate of BVOCs at night to form organic nitrate is 0.11 $\pm$ 0.09 ppbv h^{-1}, which is a potentially important source of SOA. The NO_3 concentration level is low in winter, and the oxidation ability is even lower than the contribution of O_3 at night.
2. During the summer pollution episodes, N_2O_5 heterogeneous has a large contribution to particulate nitrate formation, which can be equivalent to the contribution of $OH + NO_2$. The average daily contribution of N_2O_5 heterogeneous reaction to nitrate production reached 57 $\mu g\ m^{-3}$ during the PKU summer campaign, demonstrated this pathway is an important channel for nitrate production. Although the $OH + NO_2$ gas-phase reaction dominates in winter, the contribution of the N_2O_5 heterogeneous reaction cannot be ignored with a contribution of 17% in suburban Beijing.
3. The N_2O_5 heterogeneous uptake produces $ClNO_2$ can effectively generate Cl radicals in the photolysis process in the next day. The average daily production rate peak during the Changping campaign reached 5.2×10^6 cm^{-3} s^{-1}, which is highly oxidative during the day and made an important impact. Based on the box model, the maximum contribution of $ClNO_2$ to the primary sources of O_3 and RO_x during the winter pollution in Huairou was estimated. It was found that adding the $ClNO_2$ mechanism can increase the primary sources of O_3 and RO_x by 21 and 13%, indicating that the winter $ClNO_2$ may be critical to wintertime photochemistry. The study of $ClNO_2$ chemistry in winter may help to understand the budgets of O_3 and RO_x at the daytime.

References

1. Bannan TJ, Bacak A, Le Breton M, Flynn M, Ouyang B, McLeod M et al (2017) Ground and airborne UK measurements of nitryl chloride: an investigation of the role of Cl atom oxidation at Weybourne atmospheric observatory. J Geophys Res Atmos 122(20):11154–11165
2. Bannan TJ, Booth AM, Bacak A, Muller JBA, Leather KE, Le Breton M et al (2015) The first UK measurements of nitryl chloride using a chemical ionization mass spectrometer in central London in the summer of 2012, and an investigation of the role of Cl atom oxidation. J Geophys Res Atmos 120(11):5638–5657
3. Bertram TH, Thornton JA (2009) Toward a general parameterization of N_2O_5 reactivity on aqueous particles: the competing effects of particle liquid water, nitrate and chloride. Atmos Chem Phys 9(21):8351–8363
4. Edwards PM, Aikin KC, Dube WP, Fry JL, Gilman JB, de Gouw JA et al (2017) Transition from high- to low-NO_x control of night-time oxidation in the southeastern US. Nat Geosci 10(7):490–+
5. Faxon CB, Bean JK, Hildebrandt Ruiz L (2015) Inland concentrations of Cl-2 and $ClNO_2$ in Southeast Texas suggest chlorine chemistry significantly contributes to atmospheric reactivity. Atmosphere 6(10):1487–1506
6. Geyer A, Alicke B, Konrad S, Schmitz T, Stutz J, Platt U (2001) Chemistry and oxidation capacity of the nitrate radical in the continental boundary layer near Berlin. J Geophys Res Atmos 106(D8):8013–8025
7. Goliff WS, Stockwell WR, Lawson CV (2013) The regional atmospheric chemistry mechanism, version 2. Atmos Environ 68:174–185
8. Le Breton M, Hallquist ÅM, Pathak RK, Simpson D, Wang Y, Johansson J et al (2018) Chlorine oxidation of VOCs at a semi-rural site in Beijing: significant chlorine liberation from $ClNO_2$ and subsequent gas and particle phase Cl-VOC production. Atmos Chem Phys Discuss 1–25
9. Lu KD, Rohrer F, Holland F, Fuchs H, Bohn B, Brauers T et al (2012) Observation and modelling of OH and HO_2 concentrations in the Pearl River Delta 2006: a missing OH source in a VOC rich atmosphere. Atmos Chem Phys 12(3):1541–1569
10. Lu KD, Rohrer F, Holland F, Fuchs H, Brauers T, Oebel A et al (2014) Nighttime observation and chemistry of HO_x in the Pearl River Delta and Beijing in summer 2006. Atmos Chem Phys 14(10):4979–4999
11. Mielke LH, Furgeson A, Odame-Ankrah CA, Osthoff HD (2015) Ubiquity of $ClNO_2$ in the urban boundary layer of Calgary, Alberta, Canada. Can J Chem 94(4):414–423
12. Mielke LH, Stutz J, Tsai C, Hurlock SC, Roberts JM, Veres PR et al (2013) Heterogeneous formation of nitryl chloride and its role as a nocturnal NOx reservoir species during CalNex-LA 2010. J Geophys Res Atmos 118(18):10638–10652
13. Osthoff HD, Roberts JM, Ravishankara AR, Williams EJ, Lerner BM, Sommariva R et al (2008) High levels of nitryl chloride in the polluted subtropical marine boundary layer. Nat Geosci 1(5):324–328
14. Pathak RK, Wu WS, Wang T (2009) Summertime $PM_{2.5}$ ionic species in four major cities of China: nitrate formation in an ammonia-deficient atmosphere. Atmos Chem Phys 9:1711–1722
15. Pathak RK, Wang T, Wu WS (2011) Nighttime enhancement of $PM_{2.5}$ nitrate in ammonia-poor atmospheric conditions in Beijing and Shanghai: plausible contributions of heterogeneous hydrolysis of N_2O_5 and HNO_3 partitioning. Atmos Environ 45:1183–1191
16. Phillips GJ, Tang MJ, Thieser J, Brickwedde B, Schuster G, Bohn B et al (2012) Significant concentrations of nitryl chloride observed in rural continental Europe associated with the influence of sea salt chloride and anthropogenic emissions. Geophys Res Lett 39
17. Rohrer F, Berresheim H (2006) Strong correlation between levels of tropospheric hydroxyl radicals and solar ultraviolet radiation. Nature 442(7099):184–187
18. Rollins AW, Kiendler-Scharr A, Fry JL, Brauers T, Brown SS, Dorn HP et al (2009) Isoprene oxidation by nitrate radical: alkyl nitrate and secondary organic aerosol yields. Atmos Chem Phys 9(18):6685–6703

19. Spittler M, Barnes I, Bejan I, Brockmann KJ, Benter T, Wirtz K (2006) Reactions of NO3 radicals with limonene and alpha-pinene: product and SOA formation. Atmos Environ 40:S116–S127
20. Tan Z, Fuchs H, Lu K, Hofzumahaus A, Bohn B, Broch S et al (2017) Radical chemistry at a rural site (Wangdu) in the North China Plain: observation and model calculations of OH, HO_2 and RO2 radicals. Atmos Chem Phys 17(1):663–690
21. Tham YJ, Wang Z, Li QY, Yun H, Wang WH, Wang XF et al (2016) Significant concentrations of nitryl chloride sustained in the morning: investigations of the causes and impacts on ozone production in a polluted region of northern China. Atmos Chem Phys 16(23):14959–14977
22. Tham YJ, Yan C, Xue LK, Zha QZ, Wang XF, Wang T (2014) Presence of high nitryl chloride in Asian coastal environment and its impact on atmospheric photochemistry. Chin Sci Bull 59(4):356–359
23. Thornton JA, Kercher JP, Riedel TP, Wagner NL, Cozic J, Holloway JS et al (2010) A large atomic chlorine source inferred from mid-continental reactive nitrogen chemistry. Nature 464(7286):271–274
24. Wang H, Lu K, Chen X, Zhu Q, Chen Q, Guo S et al (2017) High N_2O_5 concentrations observed in urban Beijing: implications of a large nitrate formation pathway. Environ Sci Technol Lett 4(10):416–420
25. Wang H, Lu K, Tan Z, Sun K, Li X, Hu M et al (2017) Model simulation of NO_3, N_2O_5 and $ClNO_2$ at a rural site in Beijing during CAREBeijing-2006. Atmos Res 196:97–107
26. Wang T, Tham YJ, Xue LK, Li QY, Zha QZ, Wang Z et al (2016) Observations of nitryl chloride and modeling its source and effect on ozone in the planetary boundary layer of southern China. J Geophys Res Atmos 121(5):2476–2489
27. Wang Z, Wang WH, Tham YJ, Li QY, Wang H, Wen L et al (2017) Fast heterogeneous N_2O_5 uptake and $ClNO_2$ production in power plant and industrial plumes observed in the nocturnal residual layer over the North China Plain. Atmos Chem Phys 17(20):12361–12378
28. Wu Z, Wang Y, Tan T, Zhu Y, Li M, Shang D et al (2018) Aerosol liquid water driven by anthropogenic inorganic salts: implying its key role in Haze formation over the North China Plain. Environ Sci Technol Lett
29. Ye CX, Zhang N, Gao HL, Zhou XL (2017) Photolysis of particulate nitrate as a source of HONO and NO_x. Environ Sci Technol 51(12):6849–6856
30. Ye CX, Zhou XL, Pu D, Stutz J, Festa J, Spolaor M et al (2016) Rapid cycling of reactive nitrogen in the marine boundary layer. Nature 532(7600):489–491
31. Young CJ, Washenfelder RA, Roberts JM, Mielke LH, Osthoff HD, Tsai C et al (2012) Vertically resolved measurements of nighttime radical reservoirs; in Los Angeles and their contribution to the urban radical budget. Environ Sci Technol 46(20):10965–10973

Chapter 6
Conclusions and Outlook

Abstract This chapter gives the conclusions and outlook of this study.

6.1 Conclusions

In this paper, systematic research was conducted on the atmospheric NO_3 radical and N_2O_5 chemistry in urban and suburban Beijing. NO_3 radical and N_2O_5 field detection system was first established based on the broadband cavity-enhanced absorption spectroscopy technology. This system achieved the portability and high stability required for field measurement. N_2O_5 observation was conducted in four field campaigns. The total NO_3 reactivity and the heterogeneous uptake coefficient of N_2O_5 are quantified; the impacts of NO_3 and N_2O_5 chemistry on atmospheric oxidation, nitrate formation, and daytime photochemical processes were evaluated. The main results are summarized as follows:

1. Set up a high-precision NO_3-N_2O_5 online measurement system (PKU-CEAS), which is successfully applied to the field measurement of N_2O_5. A novel non-adjustable mechanically aligned mirror mounts was designed and tested to be working. The new design offers us a fast setup of the instrument in the field and proved to be stably running as evident by the high stability of the calibrated mirror reflectivity. An addition chemical titration module by adding NO into the sample flow is tested and proved to be very helpful for the ambient spectrum analysis which enhanced the fitting precision by avoiding the complicated fitting of the water vapor absorption and the possible wavelength and power drift of LED. The sampling loss efficiency of NO_3 and N_2O_5 during the measurement is accurately quantified. At 1 s integration time, the detection limits of NO_3 and N_2O_5 are 2.4 pptv and 2.7 pptv, respectively, and the uncertainties are 19% and 22%–36%, respectively.
2. Four campaigns were carried out in the urban and suburban areas of Beijing for the study of the chemical mechanism of NO_3 and N_2O_5. It was found that there are significant N_2O_5 in Beijing, and there are clear diurnal profiles in NO_3 and N_2O_5. The seasonal and regional differences are significant. The nighttime peaks of NO_3 and N_2O_5 often appear about 2 hours after sunset. The nighttime

H. Wang, *The Chemistry of Nitrate Radical (NO_3) and Dinitrogen Pentoxide (N_2O_5) in Beijing*, Springer Theses, https://doi.org/10.1007/978-981-15-8795-5_6

average concentration level of N_2O_5 is between 10-100 pptv, and the peak value can reach 1.0–1.5 ppbv (except for the winter campaign in PKU, which is 375 pptv). The suburban N_2O_5 is significantly higher than the urban area. The average NO_3 concentration level is between 0.1–10 pptv, and the NO_3 concentration in summer is larger than that in winter. These differences in temporal and spatial distribution are due to seasonal temperature changes and ozone changes. The NO_x concentration levels in urban and suburban areas are quite different, which affects the production rate and thermodynamic equilibrium.

3. The NO_3 reactivity in summer is mainly contributed by the BVOCs. NO_3 is a very important atmospheric oxidant in summer and dominates the oxidation of nocturnal biogenic VOCs, but its contribution to atmospheric oxidation is weak in winter. The NO_3 reactivity in Beijing area in winter is 6.6×10^{-3} s^{-1} (HR), and 3.7×10^{-3} s^{-1} (PKU), the main source of olefins is emitted by anthropogenic activities; the NO_3 reactivity to VOCs in the suburbs of summer is 1.9×10^{-2} s^{-1}, which is 2–5 times higher than that in winter. The NO_3 contribution to the oxidation of biogenic VOCs at night in Beijing in summer exceeds 90%, accounting for 28% of the average daily contribution, highlight the importance of NO_3 in summer. The NO_3 oxidation rate of VOCs in winter is more than an order of magnitude lower than that in summer. Compared with the oxidation of OH and O_3, the contribution of NO_3 to oxidation in winter is relatively small.
4. The parameterized model based on the laboratory studies were found not applicable in Beijing. Quantitative results indicate that the summer N_2O_5 uptake coefficient in Beijing is between 0.012 and 0.072, with an average value of 0.04, which is higher than the field results in Europe and the United States. It may be related to the high aerosol water content in Beijing during the summertime. The winter N_2O_5 uptake coefficient is low, with an average value of 0.005, which may be affected by the low water content and the suppression of high particulate nitrate in winter. The parameterization generally fails to predict the N_2O_5 uptake coefficient. The overestimates of the model may be due to the suppression of organic coatings on the particle surface. The coexistence of high N_2O_5 concentration, aerosol surface area, and N_2O_5 uptake coefficient during the summer pollution process resulted in the N_2O_5 heterogeneous process contributing about 50% of the daily average of particulate nitrate production, which is equivalent to the gas phase reaction ($OH + NO_2$). In winter compaigns, the N_2O_5 heterogeneous contributed less than 20% to the daily average of nitrate production, which implies that the gas phase reaction is the main channel for nitrate production in winter. The model simulation found that winter $ClNO_2$ photolysis can effectively increase the primary source of O_3 and RO_x (10%–20%), which may be critical to understanding the source of RO_x in winter.

6.2 Outlook

1. Improve field measurement technology of NO_3 and N_2O_5. Although the field measurement of NO_3 has been widely implemented based on the closed optical cavity technology at home and abroad, the sampling efficiency of NO_3 is low, and high variated. Therefore, accurate quantification is important to achieve high-precision measurement of NO_3. Open optical cavity technology can achieve NO_3 loss free measurement, which can essentially avoid the loss of sampling. It may be a choice for future NO_3 measurement technology. Although the acquisition of reference spectra and the calibration of reflectance are not so easy in practical applications, the optimization of instrument hardware design may help to solve these problems. Besides, the open path cavity system needs to retrieve water vapor absorption well in the atmosphere. The currently established lookup table-based H_2O water vapor retrieve method can be used to remove water vapor absorption and ensure accurate retrieval of NO_3.
2. Establish direct measurement methods for NO_3 reactivity and N_2O_5 uptake coefficient. The reaction of NO_3 and VOCs and the heterogeneous uptake of N_2O_5 are the two most important removal pathways in the NO_3–N_2O_5 chemistry and the main uncertainty in the budget analysis. The establishment of a direct online measurement technique for NO_3 reactivity and N_2O_5 uptake coefficient can greatly improve the understanding of the above two reactions. Based on the existing NO_3 and N_2O_5 field measurement technology, using the flow tube as the reaction zone, measuring the decay of NO_3 and N_2O_5 can achieve the quantification of the removal rate of NO_3 and N_2O_5, quantify the wall effect in the flow tube may be a key issue in the system.
3. Develop laboratory studies on the reaction of NO_3 and BVOCs. At present, the community generally believes that the reaction of NO_3 and BVOCs has a great contribution to the formation of organic aerosols, which has an important impact on the global aerosol formation and climate change. However, the related research on the reaction of NO_3 and BVOCs is still lacking. The chemical mechanism, reaction products, and subsequent influence mechanism of the reaction between NO_3 and BVOCs are unclear, especially the reaction of NO_3 and monoterpenes. Based on the development of NO_3 measurement technology, combined with new analysis methods such as CIMS, PTR-MS, and 2D-GC, in-depth laboratory research on the reaction channels of NO_3 and BVOCs will help to clarify the role of NO_3 oxidation reactions in atmospheric chemistry.
4. Explore the main control factor of the N_2O_5 uptake coefficient and establish a localized N_2O_5 uptake coefficient parameterization method. The research on the key factors influencing the N_2O_5 uptake has a history of more than 20 years. Existing studies have shown that different particulate matter components, relative humidity, mixed state, and other parameters have certain effects. However, in the actual atmosphere, the coupling of multiple factors makes it difficult to find which are the main factors. Based on the establishment of a direct measurement method for the N_2O_5 uptake coefficient, to achieve long-term measurement of

the N_2O_5 uptake coefficient and related parameters, combined with statistical analysis methods may help to screen out the main control factors that affect the local N_2O_5 uptake coefficient and help to test the parameterization proposed by laboratory studies. Based on the selection of main control factors, establishing a localized N_2O_5 uptake parameterization and updating to regional and global models will help improve the accuracy of model simulation and air quality forecasting.

5. Carry out the vertical profile research of NO_3 and N_2O_5, especially in China. Existing research shows that there is a clear vertical distribution of nighttime chemistry with NO_3 and N_2O_5, which is limited by instrumentation and platform. Nighttime chemistry in China is still in the leading stage of near-ground research, but near-ground night chemistry maybe cannot represent the entire process in the boundary layer at night. There is an urgent need to conduct a comprehensive study of the combination of near-ground and vertical scales. High-altitude surveying with towers and airplanes is currently the main method of vertical profile research. The measurement position of the tower is fixed, the height is low, and it has a relatively large location restriction. The airborne measurement is relatively flexible in spatial scale, but it has high requirements on the instrument size and stability. Combined with the ground and vertical measurements, we can describe the atmospheric chemical reaction rules of NO_3 and N_2O_5, and provide a scientific basis for the subsequent formulation of air pollution control strategies.